

12-2014

Retinal synaptic function in the absence of the on pathway.

Kathryn Marie Heath Fransen
University of Louisville

Follow this and additional works at: <https://ir.library.louisville.edu/etd>

 Part of the [Ophthalmology Commons](#)

Recommended Citation

Fransen, Kathryn Marie Heath, "Retinal synaptic function in the absence of the on pathway." (2014). *Electronic Theses and Dissertations*. Paper 1709.
<https://doi.org/10.18297/etd/1709>

This Doctoral Dissertation is brought to you for free and open access by ThinkIR: The University of Louisville's Institutional Repository. It has been accepted for inclusion in Electronic Theses and Dissertations by an authorized administrator of ThinkIR: The University of Louisville's Institutional Repository. This title appears here courtesy of the author, who has retained all other copyrights. For more information, please contact thinkir@louisville.edu.

RETINAL SYNAPTIC FUNCTION IN THE ABSENCE OF THE ON PATHWAY

By

Kathryn Marie Heath Fransen
B.S., Indiana University, 2007

A Dissertation
Submitted to the Faculty of the
College of Arts and Sciences of the University of Louisville
in Partial Fulfillment of the Requirements
for the Degree of

Doctor of Philosophy

Department of Psychological and Brain Sciences
University of Louisville
Louisville, Kentucky

December 2014

RETINAL SYNAPTIC FUNCTION IN THE ABSENCE OF THE ON PATHWAY

By

Kathryn Marie Heath Fransen
B.S. Indiana University 2007

A Dissertation Approved on

November 14, 2014

by the following Dissertation Committee:

Maureen McCall, Ph.D.

Bart Borghuis, Ph.D.

Paul DeMarco, Ph.D.

Ronald Gregg, Ph.D.

Keith Lyle, Ph.D.

Pavel Zahorik, Ph.D.

ACKNOWLEDGMENTS

I would like to express my gratitude for the people who have helped me complete this work. I could not have made it this far without the support and love of many people. I would like to thank my committee members, Dr. Borghuis, Dr. DeMarco, Dr. Gregg, Dr. Lyle, and Dr. Zahorik. Your wisdom, advice, and support throughout my graduate school experience has been extremely valuable. In addition, my fellow lab mates have been a great source of learning, support and comradery. My husband, James Fransen, has been my biggest source of support along this journey and I am so grateful to have him by my side. Throughout the good, the bad and the ugly James has been there with wise words and love. My parents and grandparents have always nurtured my curiosity and love for learning and I am thankful for all of the love and support they have shown me throughout my life. Lastly, I would like to thank my mentor Dr. Maureen McCall. You have helped guide and teach me over many years and have helped to mold me into a budding scientist. I am truly grateful for all of your support and direction and am thankful to have a strong female scientist as a role model. Thank you.

ABSTRACT

RETINAL SYNAPTIC FUNCTION IN THE ABSENCE OF THE ON PATHWAY

Kathryn Marie Heath Fransen

December 18, 2014

Complete Congenital Stationary Night Blindness (cCSNB) is a rare hereditary retinal disorder characterized by abnormal night vision. cCSNB is caused by postsynaptic defects in On bipolar cells (BCs) and is identified by the presence of an electroretinogram (ERG) with a normal a-wave, corresponding to photoreceptor function, and the absence of a b-wave, corresponding to a failure of On BC function. Through the study of genetic mutations in mouse that result in no b-wave ERG phenotypes, several proteins have been identified that play crucial roles in On BC signal transmission.

I focused on four mouse models of cCSNB; *Nyx^{nob}* (Nyctalopin mutant), *mGluR6^{-/-}* (mGluR6 knockout), *Gpr179^{nob5}* (GPR179 mutant), and *Lrit3^{-/-}* (LRIT3 knockout). These mutations effect proteins expressed by On BCs (rod and On Cone BCs). While all models of cCSNB share a no b-wave ERG phenotype I have discovered that several models differ. The differences between cCSNB animal models provide important clues into the functional roles of the proteins effected by the

mutations. Specifically, *Nyx^{nob}* retinal ganglion cells (RGCs), the output neurons of the retina, exhibit robust 3-5 Hz rhythmic spiking while *mGluR6^{-/-}* RGCs rarely do. I explored potential mechanisms which underlie this phenomenon, not only by examining RGC activity, but also the properties of the upstream rod BCs which provide excitatory input to RGCs. I found that differences in the resting state of *Nyx^{nob}* and *mGluR6^{-/-}* rod BCs correlate with the differences in RGC rhythmic spiking activity. Also, I discovered that nyctalopin is required for normal potassium conductance in rod BCs.

Additionally, I examined the role of two recently identified proteins expressed in On BCs, GPR179 (Peachey et al., 2012; Ray et al., 2014) and LRIT3 (Zeitz et al., 2013; Neuille et al., 2014). I discovered that GPR179 sets the sensitivity of the TRPM1 channel and is critical for a normal light-evoked response in rod BCs. I also discovered that LRIT3 is critical for the modulation and expression of TRPM1 channels in rod BC dendritic tips. My data not only add to the literature on animal models of cCSNB, but to the understanding of retinal circuitry in the normal retina.

TABLE OF CONTENTS

	PAGE
Abstract.....	iv
List of Figures.....	viii
Chapter I.....	1
Introduction to Retinal Structure and Function	
Chapter II.....	36
General Materials and Methods	
Chapter III.....	44
Comparison of <i>Nyx^{nob}</i> and <i>mGluR6^{-/-}</i> RGCs	
Introduction.....	44
Materials and Methods.....	49
Results.....	53
Discussion.....	68
Chapter IV.....	75
Comparison of <i>Nyx^{nob}</i> and <i>mGluR6^{-/-}</i> Rod BCs	
Introduction.....	75
Materials and Methods.....	82
Results.....	85
Discussion.....	104
Chapter V.....	111
Critical Role of GPR179 in Rod BC Response	
Introduction.....	111
Materials and Methods.....	114
Results.....	115

Discussion.....	123
Chapter VI.....	128
Critical Role of LRIT3 in Rod BC Response	
Introduction.....	128
Materials and Methods.....	135
Results.....	136
Discussion.....	143
Chapter VII.....	145
Summary and Future Directions.....	145
Implications of my Research.....	149
References.....	151
Curriculum Vitae.....	167

LIST OF FIGURES

FIGURE	PAGE
1. Diagram of retina.....	2
2. Basic functional pathways of the retina.....	4
3. Bipolar cell classes.....	8
4. The three rod pathways.....	11
5. Four major types of inhibition.....	18
6. Morphological classes of On bipolar cells.....	24
7. On BC response.....	25
8. Electroretinogram from WT and <i>mGluR6</i> ^{-/-} mouse.....	29
9. WT and <i>Trpm1</i> ^{-/-} BC pharmacological responses.....	32
10. WT and <i>Trpm1</i> ^{-/-} BC light responses.....	33
11. RGC Fast Fourier Transform.....	51
12. Among RGCs that exhibit spiking activity, most <i>Nyx</i> ^{nob} but only a few <i>mGluR6</i> ^{-/-} RGCs exhibit rhythmic spiking activity.....	55
13. Almost all of <i>Nyx</i> ^{nob} and slightly less than half of <i>mGluR6</i> ^{-/-} RGCs exhibit rhythmic membrane oscillations.....	57
14. The distribution of recorded <i>Nyx</i> ^{nob} and <i>mGluR6</i> ^{-/-} RGCs and distribution of rhythmic spiking based on morphology and light response class.....	59
15. WT, <i>mGluR6</i> ^{-/-} and <i>Nyx</i> ^{nob} RGC V_{rest}	61

16. WT, <i>mGluR6</i> ^{-/-} and <i>Nyx^{nob}</i> RGC spontaneous activity.....	63
17. <i>Nyx^{nob}</i> RGC spontaneous activity is decreased in membrane oscillation only RGCs compared to rhythmic spiking RGCs.....	67
18. Summary schematic of rhythmic RGCs in <i>mGluR6</i> ^{-/-} and <i>Nyx^{nob}</i>	69
19. <i>Nyx^{nob}</i> rod BC V_{rest} is more depolarized than WT and <i>mGluR6</i> ^{-/-}	86
20. <i>Nyx^{nob}</i> rod BCs do not exhibit TRPM1-mediated currents at dendritic tips nor soma.....	89
21. Transient peak and steady-state potassium current components were decreased in amplitude in <i>Nyx^{nob}</i> rod BCs compared to WT or <i>mGluR6</i> ^{-/-}	92
22. Transient peak and steady-state components of the Cs/TEA-insensitive currents were similar in WT, <i>Nyx^{nob}</i> and <i>mGluR6</i> ^{-/-} rod BCs.....	95
23. Transient but not persistent currents were decreased in <i>Nyx^{nob}</i> rod BCs compared to WT and <i>mGluR6</i> ^{-/-}	100
24. The input conductance of <i>Nyx^{nob}</i> rod BCs was similar to WT and <i>mGluR6</i> ^{-/-} rod BCs.....	103
25. A small amplitude, concentration-dependent CPPG response in <i>Gpr179^{nob5}</i> and <i>RGS7</i> ^{-/-} / <i>RGS11</i> ^{-/-} rod BCs.....	118
26. Capsaicin-evoked TRPM1 responses are normal in <i>RGS7</i> ^{-/-} / <i>RGS11</i> ^{-/-} and decreased in <i>Gpr179^{nob5}</i> rod BCs.....	120
27. <i>Gpr179^{nob5}</i> , <i>Trpm1</i> ^{-/-} , and <i>RGS7</i> ^{-/-} / <i>RGS11</i> ^{-/-} rod BCs have decreased standing currents and channel open probability.....	122
28. <i>Lrit3</i> ^{-/-} ERG recordings exhibit the classic cCSNB no b-wave phenotype under dark and light-adapted conditions.....	131

29. <i>Lrit3</i> ^{-/-} rod BCs lack expression of nyctalopin, have mislocalized TRPM1, and normal expression of mGluR6.....	133
30. <i>Lrit3</i> ^{-/-} rod BCs have normal expression of RGS complex proteins and GPR179 in rod BCs.....	134
31. <i>Lrit3</i> ^{-/-} rod BCs lack a CPPG mediated response at short and long duration stimulation.....	138
32. Capsaicin-evoked TRPM1 responses are absent in <i>Lrit3</i> ^{-/-} rod BCs.....	140
33. <i>Lrit3</i> ^{-/-} and <i>Trpm1</i> ^{-/-} rod BCs have decreased standing currents and channel open probability.....	142

CHAPTER I

INTRODUCTION TO RETINAL STRUCTURE AND FUNCTION

Retinal Structure

The neural retina is a laminated structure at the back of the eye which encodes light information from the world around us. The retina transduces photons into electrical signals producing a neural code, transfers the information to higher visual structures in the brain and creates the foundation of visual perception. The retina consists of three nuclear layers and two synaptic layers and is populated by five major cell classes (Figure 1). Its outer nuclear layer (ONL) contains two types of photoreceptors (PRs), rods and cones. The PRs synapse with the dendrites of bipolar cells (BCs) and horizontal cells (HCs) in the outer plexiform layer (OPL). The somas of the BC, HC, and amacrine cells (AC) are located in the inner nuclear layer (INL). The BCs and ACs synapse with each other and with ganglion cell (RGC) dendrites in the inner plexiform layer (IPL). The RGC somas compose the final nuclear layer, the ganglion cell layer (GCL) and their axons form the optic nerve which transmits the retinal signal to higher visual structures in the brain.

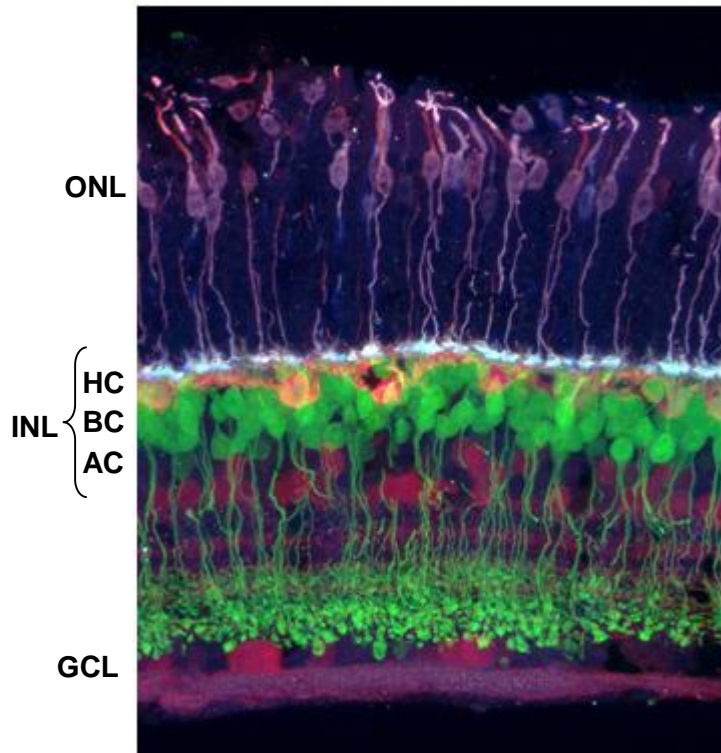


Figure 1. Diagram of retina. The outer nuclear layer contains the rod and cone photoreceptors. The photoreceptors synapse onto the bipolar cells and horizontal cells located in the inner nuclear layer. The amacrine cells also reside in the inner nuclear layer. The bipolar cells and amacrine cells synapse onto the ganglion cells located in the ganglion cell layer. From Wong et al., 2006.

PR outer segments are packed with opsin molecules, which change conformation when they absorb a photon of light. This absorption initiates a G-

protein coupled cascade which culminates in the hyperpolarization of the PR and a decrease in its glutamate release onto its postsynaptic partners, the BCs and HCs. During light stimulation PRs cease glutamate release. HCs respond with graded potential changes and provide modulatory feedback to PRs to provide gain control and create the first level of surround input to BCs. Cone PR responses to light increments lead to graded responses in BCs; namely hyperpolarization in Off cone BCs and depolarization in On cone BCs. The cone BCs then transmit graded potentials to RGCs. Rod PR responses to light increments lead to depolarization of rod BCs. Rod BCs use the All AC interneuron to piggy-back onto the On cone BCs to transfer the rod BC signal to RGCs (Famiglietti & Kolb, 1974). The processes of ACs ramify within the IPL. ACs respond with either graded or action potentials and modulate feedback inhibition to BCs and feed-forward inhibition to RGCs. The axons of BCs and ACs ramify in specific laminae of the IPL based on their functional light responses. Off cone BC axons ramify in the Off sublamina, located near the INL, while rod BCs and On cone BCs ramify in the On sublamina (Figure 2), near the GCL. This distinct lamination pattern is matched by the ramification of RGC dendrites that also correspond to their functional light response. On RGCs produce action potentials to increments of light and their dendrites ramify in the On sublamina, whereas Off RGCs respond with action potentials to decrements of light and their dendrites ramify in the Off sublamina. Bistratified RGC dendrites ramify in both substratum and either depolarize to both the onset and offset of light, or onset only.

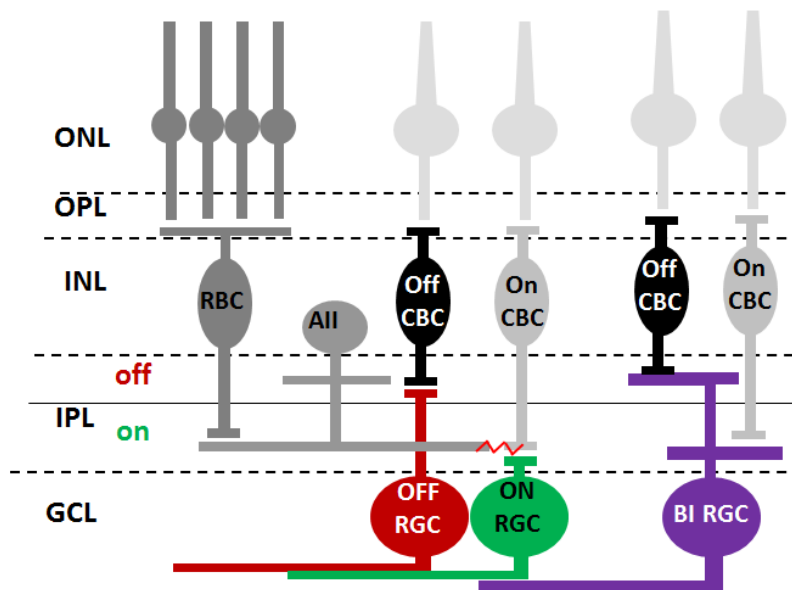


Figure 2. Basic functional pathways of the retina. Cone PRs synapse with On and Off cone BCs which synapse with On and Off RGCs, respectively. The rod PRs synapse with rod BCs, which synapse with All ACs, providing excitatory rod input to the On cone pathway and inhibitory input to the Off pathway.

Retinal Pathways

Introduction

The visual signal is transferred through the excitatory pathway from PRs to BCs and from BCs to RGCs. These excitatory signals are modulated by lateral inhibitory inputs from HCs in the outer retina and ACs in the inner retina. These inputs create center/surround organization in BCs, ACs, and RGCs and produce

contrast gain, temporal and spatial frequency selectivity, as well as selectivity to the direction of motion. Within the retina these neural elements also segregate and form the parallel rod/cone as well as the On/Off pathways which are described in detail below.

Cone Pathway

Cone PRs are responsible for photopic vision, high visual acuity and color vision. There are 180,000 cones spread evenly across the mouse retina (Jeon et al., 1998). There are two types of murine cone PRs, one sensitive to ultraviolet light (peak sensitivity 360 nm) and another to medium wavelength light (peak sensitivity 508 nm; Nikonov et al., 2006). Cones release glutamate at their synaptic terminal, the cone pedicle. HC and On cone BC dendrites invaginate the cone pedicle, while Off cone BCs make their contacts at its base. Approximately eight BCs innervate the pedicle of one cone PR, allowing for multiple pathways to originate at this first synapse (Wassle, 2004).

On and Off Pathways

The cone pathway subdivides into the On and Off pathways, which are initiated at the PR to BC synapse based on the expression of either a metabotropic or ionotropic glutamate receptor on the BC dendrites. On BCs express mGluR6 receptors, while Off BCs express ionotropic glutamate receptors. As a result of this differential glutamate receptor expression, On BCs depolarize to light onset, while Off BCs depolarize to light offset.

On and Off Bipolar Cell Classes

In the mouse, Off BCs, or hyperpolarizing BCs, express the ionotropic glutamate receptor kainate on their dendritic tips (Borghuis et al., 2014), although it was previously reported that they also express AMPA (Puller et al., 2013). Off BCs have a sign-conserving synapse which results in a depolarization to PR glutamate release by the binding of glutamate to the ionotropic receptors. The second-order BCs are the first cell class in the visual process to exhibit different temporal response properties. In ground squirrel, glutamate bound to Off BC AMPA receptors mediate transient signals while glutamate bound to kainate receptors mediate sustained signals resulting in temporally distinct signals within the Off Pathway (DeVries, 2000). In the mouse and primate, kainate receptors mediate both sustained and transient signals (Borghuis et al., 2014; Taylor, 2014).

On BCs, or depolarizing BCs, express the metabotropic glutamate receptor mGluR6 on their dendritic tips. On BCs have a sign-inverting synapse. When the concentration of glutamate in the synapse decreases, the absence of glutamate bound to the mGluR6 receptor opens a non-specific cation channel, TRPM1, and depolarizes the cell. In the mouse, transient On BCs possess voltage-gated sodium channels on their dendrites or somas, which enhance transmission to transient RGCs (Ichinose et al., 2005). Sustained On BCs do not possess these voltage-gated sodium channels (Ichinose et al., 2005). The sodium channels in transient On BCs contribute to the temporal segregation of

transient and sustained signals by the selective enhancement of the responses of On transient RGCs to light (Ichinose et al., 2005). Transient On and Off BC axons terminate toward the center of the IPL while more sustained On and Off BCs terminate within the outer portions of the IPL (Awatramani & Slaughter, 2000; Wu et al., 2000; Borghuis et al., 2013). This creates yet another parallel channel system within the retina.

BCs can also be characterized by their morphology. BC structure and physiological response follow a typical distribution where Off BCs ramify within the OFF sublamina (1-2) of the IPL while the On BCs ramify within the ON sublamina (3-5; Euler et al., 1996; Ghosh et al., 2004; Figure 3). In the mouse retina, there are four morphological Off BC types, five On cone BCs, and one type of rod BC (Figure 3A; Ghosh et al., 2004). Utilizing molecular markers there are five Off BC types, six On cone BCs, and one type of rod BC (Figure 3B; Wassle et al., 2009).

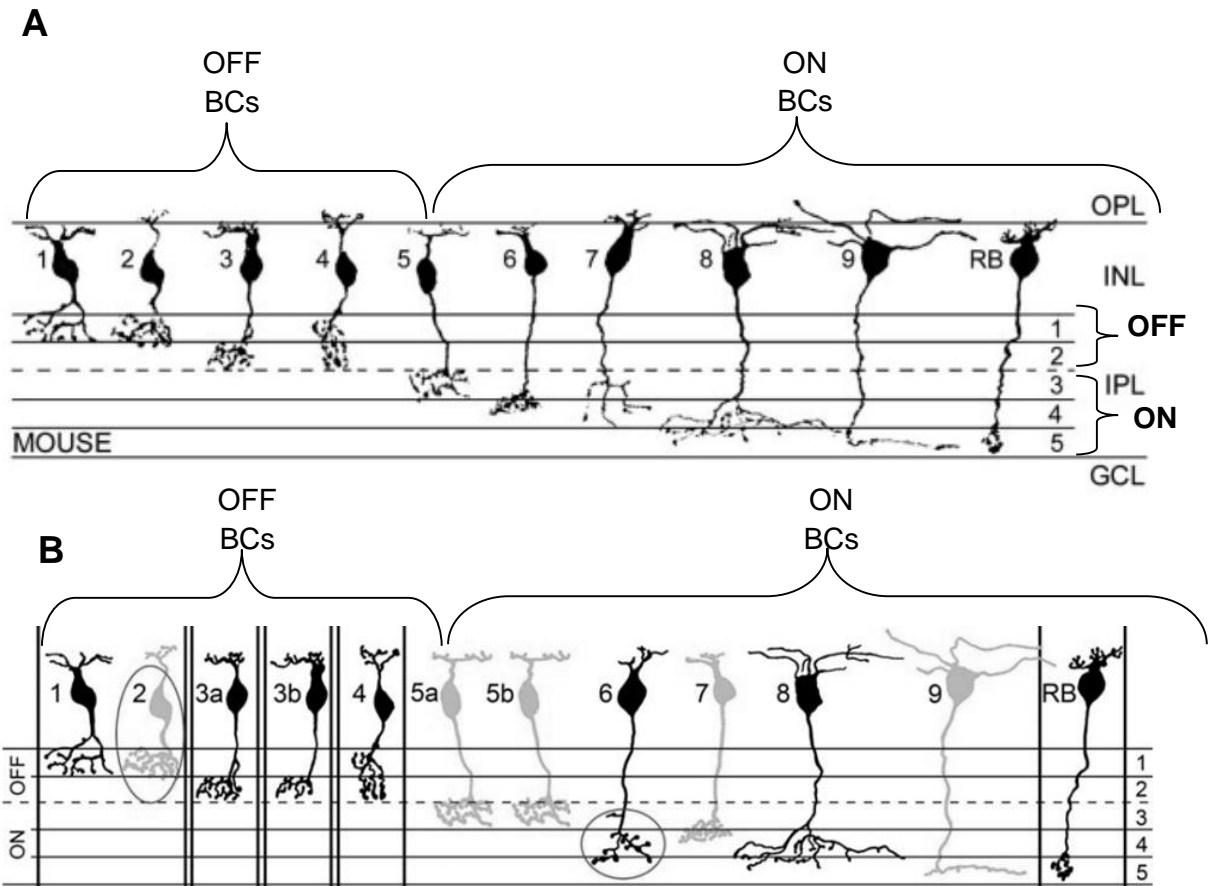


Figure 3. Bipolar cell classes. **A.** Morphological classes: There are four Off BCs, five On cone BCs and one type of rod BC. Modified from Ghosh et al., 2004. **B.** Molecular marker identified classes: There are five Off BCs, six On cone BCs, and one type of rod BC. Modified from Wassle et al., 2009.

BCs utilize graded potentials to transmit the visual signal. Rod BCs release glutamate via calcium-dependent exocytosis at ribbon-style active zones (Dowling & Boycott, 1966). Glutamate filled vesicles are tethered to ribbons,

which are closely located to the voltage-gated calcium channels at the presynaptic membrane. The ribbon synapse facilitates a fast release of vesicles from the readily releasable pool while vesicles tethered further up the ribbon contribute to a second more sustained component of release (Wan & Heidelberger, 2011). Rod BC depolarization from a holding potential of -60 mV to -10 mV for 25 msec will release the readily releasable pool of glutamate at the axon terminal (Mennerick & Matthews, 1996; Palmer, 2010). The faster the BC membrane is depolarized, the more pronounced the transient component of the excitatory postsynaptic current (EPSC) measured in downstream RGCs, while slower rates of depolarization lead to more sustained release of glutamate and sustained EPSCs (Snellman et al., 2009). Therefore, the intrinsic membrane properties of BCs are crucial for the release of glutamate and the shape and characteristics of EPSCs recorded in the postsynaptic cell.

Rod Pathways

The rod pathway is responsible for low light, or scotopic vision. Rods can detect a single photon of light (Rieke & Baylor, 1998). There are 6.4 million rods in the mouse retina (Jeon et al., 1998). The rod PR terminal, termed the rod spherule, is invaginated by HCs and rod BCs. One to three rod BC dendrites invaginate one rod spherule. One rod BC contacts 20-80 rods (Wassle, 2004). Since rod PRs are sensitive to one photon of light and rod BCs converge the signal of several rods, the rod pathway is sensitive to very low light levels. Rod input to rod BCs exhibit slower temporal signals than cones to cone BCs

(Ashmore & Copenhagen, 1980; Cadetti et al., 2005). The rod BC expresses the same mGluR6 receptor as On cone BCs and communicates with RGCs via the All AC. Thus, the rod pathway functions as part of the On and Off pathways.

There are three different pathways for the rod system and they appear to be segregated according to their sensitivity to light. The primary rod pathway is the most sensitive and transmits rod signals to rod BCs and to the On and Off cone pathway via the All AC (Figure 4; Kolb & Famiglietti, 1974). The On response of rod BCs is transmitted through an excitatory synapse with the All AC, resulting in All depolarization. The All is electrically coupled through gap junctions to On cone BCs, which create a sign-conserving signal to the On cone pathway. The All also has a sign-inverting glycinergic inhibitory synapse with Off cone BCs resulting in hyperpolarization of Off cone BCs. The On and Off cone BCs then transmit the signal to their corresponding On and Off RGCs (Kolb & Famiglietti, 1974).

The secondary rod pathway with intermediate sensitivity transmits the PR rod signal to cone PRs via gap junctions. The rod signal is then carried through On and Off cone BCs to RGCs (Figure 4; Volgyi et al., 2004). The tertiary rod pathway, the least sensitive, transmits the rod signal directly through a chemical synapse with Off cone BCs (Volgyi et al., 2004) and type 7 On cone BCs (Tsukamoto et al., 2007). This final pathway provides another route for rod signals to reach the Off and On cone pathways (Figure 4; Volgyi et al., 2004; Tsukamoto et al., 2007). The primary pathway mediates slow low threshold

signaling, the secondary pathway mediates faster high threshold signals (Volgyi et al., 2004), and the tertiary pathway likely mediates intensity changes at the interface of scotopic-mesopic vision, optimizing detection at dusk and dawn (Volgyi et al., 2004; Tsukamoto et al., 2007). The three rod pathways extend the rod system operating range as RGCs receive either separate or convergent inputs from one or more of the pathways (Volgyi et al., 2004; Tsukamoto et al., 2007).

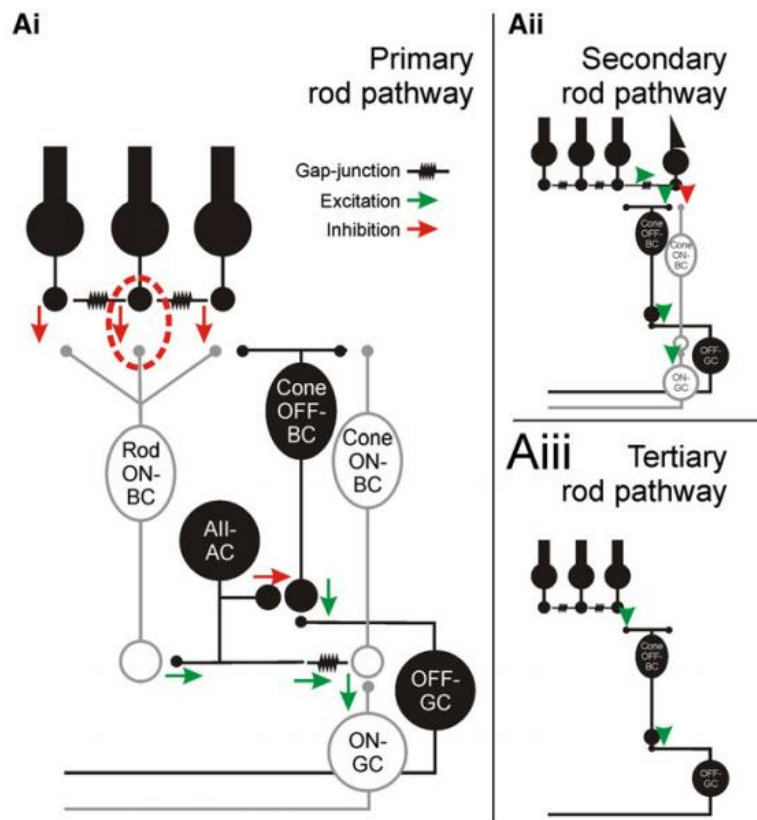


Figure 4. The three rod pathways. Ai. The primary rod pathway signals from rod PRs to rod BCs to All ACs. Aii. The secondary pathway signals from rod PRs to cones through gap junctions and then to On and Off cone BCs. Aiii. The tertiary

pathway signals from rod PRs to a class of Off cone BCs and type 7 On cone BCs (Tsukamoto et al., 2007). From van Genderen et al., 2009.

Retinal Ganglion Cells

Retinal Ganglion Cell Classes

RGCs integrate the graded inputs from second order neurons and convert them into action potentials, which are used to transmit the retinal signal to higher brain structures. There are approximately 20 morphological types of RGCs in the retina (Sun et al., 2002). RGCs are characterized based on dendritic ramification in the IPL, dendritic and soma diameters and dendritic arborization (Sun et al., 2002). RGCs can be further classified based on their excitatory response to either the onset, offset, or onset and offset of light stimuli (Hartline, 1948). Also, RGCs have been classified based on the spatial linearity of their receptive field response. “X-cells” exhibit linear responses, while “Y-cells” are non-linear (Enroth-Cugell & Robson, 1966). There also are classes of RGCs which encode direction of motion, edges and color.

On and Off RGCs exhibit different intrinsic mechanisms. Tonic excitatory input to On RGCs generate maintained spontaneous activity (action potentials), whereas spontaneous activity in Off RGCs is present without excitatory input, although it is modulated by input (Margolis & Detwiler, 2007). Consistent with this

view, Off RGCs exhibit other intrinsic properties similar to pacemaker neurons; sub-threshold oscillations, burst firing and rebound excitation, while On RGCs do not (Margolis & Detwiler, 2007). Differences in conductance may account for the difference in the spontaneous activity of On and Off RGCs. Specifically, Off and On RGCs exhibit different conductance of persistent Na^+ , hyperpolarization-activated K^+ and Na^+ channels, and low voltage activated Ca^{2+} currents (Kameneva et al., 2011). At this point nothing is known about the dependence of Bistratified RGCs on synaptic input for their spontaneous spiking activity or whether they are more similar to On or Off RGCs.

One morphological class of RGCs, the Alpha cell (referred to functionally as Y-cells), have large somas, thick axons and widely radiate dendrites. Functionally the Alpha RGCs have large concentric center-surround receptive fields. There are two subclasses of Alpha RGCs. On Alpha RGCs have dendrites that ramify in the On sublamina of the IPL and respond to light increments, while Off Alpha RGCs have dendrites that ramify in the Off sublamina of the IPL and respond to light decrements (Enroth-Cugell & Robson, 1966). In the mouse, Alpha-like cells also are called A-type RGCs. They have been divided into three subclasses. The Off morphology A-type RGCs can be divided into two functional groups: Off transient (Off-T) and Off sustained (Off-S). Off-T cells are quiet in darkness and exhibit transient spikes at a decrease in illumination, while Off-S cells exhibit spontaneous spikes in darkness and respond with a sustained response to a dark stimulus (Pang et al., 2003; Murphy & Rieke 2006). On A-type

RGCs respond with a sustained response (On-S) to an increase in illumination. On-S, Off-S, and Off-T light responses are generated by different mechanisms. On-S RGCs are driven by the modulation of tonic excitation through the On pathway. Off-S RGC light responses are driven by the modulation of direct glycinergic input from All ACs, either through the rod BC or On cone BC synapses (Van Wyk et al., 2009). Off-T RGCs have strong drive from both the On and Off pathways, while the On and Off sustained cells are driven mainly through the On pathway (Van Wyk et al., 2009).

Retinal Ganglion Cell Excitatory Receptors

The spontaneous EPSCs (sEPSCs) of RGCs are mediated by synaptically located glutamate receptors, while their light-evoked responses also recruit perisynaptic glutamate receptors (Sagdullaev et al., 2006). In mouse, On morphology RGC sEPSCs are mediated exclusively by AMPA receptors, while Off morphology RGC sEPSCs are mediated by both AMPA and NMDA receptors (Sagdullaev et al., 2006; Zhang & Diamond, 2009). Currently it is unknown what glutamate receptor(s) mediate sEPSCs in Bistratified RGCs in any species.

Receptive Field Organization

Most BC, ACs, and RGCs have concentric receptive field organization. Receptive field centers are excitatory in response to a stimulus and are encompassed by a larger, antagonistic surround (Kuffler, 1953; Rodieck & Stone, 1965a). The receptive field center correlates with the region of space where the

preferred stimulus will elicit an increased rate of firing with stimulation (Rodieck & Stone, 1965b). The receptive field surround correlates with the region of space where a stimulus larger than the receptive field center will decrease rate of firing (Rodieck & Stone, 1965b). As a larger region of the center is stimulated there is an increase in firing until the peak firing occurs and the entire center component is stimulated. Once the stimulus increases to include the surround, the center response will decrease as inhibition from the surround is recruited. The center excitation and surround inhibition are summed in a linear or non-linear fashion which generates spatial tuning (Rodieck & Stone, 1965a; Enroth-Cugell & Robson, 1966; Cook & McReynolds, 1998a).

Receptive fields are classified by their excitatory center response to light stimulation – On, Off, or On-Off (Hartline, 1948). On center cells have an Off antagonistic surround, and Off center cells have an On antagonistic surround. There are also more complex receptive fields such as direction selective receptive fields and, in primates, there are chromatically opponent center-surround receptive fields (Dacey & Packer, 2003; Wässle, 2004).

BCs exhibit a center-surround receptive field. Direct inputs from PRs contribute to the center response, while HCs feedback inhibition to the cones as well to BCs (Dowling, 1970; Fisher & Boycott, 1974; Kolb & Jones, 1984). The BC surround is thought to be passed along to the ACs although it is possible that AC-AC interactions also make a contribution. ACs modulate the BC and RGC surrounds via inhibitory synapses in the IPL.

Inhibitory Retinal Circuitry

Inhibition shapes retinal responses based on inhibitory neurotransmitter released, the characteristics of release (tonic or phasic), the type of postsynaptic receptors and network interactions that create different types of inhibition; feedforward, feedback, or serial (Eggers & Lukasiewicz, 2011). The inhibitory neurotransmitters of the retina are gamma amino butyric acid (GABA) and glycine.

Types of Inhibitory Circuitry

In feedforward inhibition, the presynaptic cell releases inhibitory neurotransmitter directly onto its postsynaptic partner. An example of feedforward inhibition occurs when an AC provides input to a postsynaptic receptor on a RGC (Figure 5B). In feedback inhibition, the presynaptic cell releases excitatory neurotransmitter directly onto its postsynaptic partner, which is an inhibitory neuron. The inhibitory neuron releases neurotransmitter back onto its presynaptic partner modulating its excitatory neurotransmitter release. The A17 AC/rod BC circuit is a classic example of feedback inhibition. Glutamate release from the rod BC axon terminals excite the A17 that releases GABA onto the rod BC and activates GABA_c receptors to reduce rod BC output (Figure 5A; Sagdullaev et al., 2006; Chavez et al., 2010).

In serial inhibition, the presynaptic cell releases inhibitory neurotransmitter onto its postsynaptic partner, which is an inhibitory neuron. The inhibitory neuron

then decreases its release of inhibitory neurotransmitter onto another postsynaptic cell. Therefore, serial inhibition from one cell acts to shape inhibitory inputs to cells downstream of its direct postsynaptic partner (Figure 5C). Serial inhibition is a mechanism of control for feedback and feedforward gain and regulation of temporal characteristics of inhibition (Zhang et al., 1997). Serial inhibition can also be a form of dis-inhibition if the connection involves an even number of synapses, which will result in a decrease of inhibition (inhibition of an inhibitory cell). Serial connections are important for spatial tuning (Eggers & Lukasiewicz, 2010). Crossover inhibition is the inhibition of one pathway via excitation of another parallel pathway (Figure 5D). Crossover inhibition works with excitation to linearize signaling in some pathways (Werblin, 2010). The most well studied form of crossover inhibition is the excitation of the All AC by the On pathway which leads to inhibition of the Off pathway (Manookin et al., 2008).

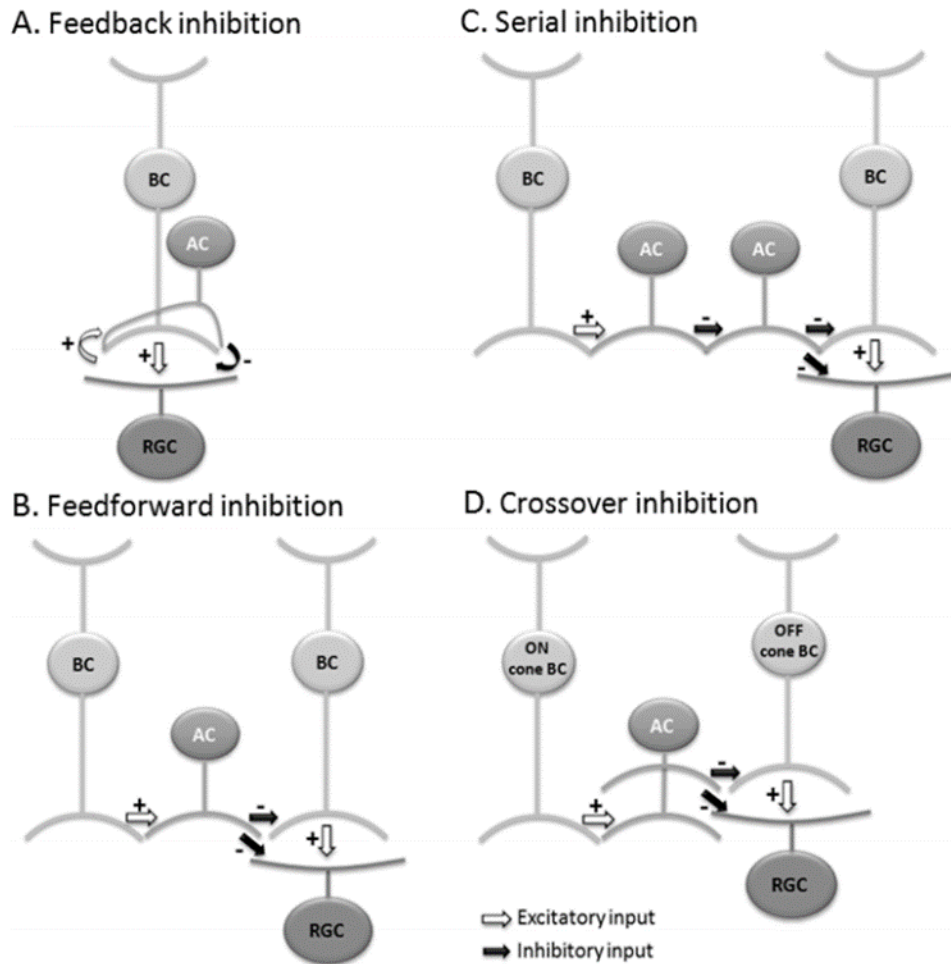


Figure 5. Four major types of inhibition. A. Feedback inhibition modulates the release of glutamate from BCs to RGCs. B. Feedforward inhibition provides direct inhibition to BCs or RGCs. C. Serial inhibition shapes other inhibitory inputs. D. Crossover inhibition enables reinforcement of signals by crosstalk between On and Off pathways.

GABAergic Inhibition

GABA is the major inhibitory neurotransmitter in the central nervous system. GABA is released by HCs and ACs (Wu, 1991; Marc et al., 1995). Mouse BC, AC, and RGC processes express GABA receptors (Zhang et al., 1997; Eggers & Lukasiewicz 2006a). Wide-field GABAergic ACs mediate large regions of surround inhibition and carry signals laterally within a single layer of the IPL (Pourcho & Goebel, 1983; Vaney, 1991). GABAergic inhibition has been shown to shape most aspects of visual signaling; for example GABAergic inhibition is important for spatial tuning (Cook & McReynolds, 1998; Eggers & Lukasiewicz, 2011) and temporal signaling (Dong & Werblin, 1998; Dong & Hare, 2003; Singer & Diamond, 2003; Chavez et al., 2006; Sagdullaev et al., 2006).

Both GABA_A and GABA_C receptors are ionotropic and permeable to chloride ions (Bormann & Feigenspan 1995). In the mouse retina, GABA_C receptors are only expressed on BCs (Feigenspan et al., 1993; Koulen et al., 1997; Eggers & Lukasiewicz, 2006; Sagdullaev et al., 2006). The GABA_C receptor appears to primarily mediate feedforward inhibition in the OPL and feedback inhibition in the IPL. Rod BC inhibition is mostly mediated by GABA_C receptors. On cone BC inhibition is mostly mediated by GABA_C receptors, but with a larger amount of GABA_A receptor contribution compared with rod BCs. Off cone BC inhibition is mediated by equal contributions of GABA_A and GABA_C receptors (Eggers et al., 2007).

GABA_A receptors are much more widespread and are expressed on HC, BCs, ACs, and RGCs (Tian et al., 1998; Feigenspan and Weiler, 2004; Eggers and Lukasiewicz, 2011). They are known to mediate feedforward, feedback, and serial inhibition. For example, BCs receive inhibition from ACs mediated by GABA_A receptors (Zhang et al., 1997; Eggers & Lukasiewicz 2006a; 2010). Serial inhibition limits direct GABAergic inhibition to BCs and affects the kinetics of transmission between BCs and RGCs (Zhang et al., 1997; Roska et al., 1998).

Glycinergic Inhibition

Glycine is present in 40-50% of ACs (Pourcho, 1996). Glycinergic ACs mediate excitation from BCs, AC, and RGCs in a narrow spatial field and transmit signals vertically between layers of the IPL (MacNeil & Masland, 1998; Menger et al., 1998). There are four types of glycine receptor subunits expressed in the retina. They are found on certain BC axons, ACs and RGC dendrites (Grunert & Wassle, 1993; Wassle et al., 2009). Half of all RGCs receive spontaneous inhibition via glycine receptors (Tian et al., 1998).

Consistent with their processes extending through the IPL sublamina, glycinergic ACs mediate crossover inhibition between On and Off layers of the IPL (Roska et al., 2006; Chavez & Diamond, 2008; Manookin et al., 2008; Molnar et al., 2009). For example, All ACs mediate glycinergic crossover inhibition, as they receive excitatory input from the On pathway and transmit inhibitory outputs to the Off pathway (Manookin et al., 2008). Off BCs receive the most glycinergic

input (Eggers et al., 2007), On BCs do not receive any light-evoked glycine input (Ivanova et al., 2006; Eggers et al., 2007), and rod BCs receive only a small amount of glycinergic inhibition (Eggers et al., 2007).

Circuits that challenge the dogma of separate parallel pathways

All Amacrine Cell

The All AC is one of the most widely studied ACs (Famiglietti & Kolb, 1974; Strettoi et al., 1992). As mentioned previously, the All is a glycinergic narrow-field bistratified AC that participates in crossover inhibition from the On pathway to the Off pathway (Manookin et al., 2008). In addition, the All AC provides crosstalk between the rod and cone pathways. This is evident as All ACs respond over a wider range of light levels than rods and rod BCs (Xin & Bloomfield, 1999; Pang et al., 2004), suggesting the All not only mediates rod signals but also cone signals (Pang et al., 2007). The All AC has been shown to transmit cone signals through On cone BC-All AC bidirectional electrical synapses (Strettoi et al., 1992; Veruki & Hartveit, 2002b; Pang et al., 2007). Thus, the All AC can integrate rod and cone signals, which provide a wide range of outputs to RGCs (Pang et al., 2003). Under photopic light conditions inputs from On cone BCs depolarize the All AC, which provides glycinergic inhibition to Off cone BCs and RGCs (Muller et al., 1988). In this way the Off pathway is inhibited not only under scotopic illumination but while cone signals dominate the All circuitry. Most recently the All AC-cone BC network has been the focus of

work exploring the network that generates rhythmic activity in the retina of mouse models of PR degeneration (Borowska et al., 2011).

Excitatory Crosstalk

Several publications have suggested the presence of masked responses of opposite polarity, e.g., On response from OFF morphology RGC or vice versa (Ariel & Daw, 1982; Nirenberg & Meister, 1997; Roska & Werblin, 2001; Renteria et al., 2006; Ackert et al., 2009). Although initially considered an artifact, further evidence challenged the dogma of On and Off pathway segregation. For example, over one-third of RGCs in the mouse and rabbit retina with On or Off responses also exhibit opposite polarity responses when GABAergic inhibition is blocked (Farajian et al., 2011). As further evidence for crosstalk between pathways, Off RGCs can alter their response sign to On-Off or On, in response to a change in size or intensity of light stimulus (Sagdullaev & McCall, 2005). The above circuits demonstrate crosstalk between pathways, which have been characteristically viewed as separate.

In addition, the All AC-On cone BC circuit has been implicated in the generation of rhythmic oscillations in all morphological classes of RGCs in the mouse models of retinitis pigmentosa, *rd1* and *rd10* (Margolis et al., 2008; Borowska et al., 2011; Stasheff et al., 2011; Trenholm et al., 2012). In *rd* PR degeneration eliminates visual signaling through the retina and alters the circuit such that either the network of All-On cone BC coupling or Alls alone drive

oscillations across all classes of RGCs. These oscillations are not found in the WT retina, because the PR input and interaction between retinal pathways maintain the absence of oscillations.

In conclusion, there is growing evidence which challenges the dogma of separate and parallel pathways. The current thought is that there are interactions between excitatory On and Off signals in the inner retina, but inhibitory synaptic circuitry masks crosstalk between pathways to maintain the fidelity of the receptive field center response and the dendritic lamination pattern.

On Bipolar Cells

On BCs consist of one morphological class of rod BC and five On cone BCs (Figure 6; Ghosh et al., 2004; Pignatelli & Strettoi, 2004). Different BC response kinetics have been correlated with morphological classes (Awatramani & Slaughter 2000; DeVries et al., 2000). Rod BC light responses have a robust sustained depolarization at light onset, followed by a small hyperpolarization at light offset (Euler & Masland, 2000). On cone BCs exhibit either transient or sustained On responses (Euler & Masland, 2000). Different temporal response properties are likely shaped by a varied distribution of inhibitory receptors with different subunit compositions on different BC types (Ivanova & Muller 2006; Eggers & Lukasiewicz, 2011). Different morphological types of BCs segregate specific aspects of the light signal in order to maintain parallel processing of visual information (Awatramani & Slaughter, 2000).

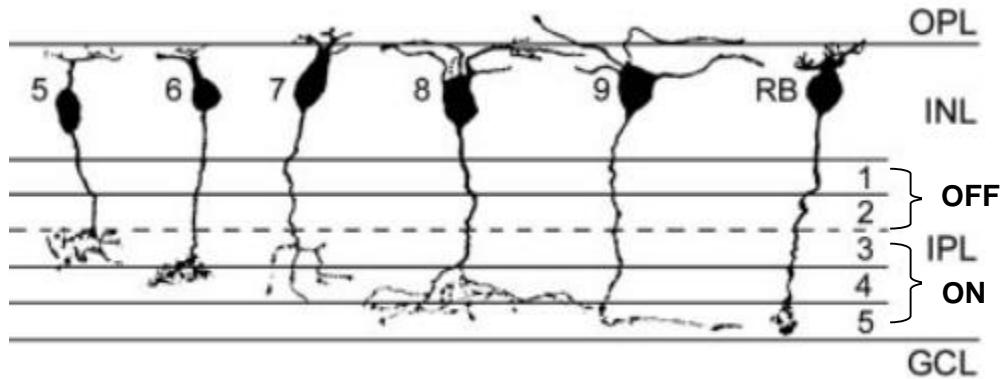


Figure 6. Morphological classes of On bipolar cells. Types 5-9 are On cone BCs. There is one type of rod BC. Modified from Ghosh et al., 2004.

The mGluR6 G-Protein Cascade and Its Associated Proteins mediate signaling in On BCs

Photoreceptors are continuously depolarized in the dark. Light produces a graded hyperpolarization whose amplitude and duration vary with light intensity. This translates into a graded decrease in glutamate release (Trifonov, 1968). At light onset, the depolarization in On BCs results from a mGluR6 mediated mechanism. At light offset (in the dark), glutamate is bound to the mGluR6 receptor and a sequence of cascade events occur which culminate in the opening of the TRPM1 channel and depolarization of the On BC. The On BC response cascade is described in detail below in Figure 7.

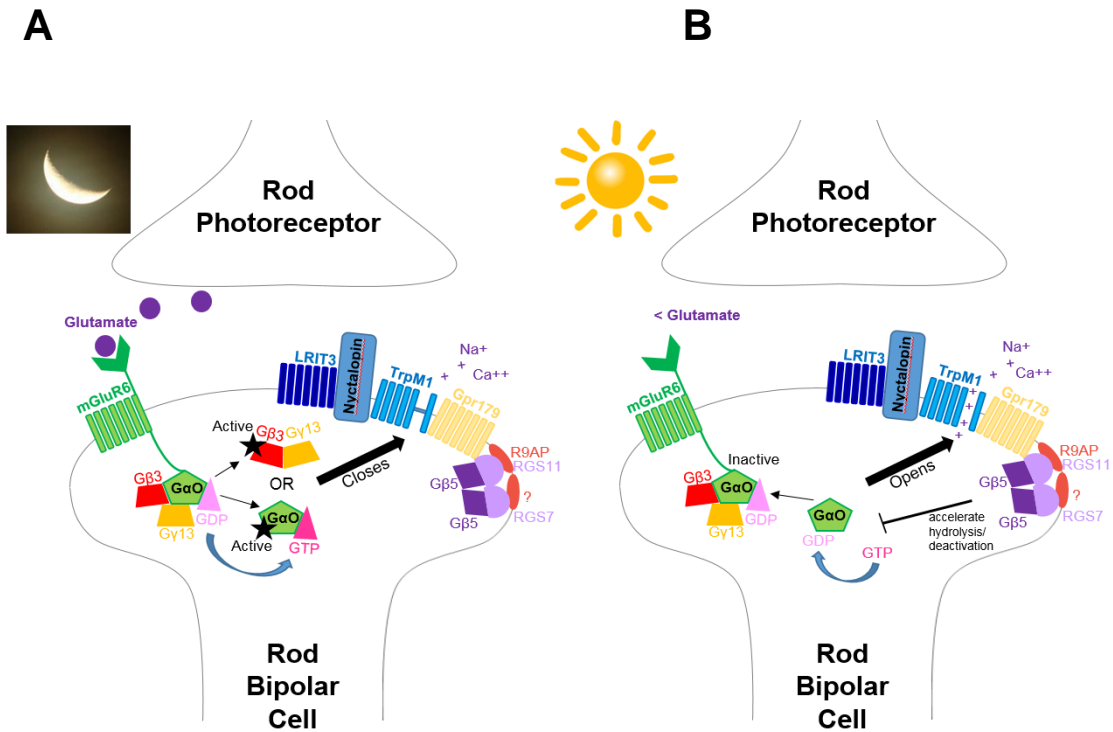


Figure 7. On BC response. A. In the dark glutamate is released from rods and binds mGluR6. mGluR6 activates a trimeric G-protein complex, G_0 (Vardi et al., 1993; Nawy 1999; Dhingra et al., 2000). The trimeric G-proteins are activated when GDP is exchanged for GTP on $G\alpha_0$, which dissociates into $G\alpha_0$ -GTP (Vardi et al., 1993; Nawy 1999; Dhingra et al., 2000) and the dimer $G\beta_3$ / $G\gamma_{13}$ (Dhingra et al., 2012; Huang et al., 2003). The activated G-protein complex leads to the closure of the non-selective cation channel, TRPM1, and relative hyperpolarization of the rod BC, either through interaction with $G\alpha_0$ -GTP and/or $G\beta_3$ / $G\gamma_{13}$ or another intermediate effector not yet identified. B. In the light glutamate release is decreased and no longer binds mGluR6. Hydrolysis of GTP into guanine dinucleotide (GDP) forms the inactive state of $G\alpha_0$ ($G\alpha_0$ -GDP; Hooks et al., 2003) which recombines with $G\beta_3$ and $G\gamma_{13}$ to form the trimeric G-

protein complex. RGS7 and RGS11, regulator of G-protein signaling (RGS) proteins (Cao et al., 2012; Shim et al., 2012), form heterodimers with G β 5 (Rao et al., 2007). These heterodimers are GTPase-activating protein (GAP) complexes, which accelerate the hydrolysis of GTP to GDP by G α_0 , (Hooks et al., 2003; Rao et al., 2007), resulting in accelerated deactivation of the G-protein and culminates in the opening of TRPM1 and depolarization of the BC (Audo et al., 2009; Li et al., 2009; Morgans et al., 2009, 2010; Shen et al., 2009; Koike et al., 2010; Peachey et al., 2012a). R9AP is a membrane anchor protein for RGS11 and critical for its proper localization in the membrane at the dendritic tips (Jeffrey et al., 2010); nyctalopin, a leucine-rich repeat protein is critical for proper trafficking or localization of TRPM1 (Gregg et al., 2003; Pearing et al., 2011); GPR179 is required for proper dendritic tip localization of RGS7 and RGS11 (Orlandi et al., 2012) and LRIT3 is critical for rod BC light-mediated response (Zeitz et al., 2013; Neuille et al., 2014).

mGluR6 Receptor

mGluR6 (Nakajima et al., 1993; Nomura et al., 1994) is one of several metabotropic receptors that have a G-protein coupled cascade and utilize second messengers to produce cell responses. Three classes of mGluRs are defined on the basis of amino acid sequence, transduction mechanisms, and pharmacological sensitivity. Group I receptors, mGluR1 and mGluR5, are coupled to the stimulation of phospholipase C, while Groups II, mGluR2 and 3, and Group III, mGluR4, 6, 7, and 8 are coupled to the inhibition of the cyclic

adenosine monophosphate (cAMP) cascade. Group III receptors are distinct due to their sensitivity to 2-Amino-4-Phosphonobutyric Acid (APB; Slaughter & Miller 1981; Quraishi et al., 2007). All mGluRs contain a large (500-600 residues) N-terminal extracellular domain, which contains the glutamate binding site that is linked to a G-protein coupled receptor seven-transmembrane domain that mediates G-protein activation (Bhave et al., 2003; Pin et al., 2003). mGluRs likely form dimers (Pin & Acher, 2002). mGluRs are bi-lobed with a large cleft between the lobes in the absence of a ligand. The glutamate binding mechanism is called the “Venus flytrap” module as the ligand binding changes the protein conformation with the ligand trapped between the two lobes, similar to a Venus flytrap’s mechanism to trap insects (Pin & Acher, 2002). Slaughter and Miller (1981) discovered that APB selectively blocked the On pathway in the retina, while the Off pathway remained intact at the BC level.

TRPM1 Channel

TRPM1, also known as Melastatin 1, is a member of the transient receptor potential (TRP) channel family and consists of six transmembrane domains (Koike et al., 2010). The TRPM1 channel mediates the non-selective cation current that depolarizes On BCs (Bellone et al., 2008; Morgans et al., 2009; Shen et al., 2009; Koike et al, 2010). The activation/inactivation of the trimeric G-protein G_o is linked to the opening/closing of the TRPM1 channel (Vardi 1998; Nawy 1999; Dhingra et al., 2002), but the mechanism remains undetermined,

although two possible candidates are G_oα (Dhingra et al., 2000) and G_γ13/G_β3 (Dhingra et al., 2012).

Nyctalopin

Nyctalopin is a member of the small leucine-rich repeat family (LRR) of proteins. LRR proteins facilitate protein-protein interactions and are involved in signal transduction, cellular trafficking, cell adhesion, and tissue organization (Poopalasundaram et al., 2005). Nyctalopin interacts with TRPM1 and plays a critical role in its localization to the On BC dendritic tips (Pearing et al., 2011). The exact role of nyctalopin in the mGluR6 cascade or the assembly of the entire signaling complex remains unknown (Pearing et al., 2011).

GPR179

Like mGluR6, the G-protein coupled receptor 179 (GPR179) is a seven transmembrane G-protein coupled receptor. GPR179 also is localized to the dendritic tips of the On BCs in the mouse retina (Peachey et al., 2012b), where it co-localizes with mGluR6 and TRPM1.

LRIT3

The recently identified gene, *LRIT3*, encodes another LRR protein, with immunoglobulin-like, and transmembrane-domain 3 moieties (Zeitz et al., 2013). The loss of LRIT3 protein causes the loss of nyctalopin and TRPM1 channels from the dendritic tips of rod BCs.

On BC Mutations Result in No b-wave ERG Phenotype

mGluR6

GRM6 is the gene that encodes the mGluR6 receptor. The *mGluR6*^{-/-} mouse exhibits a no b-wave ERG phenotype (Masu et al., 1995; Figure 8) and therefore lacks proper function of On BCs. The *mGluR6*^{-/-} mouse does not differ from WT in a shuttle box avoidance task, which demonstrates a level of visual signal preservation (at dim illumination of 1.2 cd/m²; Masu et al., 1995). The *mGluR6*^{-/-} mouse Superior Colliculus exhibits delayed On responses (dOn; Masu et al., 1995; Sugihara et al., 1997). The *mGluR6*^{-/-} mouse exhibits a decrease in the percent of cells with On responses in the visual cortex (WT= 100%, *mGluR6*^{-/-} = 79%) and RGCs (WT = 79%, *mGluR6*^{-/-} = 43%) compared to WT (Renteria et al., 2006). In addition, only Off and dOn responses were found in the visual cortex and RGCs (Renteria et al., 2006).

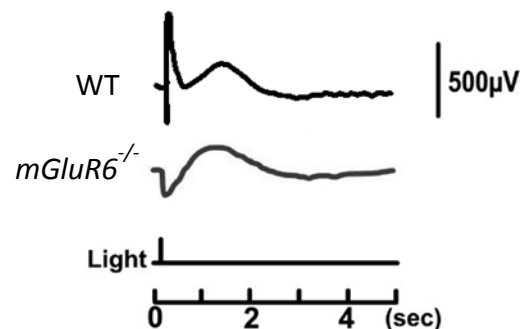


Figure 8. Electroretinogram from WT and *mGluR6*^{-/-} mouse. The positive going b-wave is absent in the *mGluR6*^{-/-} mouse. All nob mutants exhibit a no b-wave phenotype. Modified from Masu et al., 1995.

In the WT mouse retina, a dOn response, similar to that found in the *mGluR6*^{-/-}, can be unmasked by block of the On pathway with the mGluR6 agonist APB (Renteria et al., 2006). The abnormal On response is likely produced by the Off pathway (Renteria et al., 2006; Farajian et al., 2011). As described earlier, the On pathway has inhibitory input to the Off pathway (Cohen, 1998; Zaghloul et al., 2003). Under normal conditions, the dOn response from the Off Pathway would be suppressed by inhibitory ACs driven by the On pathway (Renteria et al., 2006). In WT retina the normal interaction between On and Off pathways results in correctly timed responses to the onset and offset of a stimulus (Renteria et al., 2006).

TRPM1

A TRPM1 mutation was first identified in the Appaloosa horse (Bellone et al., 2008). Mutations in TRPM1 result in a no b-wave ERG in both animal models and humans. Human individuals with TRPM1 mutations have 15 Hz flicker cone ERGs but no response through the primary rod pathway (van Genderen et al., 2009). In *Trpm1*^{-/-} mice optokinetic responses, used to measure spatial frequency and contrast sensitivity thresholds, reveal a 10% reduction of spatial frequency threshold, as well as a three-fold decrease in contrast sensitivity compared to WT (Morgans et al., 2009).

Trpm1^{-/-} rod BCs lack a response to exogenous application of the mGluR6 antagonists CPPG (Morgans et al., 2009) or LY341495 (Pearing et al., 2011). All

WT On cone BCs respond with sustained currents to CPPG (Morgans et al., 2009), while half of *Trpm1*^{-/-} On cone BCs exhibit no response. Unexpectedly, the remaining *Trpm1*^{-/-} On cone BCs exhibit a small transient current (Figure 9; Morgans et al., 2009). This suggests that a subset of On cone BCs possess additional receptors/channels that are modulated by CPPG.

In contrast to Morgans et al., (2009), Koike et al. (2010) measured *Trpm1*^{-/-} On BC light responses instead of pharmacologically-stimulated responses. Koike et al. found that neither *Trpm1*^{-/-} rod BCs nor On cone BCs exhibited light-evoked responses (Figure 10; 2010). Also, in the dark, *Trpm1*^{-/-} On BC membrane current fluctuations are smaller than in WT, which suggests no functional transduction channel in the *Trpm1*^{-/-} mice (Koike et al., 2010). As Koike et al. (2010) explained, the conflicting results with Morgans et al. (2009) may be explained by Morgans et al.'s use of pharmacological stimulation, as L-AP4 also affects cone PRs and there is no conclusive evidence that CPPG affects only On BCs in the retina (Hosoi et al., 2005) or that the mGluR6/TRPM1 cascade is the only effector of CPPG in On BCs. Ray et al. (2014) also reported a residual current in *Trpm1*^{-/-} rod BCs that is not mediated by capsaicin, a non-selective TRP channel agonist, providing further evidence of a small unidentified current in rod BCs. Thus, light stimulation versus pharmacological stimulation may yield different results.

Capsaicin gates TRPM1 in rod BCs (Shen et al., 2009). *Trpm1*^{-/-} rod BCs do not respond to capsaicin (Pearing et al., 2011), however, small capsaicin-

activated current is present in at least some *Trpm1*^{-/-} On BCs (Morgans et al., 2009). Morgans et al. (2009) speculated that in addition to TRPM1, there is another type of channel which is sensitive to capsaicin. Therefore, it is possible that capsaicin does not act on the TRPM1 channel in isolation in rod or On cone BCs.

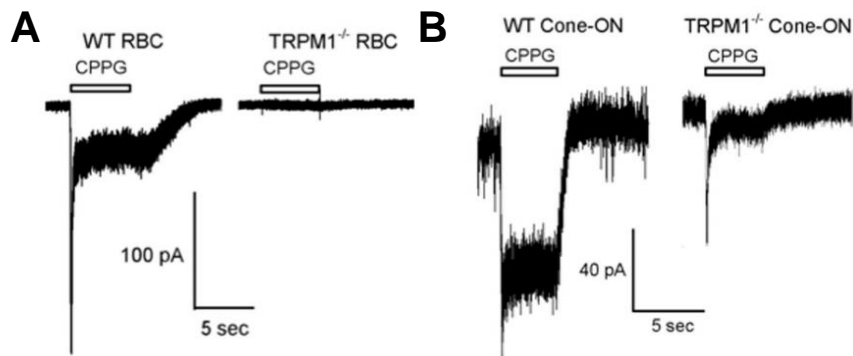


Figure 9. WT and *Trpm1*^{-/-} BC pharmacological responses. A. WT rod BCs respond to CPPG and *Trpm1*^{-/-} rod BCs do not. B. WT On cone BCs respond to CPPG and a population of *Trpm1*^{-/-} On cone BCs maintain a small transient response. From Morgans et al., 2009.

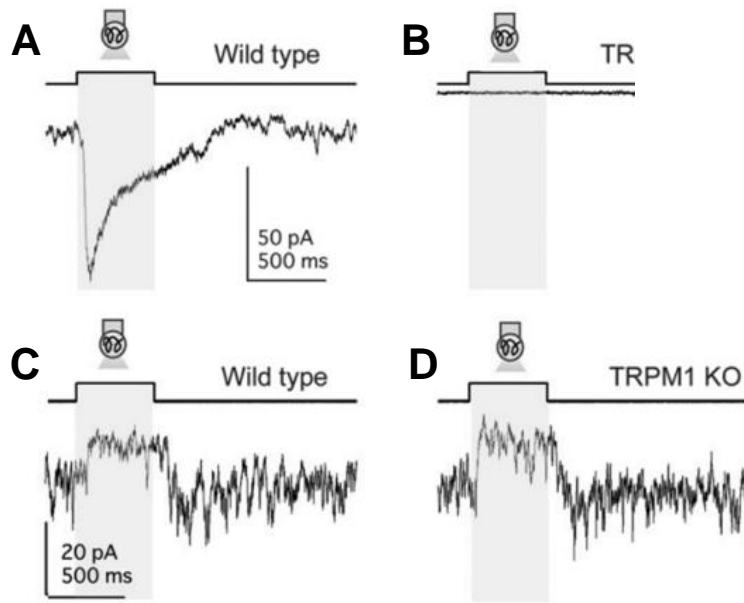


Figure 10. WT and *Trpm1*^{-/-} BC light responses. A. WT On BC response to light
 B. *Trpm1*^{-/-} On BCs are non-responsive to light. C. WT Off BC response to light.
 D. *Trpm1*^{-/-} Off BCs maintain outward current in response to light. From Koike et al., 2010.

Nyctalopin

The *Nyx^{nob}* mouse, a mouse with a mutation in the nyctalopin gene, was the first no b-wave ERG animal mutant to be identified (Pardue et al., 1998). An active avoidance behavioral paradigm demonstrated that *Nyx^{nob}* mice have decreased sensitivity to light (Gregg et al., 2003). *Nyx^{nob}* RGCs exhibit abnormal

periodic bursting that arises around postnatal day (P) 15, after a period of relatively normal development, as well as persistence of waves past normal developmental stages (Demas et al., 2006). *Nyx^{nob}* RGCs have a common fundamental frequency of bursting activity (3-5 Hz; Demas et al., 2006), although the cells do not burst in unison. Due to abnormal spontaneous activity of RGCs, the *Nyx^{nob}* dorsal lateral geniculate nucleus exhibits desegregation of RGC axons in mice up to age P22 (Demas et al., 2006). *Nyx^{nob}* On BCs do not respond to exogenous glutamate puffs (Gregg et al., 2007), the mGluR6 antagonist LY341495, or to the TRP agonist capsaicin (Pearing et al., 2011). The TRPM1 channel is absent in *Nyx^{nob}* On BC dendritic tips (Gregg et al. 2007; Pearing et al., 2011).

Gpr179

The *Gpr179^{nob5}* mouse has a severely decreased ERG b-wave amplitude (Ray et al., 2014). When GPR179 is absent, expression of two regulator of G-protein signaling (RGS) proteins, RGS7 and RGS11, which accelerate the opening of the TRPM1 channel, also are absent in rod BC dendritic tips (Orlandi et al., 2012). My experiments further examine the role of GPR179 in Chapter V.

LRIT3

The *Lrit3^{-/-}* mouse has a no b-wave ERG phenotype (Neuille et al., 2014; McCall/Gregg lab, unpublished observation), similar to a certain population of

human patients diagnosed with cCSNB (Zeitig et al., 2013). My experiments in Chapter VI will help elucidate the role of LRIT3 in rod BC signaling.

Phenotypic differences across no b-wave mutants

When no b-wave mutants are compared, some unexpected differences in RGC functional responses have been observed (Pinto et al., 2007; Maddox et al., 2008). Two variants of the mGluR6 gene (*mGluR6^{nob3}* and *mGluR6^{nob4}*) result in different distributions of RGC functional classes, which are defined by the RGC response to light stimuli (Pinto et al., 2007; Maddox et al., 2008). There are also significant differences in *mGluR6^{nob3}* and *mGluR6^{-/-}* in regards to their excitatory and inhibitory input to RGCs (Heath, unpublished data). In addition, *Nyx^{nob}*, *Trpm1^{-/-}* and *Lrit3^{-/-}* generate rhythmic bursting activity (Demas et al., 2006; McCall lab observation), while *mGluR6^{-/-}* does not exhibit this phenotype (Renteria et al., 2006).

CHAPTER II

GENERAL MATERIALS AND METHODS

Animals

In experiments that examined BC function, three-to-six week old male and female mice of various genotypes were used. In experiments that examined RGC function, two to six month old male and female mice were used. The genotypes of all mice used are shown in Table 1.

All mice were housed in a 12h/12h light/dark cycle. Animals had access to food and water *ad libitum*. All procedures were performed in accordance with the ARVO Statement for the Use of Animals in Ophthalmic and Vision Research and approved by the University of Louisville Institutional Animal Care and Use Committee.

Mouse line	Publication	Source	Source No. (if available)
wild type C57BL/6J		Jackson Labs (ME, USA)	664 (Jax)
<i>mGluR6</i> ^{-/-}	Masu et al., 1995	gift from David Copenhagen	NA
<i>Nyx</i> ^{nob}	Pardue et al., 1998	gift from Neal Peachey (spontaneous BALBc/ByJ line mutant)	NA
<i>Gpr179</i> ^{nob5}	Peachey et al., 2012	gift from Gianluca Tosini (spontaneous C3H line mutant)	NA
<i>Trpm1</i> ^{-/-} (<i>Trpm1</i> ^{tm1Lex})	Shen et al., 2009	generated by Lexicon Genetics; obtained from the European Mouse Mutant Archive	NA
<i>Lrit3</i> ^{-/-} (<i>Lrit3</i> ^{emRgg1})	Heath et al., in preparation	created by Ron Gregg	NA

Table 1. All of the mouse lines used in the following experiments.

Dark and Light Adaptation

When mice were used in dark-adapted experiments, they were placed in their home cage overnight in a completely dark room. Using a dim red light, the mice were anesthetized in the dark room. When mice were used in light-adapted experiments, they were kept in their home cage under normal room illumination and were anesthetized under normal room light.

General Preparation for Retinal Recordings

Mice were anesthetized with an intraperitoneal injection of xylazine/ketamine (127 and 12 mg/kg concentration, respectively) diluted in Ringer's solution. Once the animal was deeply anesthetized, a cervical dislocation was performed and the eyes enucleated. For dark-adapted experiments the eyes were enucleated under dim red light and dissected under infrared (IR) illumination to prevent bleaching the photoreceptors. In light-adapted experiments, the eyes were enucleated under normal room light and dissected under dim light. Oxygenated (95/5%-oxygen/carbon dioxide) Ames medium (Sigma-Aldrich) with 1.9g/l sodium bicarbonate buffer was used as the extracellular solution for BC experiments. Oxygenated (95/5%-oxygen/carbon dioxide) bicarbonate buffered Ringer's solution (containing in mM: 125 NaCl, 2.5 KCl, 1 MgCl₂, 1.25 NaH₂PO₄, 20 glucose, 26 NaHCO₃ and 2 CaCl₂, at pH 7.2) was used as the extracellular solution for RGC experiments. The cornea and lens

were removed. The retina was separated from the sclera and the vitreous was manually removed from the retina with forceps.

Retinal Slice Preparation for BC Recordings

The dissected whole mount retina was placed onto nitrocellulose paper (Millipore) photoreceptor side up, which was adhered to a cover slip with vacuum grease. The tissue and paper were placed into a custom made tissue slicer and 150 μm sections were cut using a razor blade. Each slice was oriented perpendicular to the cutting plane so that each retinal layer was visible and its position was stabilized between two vacuum grease tracks. Retinal slices were stored in a dark oxygenated bath chamber until needed.

Retinal Whole Mount Preparation for RGC Recordings

Retinas were dissected under IR illumination in order to preserve photoreceptor driven responses to light stimuli. The whole mount retina was cut into four quarters and placed on a cover slip. Stainless steel harps lined with nylon stabilized the retina against the cover slip. Only one RGC was recorded from each quarter to prevent the loss of light-evoked responses in subsequent RGCs resulting from bleaching of the photoreceptors. Retinal quarters were stored in a dark oxygenated bath chamber until needed.

BC and RGC Whole Cell Patch Clamp Recording

The extracellular solution in the recording chamber was maintained at 34-35 °C. For BC experiments dark and light-adapted conditions were used. For light-adapted preparations the recorded retinal slice was exposed to light throughout the preparation and recording. For the dark-adapted preparations the retinal slice was illuminated by IR and viewed by an IR camera. For all RGC experiments, the IR camera was used to visualize the retinal tissue for recording. The BC soma was targeted in retinal slices. A blunt pipette was used to scrape off a small portion of inner limiting membrane to expose the targeted RGC soma in retinal whole mounts.

Recording electrodes were pulled from borosilicate glass (FHC, Inc., Bowdoin, ME) on a P-97 Flaming/Brown Micropipette Puller (Sutter Instruments Co., Novato, CA). For BC recordings, glass electrodes were filled with an intracellular solution of either K-gluconate (containing in mM: 120 K-gluconate, 1 CaCl₂, 1 MgCl₂, 10 Na-HEPES, 11 EGTA, 4 ATP, 1 GTP and 1% sulforhodamine) to maintain normal ion concentrations within the cell or Cs-gluconate-TEA (containing in mM: 20 CsCl, 107 CsOH, 107 D-Gluconic Acid, 10 Na⁺ HEPES, 10 BAPTA, 10 TEA and 1% sulforhodamine) to block potassium currents in the cell. For RGC recordings, K-gluconate with 1% lucifer yellow instead of sulforhodamine was used.

For BC recordings, electrodes with resistance between 6-9 M Ω were used. For RGC recordings, electrodes with resistance between 3-6 M Ω were used. As the pipette was lowered into the chamber holding the tissue, positive pressure was applied in order to keep the electrode tip clear of debris. The electrode was lowered to the retina and toward the cell until the electrode created a visible dimple in its soma. The positive pressure was released and slight suction applied. This created a G Ω seal between the electrode and BC or RGC (~2-4 or 1 G Ω , respectively). Suction was reapplied to break into the cell membrane. BCs were recorded if their input resistance was ~1 G Ω and access resistance <25 M Ω . RGCs were recorded if their input resistance was <100 M Ω . BC and RGC current and voltage responses were recorded via a Multiclamp 700A amplifier with a Digidata 1440A digitizer (MDS Analytical Technologies, Union City, CA) and filtered at 2.4 kHz with a four-pole Bessel low pass filter, sampled at 10 kHz. Clampex 10.2 software was used to generate command outputs, trigger the light stimulus and acquire and analyze analog whole cell voltage and current.

Light Stimulus

RGC light-evoked responses were elicited by full-field application of white light from a light emitting diode with the intensity of 2140 cd/m².

Morphological Identification of BCs

In the retinal slice, rod BC somas were identified and targeted for recording based on size, shape, and location of their somas in the INL (Ghosh et al., 2004). To verify their morphology, BCs were filled with intracellular solution containing 1% sulforhodamine, a red fluorescent dye. Their morphology was verified by fluorescence microscopy, and cells divided into rod, On cone, or Off cone BCs (Ghosh et al., 2004). Rod BC somas are found at the top of the INL and their axon terminals have very distinct lobular terminals that ramify within the deepest layer of the IPL. On and Off cone BC somas were found in the middle/upper-middle INL while On cone axon terminals ramify within the lower half of the IPL closest to the RGC layer and Off BCs axon terminals ramify within the upper half of the IPL.

Morphological Identification of Recorded RGCs by

Immunohistochemistry

In retinal whole mount recordings, RGCs were filled with intracellular solution containing 1% Lucifer Yellow, a fluorescent dye. At the end of each recording, the retinal whole mount quarter containing the characterized RGC was fixed in 4% paraformaldehyde in phosphate buffer (pH 7.4) (30 min), rinsed in 0.1 M phosphate buffered saline (PBS, 3X; 20 min) and stored at 4°C. The tissue was incubated in PBS with 0.5% triton-X (PBX) for 1hr, followed by blocking in 5% normal donkey serum in PBX for 1hr. Retinas were reacted with anti-lucifer

yellow antibody (rabbit, 1:1000, Molecular Probes, Eugene, OR) overnight. Tissue was washed in PBS (3X; 5-10 min), incubated in 5% normal donkey serum in PBX for 1hr, and then incubated in Alexa Fluor 488 secondary antibody (donkey anti-rabbit, 1:1000, Molecular Probes, Eugene, OR) in 5% normal donkey serum overnight at 4°C. Retinas were then washed in PBS (3X) and incubated in TO-PRO-3, a nuclear stain, (1:1000 in PBS, Molecular Probes, Eugene, OR) for 20 min. Finally, retinas were washed in PBS twice, mounted in Gelmount, cover-slipped and imaged on an Olympus FV300 confocal microscope. Confocal stacks were taken at 0.4 micron intervals.

The dendritic arbor of each RGC was reconstructed using FluoView 4.0 software (Olympus, Center Valley, PA). The stratification pattern within the IPL was determined by rotating the image stack 90° and the lamination of the RGC dendrites relative to the TO-PRO-3 stain of the INL and ganglion cell layer were compared. RGCs with dendrites that stratified in the On sublamina (the three sub-layers of the IPL located most closely to the ganglion cell layer) were defined as On morphology, dendrites in Off sublamina (the two sub-layers of the IPL located most closely to the INL) were defined as Off morphology and those with dendrites in both sublamina were defined as Bistratified.

Analysis and Statistics

Clampfit 10.2 software was used to measure BC and RGC responses in offline analysis. Prism 5.04 software (Graphpad Software, Inc., La Jolla, CA) was

used for statistical analyses. A D'Agostino and Pearson omnibus test was used to determine if data were derived from a normal distribution. For data with a normal distribution a two-tailed Student's t-test, one-way ANOVA with Bonferroni post hoc, or two-way ANOVA with Bonferroni post hoc were used to determine statistically significant differences. For data with a non-normal distribution a Mann-Whitney or Kruskal-Wallis with Dunns post-hoc were used to determine statistically significant differences. Significance was defined as $P < 0.05$. The post hoc P value is reported in the text. All data were reported as mean \pm standard error of the mean.

CHAPTER III

COMPARISON OF *Nyx^{nob}* AND *mGluR6^{-/-}* RGCS

Introduction

Spontaneous bursts of action potentials that propagate across the retina (retinal waves) are a part of normal retinal development (Meister et al., 1991; Wong et al., 1993; Wong & Oakley, 1996). In the mouse retina, these waves occur prior to PR differentiation, expression of rhodopsin and thus, before the onset of visual signaling (Galli & Maffei, 1988; Shatz et al., 1988; Wong et al., 1993). Retinal waves are critical for segregation of ON-OFF RGC axon terminals as well as the formation and maintenance of eye-specific regions in the dorsal lateral geniculate nucleus (dLGN; Wong & Oakley, 1996; Eglén, 1999; Demas et al., 2003). In normal mouse retina, three wave phases have been defined by the neurotransmitter source of the activity: stage I (E16 to P0): acetylcholinergic, mediated by nicotinic acetylcholine receptors in combination with a non-nicotinic receptor mechanism, which may be either gap junction or neurotransmitter mediated (Bansal et al., 2000; Catsica et al., 1998), stage II (0 to P11): acetylcholinergic, mediated by nicotinic acetylcholine receptors (Bansal et al., 2000), stage III (P11 to P14): glutamatergic, mediated by ionotropic glutamate

receptors (Bansal et al., 2000; Wong, 1999; Torborg & Feller, 2005). Stage III glutamatergic waves end shortly after eye-opening, at about the time that the retina becomes responsive to light (Demas et al., 2003).

Complete congenital stationary night-blindness (cCSNB) is a disease of heterogeneous etiology. Most patients and animal models of cCSNB have been identified in screens of retinal function using the ERG. The cCSNB ERG has a normal a-wave, which indicates intact photoreceptor function but lacks a b-wave, reflecting a lack of signaling in On BCs. The nyctalopin mutant (*Nyx^{nob}*) and metabotropic glutamate receptor 6 knockout (*mGluR6^{-/-}*) mice have similar no b-wave ERG phenotypes (Masu et al., 1995; Pardue et al., 1998) and are models of cCSNB.

During development, *Nyx^{nob}* retinas exhibit normal stage I and II waves, but stage III glutamatergic waves persist through at least early adulthood (P28; Demas et al., 2006). These abnormal waves increase in frequency and by P28 transition into high frequency rhythmic action potentials (Demas et al., 2006). Approximately 80% of *Nyx^{nob}* RGCs develop abnormal rhythmic spontaneous bursts when recorded *in vitro* and their fundamental frequency is between 3-5 Hz at P28 (Demas et al., 2006). The extended period of glutamatergic waves and/or the rhythmic bursting of the RGCs are correlated with desegregation of eye-specific RGC axon projections in the *Nyx^{nob}* dLGN (Demas et al., 2006). Waves in *mGluR6^{-/-}* or other cCSNB mouse models have not been examined, and the question remains whether their waves persist.

A rhythmic component in the spontaneous spiking activity of RGCs also has been reported in two mouse models of retinitis pigmentosa, *rd1* and *rd10*, where rods and then cone photoreceptors degenerate (Blanks et al., 1974; Carter-Dawson et al., 1978; Marc et al., 2007; Ye & Goo 2007 (*rd1*); Margolis et al., 2008 (*rd1*); Stasheff, 2008 (*rd1*); Borowska et al., 2011(*rd1*); Stasheff et al., 2011 (*rd1* & *rd10*); Menzler & Zeck, 2011 (*rd1*); Trenholm et al., 2012 (*rd1*); Menzler et al., 2014 (*rd1* & *rd10*)). In the *rd* retina, two mechanisms have been proposed to account for the oscillations: 1) The network of gap junction-coupled All ACs and On cone BCs are the synaptic drive which underlies the RGC bursting (Borowska et al., 2011; Menzler & Zeck, 2011; Trenholm et al., 2012) and 2) Oscillations in the *rd1* retina reflect intrinsic bursting of Alls that are directly relayed to the RGCs rather than emerging from the gap-junction-coupled network (Choi et al., 2014). This intrinsic rhythmic property of All ACs is unmasked by hyperpolarization of *rd1* All ACs when synaptic input is reduced due to photoreceptor degeneration (Choi et al., 2014).

There are differences between *rd* and cCSNB animal models and the oscillations in their RGCs: *rd* RGCs are reported to oscillate at ~10 Hz (Yee & Goo, 2007; Borowska et al., 2011(*rd1*)), ~6.8 Hz (Yee et al., 2012 (*rd1*)) or ~3-12 Hz (Toychiev et al., 2013 (*rd10*)), while *Nyx^{nob}* RGCs oscillate at ~3-5 Hz (Demas et al., 2006). Approximately half of all *rd* RGC morphological classes oscillate (Borowska et al., 2011), while almost all *Nyx^{nob}* RGCs oscillate (Demas et al., 2006). In cCSNB, the rod and On cone BCs never respond to glutamate (Gregg

et al., 2007) or light stimulation (Xu et al., 2011) regardless of whether they are recorded *in vivo*, *in vitro*, as spiking or membrane potentials, while their Off cone BCs have normal glutamate responses (Gregg et al., 2007). In *rd*, signaling is present early in postnatal development, then rod followed by cone PRs degenerate, which alters the ability of all RGCs to respond to light. However, at an early stage of degeneration in *rd1* mouse ON responses diminish before OFF responses (Stasheff, 2008). While there are differences between these two disease models, it is possible they share similar underlying mechanisms, which result in RGC oscillations.

In WT retina, although a small proportion of RGCs show some high frequency rhythmicity (Freeman et al., 2008), most RGCs exhibit spontaneous spiking activity with no temporal correlation. A correlation of RGC class with the presence of rhythmicity has not been reported (Freeman et al., 2008). The spontaneous activity of WT ON-sustained RGCs require excitatory synaptic input, whereas spontaneous activity of WT OFF-sustained and transient RGCs are set intrinsically and modulated by synaptic input (Margolis & Detwiler, 2007). Bistratified RGCs spontaneous activity has not been examined, but is likely to at least reflect excitatory input from the On pathway.

Like the *Nyx^{nob}* mouse, the *mGluR6^{-/-}* mouse lacks signaling through On BCs and thus through the On retinal pathway. Even so, delayed ON (dON) responses (responses whose onset is ≥ 400 msec) have been documented in the RGCs (Renteria et al., 2006) and superior colliculus (Sugihara et al., 1997) of the

mGluR6^{-/-} mouse. dON and dON/OFF responses also are found in *Nyx^{nob}* RGCs along with OFF responses (McCall lab, unpublished observation). In contrast, WT RGCs do not exhibit dON responses, although they can be induced in OFF-center RGCs (Renteria et al., 2006) or RGCs with OFF morphology (Farajian et al., 2011) when the ON pathway is blocked with APB or when GABAergic inhibition is blocked (Renteria et al., 2006; Farajian et al., 2011). Furthermore, under these pharmacological manipulations, over one-third of WT OFF morphology RGCs exhibit these masked ON responses (Farajian et al., 2011). This result demonstrates that ON responses are generated by or carried through the OFF pathway and are normally masked by crossover inhibition initiated in the ON pathway (Renteria et al., 2006; Farajian et al., 2011).

Using extracellular recordings, all *mGluR6*^{-/-} (Renteria et al., 2006) and *Nyx^{nob}* RGCs show spontaneous spiking, but only *Nyx^{nob}* RGCs have been reported to spike rhythmically (Demas et al., 2006). Rhythmicity is not an artifact induced by recording *in vitro*, as extracellular *in vivo* recordings from single *Nyx^{nob}* RGC axons in the optic nerve also show similar rhythmic spiking (3-5 Hz; Demas et al., 2006). Using a whole cell patch clamp approach, I found that most *Nyx^{nob}* RGCs have rhythmic membrane oscillations (96%) and many of these RGCs spike rhythmically (61%). In contrast, many *mGluR6*^{-/-} RGCs (40%) have rhythmic membrane oscillations but few have rhythmic spiking (12.5%). This dichotomy in *Nyx^{nob}* and *mGluR6*^{-/-} RGCs rhythmic spiking is unexpected, since the retinas of both mutants show no signs of remodeling, share a similar no b-

wave ERG phenotype (Masu et al., 1995; Pardue et al., 1998) and lack expression of TRPM1, the non-selective cation channel that is responsible for signaling in On BCs (Cao et al., 2011; Pearing et al., 2011; Xu et al., 2011).

This suggests that there are differences between *Nyx^{nob}* and *mGluR6^{-/-}* retinas that occur at or after the On BC output to the rest of the inner retinal circuit. To characterize the differences in this circuitry in *Nyx^{nob}* and *mGluR6^{-/-}* mutants, I recorded and compared both the intrinsic properties and synaptic inputs to *Nyx^{nob}* and *mGluR6^{-/-}* RGCs using *in vitro* whole cell patch clamp recordings so that I could correlate functional changes with RGC morphology.

Materials and Methods

RGC Whole Cell Patch Clamp Protocol

Current Clamp Protocols

Membrane Oscillations

K-Gluconate intracellular solution (containing in mM: 120 K-gluconate, 1 CaCl₂, 1 MgCl₂, 10 Na-HEPES, 11 EGTA, 4 ATP, 1 GTP and 1% sulforhodamine) was used for RGC recordings. To evaluate the presence of a rhythmic component in RGC spontaneous membrane potential activity (includes action potentials and sub-threshold membrane oscillations), I performed a Fast Fourier transform (FFT) analysis over 85 seconds of a 0 pA current clamp recording (Clampfit 10.2; Figure 11). Raw RGC current clamp recordings display

voltage change across time, while a FFT allows me to see what components are present within the raw recorded signal. Specifically, a FFT presents the RGC signal as the voltage amplitudes that are present at each frequency (Hz). A Fourier analysis converts time to frequency and the FFT is an algorithm which computes the Fourier transform, which is plotted on a graph (example in Figure 11).

RGCs were classified as 'rhythmic' if there was a peak present in their FFT. The criterion to classify a cell as rhythmic was employed if the peak of the FFT had low power (low Y-axis value at the peak) or was surrounded by high baseline/noise power (high Y-axis values to the left and/or right of the peak), in which case I used the following metric: A cursor was placed following the DC component of the power spectrum and another cursor was placed at 10 Hz to encompass the peak of the FFT (Figure 11). The following equation was utilized: mean across the selected cursor region + 3 x standard deviation. If the calculated value was larger than the power of the FFT peak (Y-axis value at the peak), then the RGC was classified as 'non-rhythmic'. If the calculated value was smaller than the power of the FFT peak, then the RGC was classified as 'rhythmic'. The principle behind the equation was to determine if the peak of the FFT was large and narrow enough to be considered a reliable measure of rhythmic frequency above noise. The rhythmic frequency was classified as the frequency (Hz) of the FFT peak (the X-axis value at the peak of the FFT).

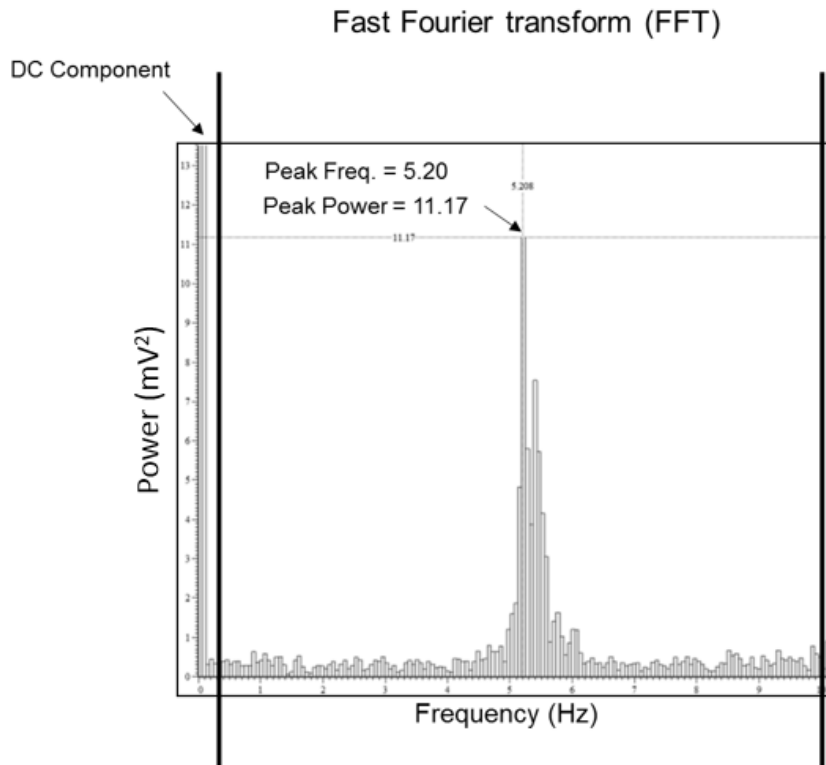


Figure 11. RGC Fast Fourier Transform. RGCs were classified as ‘oscillatory’ if they exhibited a strong peak in the FFT. Specifically, a cursor was placed following the DC component of the power spectrum and another cursor was placed at 10 Hz to encompass the peak of the FFT. If the calculated mean across the selected cursor region + 3 x standard deviation was larger than the power of the FFT peak (Y-axis value at the peak), then the RGC was classified as ‘non-oscillatory’. If the calculated value was smaller than the power of the FFT peak, then the RGC was classified as ‘oscillatory’. The oscillatory frequency is the frequency (Hz) of the FFT peak (the X-axis value at the peak of the FFT).

Resting Membrane Potential (V_{rest})

The mean V_{rest} was calculated by subtracting the peak of the membrane potential from the trough of the membrane potential across eight consecutive ten second intervals, which were averaged to calculate the mean V_{rest} (Clampfit 10.2). If action potentials were present on top of the baseline membrane potential, the action potential deflection from baseline was eliminated from the peak measurement. Action potentials were ignored in order to compare baseline membrane potentials across all cells, whether or not they exhibited action potentials.

Rhythmic Spiking

To evaluate the presence of rhythmic spiking activity in isolation of any sub-threshold membrane oscillation I used Spike2 7.02 to filter only the action potentials in each 85 second current clamp recording. Then I performed the same FFT described above, utilizing the same specified criterion to classify a cell as 'non-rhythmic spiking' or 'rhythmic spiking'.

Spontaneous Activity

Spontaneous spiking activity was calculated by setting a threshold in which Clampfit 10.2 counted all spikes which crossed a cursor in the positive direction. The threshold was set individually for each recording to ensure all spike events were included in the analysis. Spikes from each RGC were counted across 85 seconds and the average number of spikes/second was calculated.

Light Response Class

RGCs were categorized as responsive when they had action potentials or depolarized to light onset or offset in $\geq 50\%$ of the stimuli trials. The time-to-peak of the response was measured in Clampfit 10.2 and the response was then classified as either ON, ON/OFF, OFF, delayed ON (dON), or dON/OFF.

Statistical Analysis

One-way ANOVA with Bonferroni post hoc, Kruskal-Wallis with Dunns post hoc, Chi Square, Mann-Whitney or unpaired t-tests with Welch's correction were used as the statistical analyses. Post hoc *P* values are reported. Analyses were performed in Prism 5.04.

Terminology

Membrane oscillations: All membrane potential data, including spikes and sub-threshold membrane oscillations.

Rhythmic spiking: The rhythmic spikes have been isolated from sub-threshold membrane oscillations.

Results

In my *in vitro* whole-mount preparation, all WT RGCs ($n = 34$), regardless of dendritic morphology, had spontaneous and/or light-evoked spiking activity. I confined my analysis to *Nyx^{nob}* and *mGluR6^{-/-}* RGCs with spiking activity. Similar

to previous reports (Freeman et al., 2008), I found a small number of WT (3/33) and *mGluR6*^{-/-} (1/42) RGCs with rhythmic activity at frequencies >14 Hz (either ON or OFF morphology RGCs). Since this high frequency rhythmicity is a WT phenotype, I eliminated any RGC with oscillations > 14 Hz from my analysis.

Most Nyx^{nob} and few mGluR6^{-/-} RGCs have rhythmic spiking

Among spiking RGCs, 61% (33/54) of *Nyx^{nob}* RGCs (Figure 12A, B), but only 12.5% (5/40) of *mGluR6*^{-/-} RGCs exhibited rhythmic spiking activity. In the *rd1* retina, 50% of RGCs exhibit rhythmic spiking (; et al., 2011), suggesting the *Nyx^{nob}* retina may more closely resembles the *rd* retina. The distribution of fundamental frequency of *Nyx^{nob}* and *mGluR6*^{-/-} RGCs were between 2-5 Hz (Figure 12C) and their means were similar (*Nyx^{nob}* RGCs: 3.64 Hz ± 0.16; *mGluR6*^{-/-} RGCs: 3.03 Hz ± 0.35; t-test: *P* = 0.14).

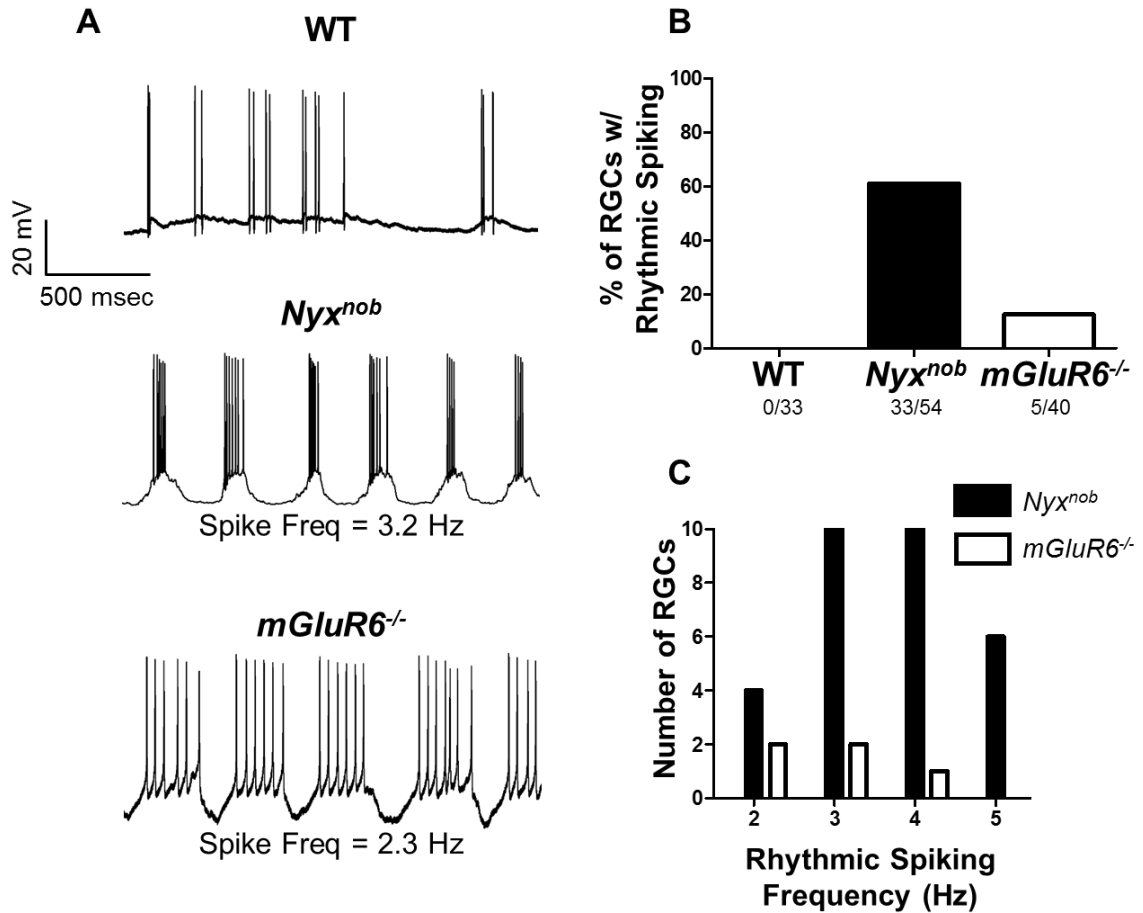


Figure 12. Among RGCs that exhibit spiking activity, most *Nyx^{nob}* but only a few *mGluR6^{-/-}* RGCs exhibit rhythmic spiking activity. A. Recordings from WT, *Nyx^{nob}* and *mGluR6^{-/-}* RGCs, demonstrate the absence of rhythmic spiking in WT RGCs and its presence in *Nyx^{nob}* and *mGluR6^{-/-}* RGCs. B. Histogram shows the frequency distribution of *Nyx^{nob}* and *mGluR6^{-/-}* RGCs that spike rhythmically. C. Histogram shows the distribution of fundamental frequency of *Nyx^{nob}* and *mGluR6^{-/-}* RGCs with rhythmic spiking.

Almost all Nyx^{nob} but less than half of mGluR6^{-/-} RGCs have rhythmic membrane oscillations

Given the difference in the proportions of *Nyx^{nob}* and *mGluR6^{-/-}* RGCs that exhibit rhythmic spiking, I characterized rhythmicity in their membrane potentials. An additional 35% of *Nyx^{nob}* RGCs (19 RGCs) and 27.5% of *mGluR6^{-/-}* RGCs (11 RGCs) exhibit only membrane oscillations. Taken together, 96% of *Nyx^{nob}* (52/54) and 40% of *mGluR6^{-/-}* (16/40) RGCs show some rhythmic activity (Figure 13B). Again, the distribution of *Nyx^{nob}* and *mGluR6^{-/-}* RGC fundamental frequencies were between 2-5 Hz (Figure 13C) and their means were similar (*Nyx^{nob}* RGCs: 3.53 Hz \pm 0.10; *mGluR6^{-/-}* RGCs: 3.11 Hz \pm 0.19; t-test: $P = 0.06$). These data indicate that rhythmic membrane oscillations in both *Nyx^{nob}* and *mGluR6^{-/-}* RGCs do not always transfer into rhythmic spiking (example of this in Figure 3A), although *Nyx^{nob}* RGCs are much more likely to show rhythmicity. This finding may result from RGCs with altered V_{rest} , therefore hindering their spiking ability, but maintaining their membrane oscillations. In addition, this finding may indicate that excitatory inputs, which cause RGC rhythmic activity, are insufficient to bring them to spike threshold, due to altered spontaneous activity. The initial results suggest a fundamental difference in the inner retinal circuits of these two models of cCSNB.

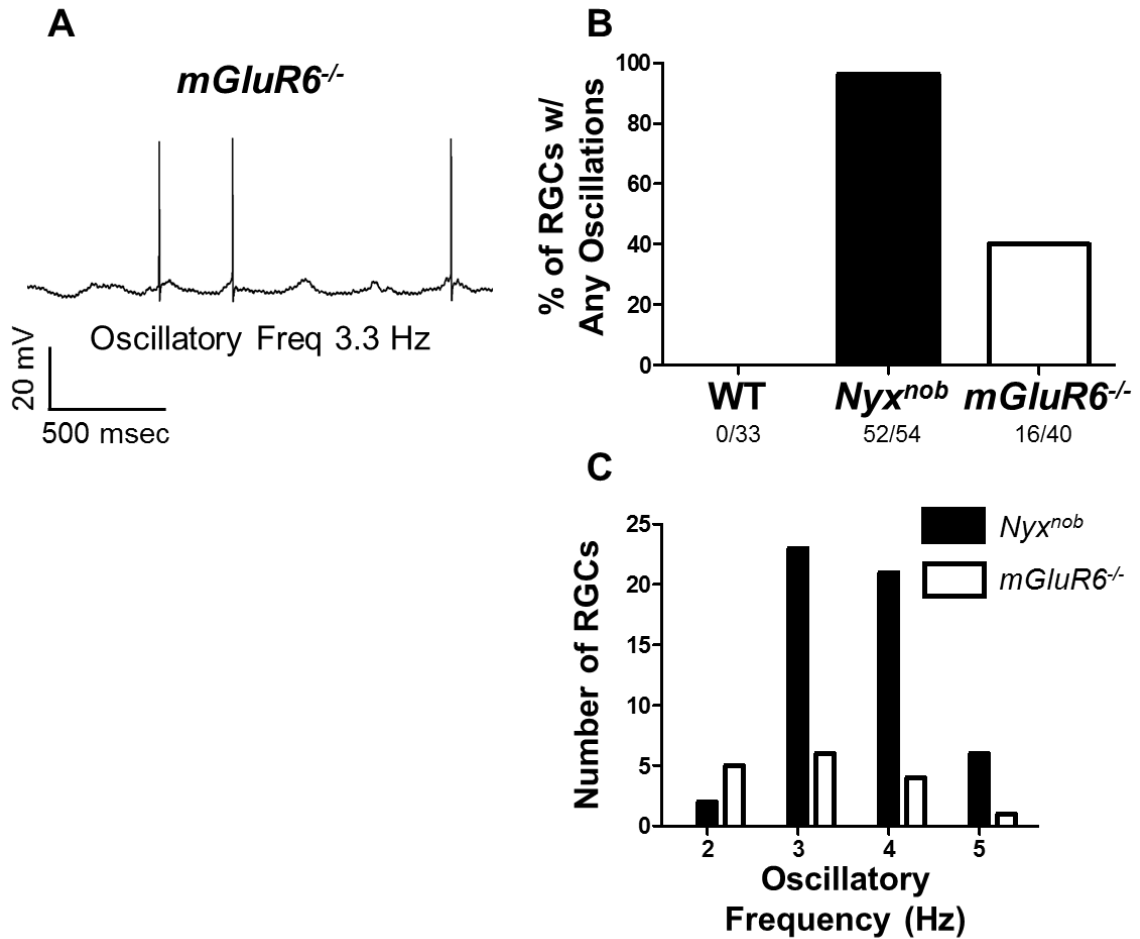


Figure 13. Almost all of *Nyx^{nob}* and slightly less than half of *mGluR6^{-/-}* RGCs exhibit rhythmic membrane oscillations. A. Recording from *mGluR6^{-/-}* RGC demonstrates the presence of rhythmic membrane oscillations without rhythmic spiking. B. Histogram shows the frequency distribution of *Nyx^{nob}* and *mGluR6^{-/-}* RGCs that have rhythmic membrane oscillations. C. Histogram shows the distribution of fundamental frequency of *Nyx^{nob}* and *mGluR6^{-/-}* RGCs with rhythmic membrane oscillations.

Nyx^{nob} and mGluR6^{-/-} RGC morphological and light response classes were evenly sampled

To determine if all morphological and light response classes were sampled evenly between *Nyx^{nob}* and *mGluR6^{-/-}* RGCs, I plotted the percent of RGCs recorded for all morphological classes (ON, OFF, Bistratified; Figure 4Ai) and light response classes (OFF, dON, dON/OFF, NR; Figure 14Bi). The RGCs recorded in both *Nyx^{nob}* and *mGluR6^{-/-}* were sampled evenly across morphological and light response classes (Figure 14Ai, Bi).

All Nyx^{nob} RGC classes but only non-responsive (NR) mGluR6^{-/-} RGCs exhibit rhythmic spiking

Next, I determined whether specific morphological or light response classes corresponded to RGCs with rhythmic spiking or membrane oscillations. I compared the distribution of *Nyx^{nob}* and *mGluR6^{-/-}* RGCs with rhythmic spiking as a function of their dendritic morphology (Figure 14Aii) or light response class (Figure 14Bii). Rhythmic spiking was found in similar proportions in all *Nyx^{nob}* and *mGluR6^{-/-}* RGC morphological classes (Figure 14Aii; Chi Square: $P = 0.53$), demonstrating no correlation between RGC morphological class and the presence/absence of rhythmic spiking. *Nyx^{nob}* and *mGluR6^{-/-}* are similar to the rd1 retina, where all morphological classes exhibit rhythmic spiking (Borowska et al., 2011). Among *Nyx^{nob}* RGCs, rhythmic spiking was found across all light response classes (OFF, dON/OFF, NR; Figure 4Bii). In contrast, only NR

mGluR6^{-/-} RGCs have rhythmic spiking (Figure 4Bii) and this is not related to their dendritic morphology (Figure 4Aii).

RGCs with rhythmic membrane oscillations are found at similar proportions in all *Nyx*^{nob} and *mGluR6*^{-/-} RGC morphological and light response classes (data not shown; morphological classes: Chi Square: *P* = 0.39; light-response classes; Chi Square: 0.12), demonstrating no correlation in RGC class and the presence/absence of membrane oscillations.

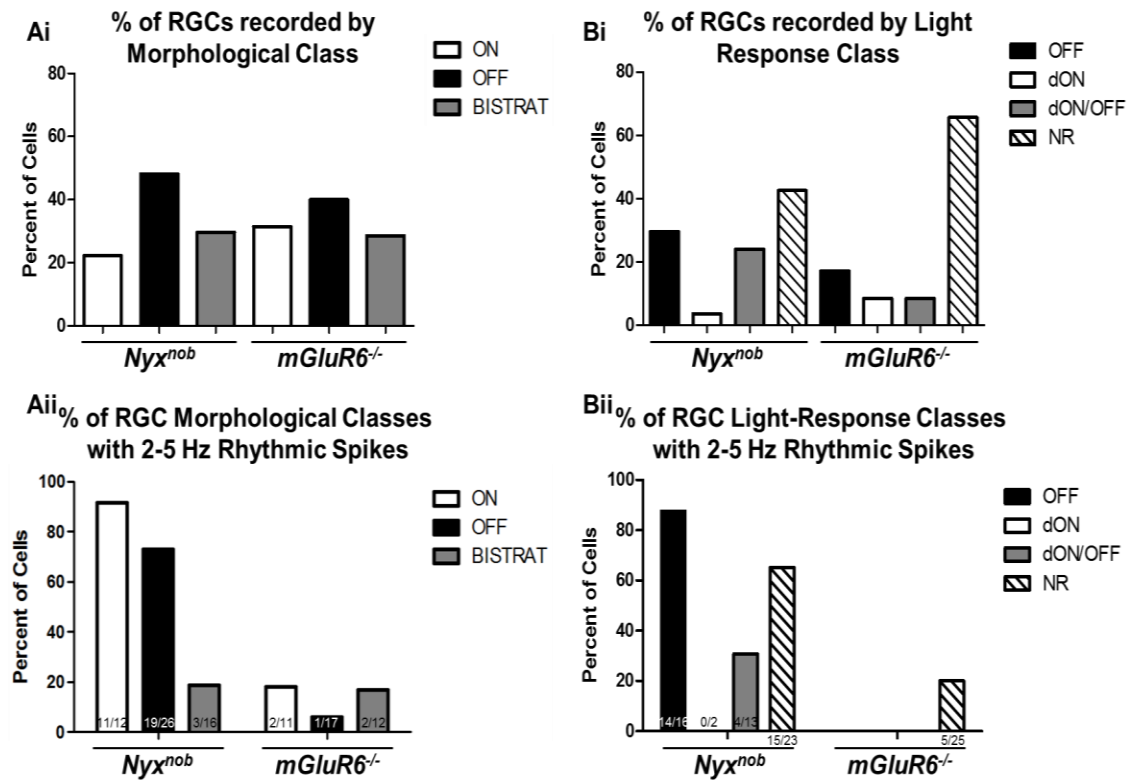


Figure 14. The distribution of recorded *Nyx*^{nob} and *mGluR6*^{-/-} RGCs and distribution of rhythmic spiking based on morphology and light response class.

Ai. Histogram of morphological classes of all *Nyx*^{nob} and *mGluR6*^{-/-} RGCs

recorded. Aii. Histogram shows the percent of morphological classes with 2-5 Hz rhythmic spikes in *Nyx^{nob}* and *mGluR6^{-/-}* RGCs. All *Nyx^{nob}* and *mGluR6^{-/-}* morphological classes (ON, OFF, Bistratified) exhibit RGCs with rhythmic spiking. Bi. Histogram of light response classes of all *Nyx^{nob}* and *mGluR6^{-/-}* RGCs recorded. Bii. Histogram shows the percent of light-response classes with 2-5 Hz rhythmic spikes in *Nyx^{nob}* and *mGluR6^{-/-}* RGCs. Almost all *Nyx^{nob}* light-response classes (OFF, dON/OFF, NR) exhibit RGCs with rhythmic spiking. Only NR *mGluR6^{-/-}* RGCs exhibit rhythmic spiking.

Nyx^{nob} and *mGluR6^{-/-}* RGCs have similar V_{rest} although both are more hyperpolarized than WT

The V_{rest} of neurons is a function of both intrinsic properties and tonic synaptic inputs. Therefore, I examined whether a difference in V_{rest} could be correlated with the difference between *Nyx^{nob}* and *mGluR6^{-/-}* RGC rhythmic spiking. Including all RGC types, WT, *mGluR6^{-/-}* and *Nyx^{nob}* RGC V_{rest} were similar (one-way ANOVA with Bonferroni post hoc: $P > 0.05$; data not shown). However, the mechanism of maintained activity is known to differ in ON and OFF morphology RGCs (Margolis & Detwiler, 2007), so I next compared V_{rest} within RGC morphological classes (Figure 15). V_{rest} was similar across OFF and Bistratified RGCs in WT, *mGluR6^{-/-}* and *Nyx^{nob}* RGCs (Kruskal-Wallis with Dunns post hoc: $P > 0.05$; Figure 15B, C). Within ON morphology RGCs, *mGluR6^{-/-}* and

Nyx^{nob} V_{rest} were more hyperpolarized compared to WT RGCs (Kruskal-Wallis with Dunns post hoc: WT v. *mGluR6^{-/-}*: $P < 0.01$; WT v. *Nyx^{nob}*: $P < 0.001$; Figure 15A), although V_{rest} of ON morphology *mGluR6^{-/-}* and *Nyx^{nob}* RGCs were similar (Kruskal-Wallis with Dunns post hoc: $P > 0.05$; Figure 15A). Thus, *mGluR6^{-/-}* and *Nyx^{nob}* RGCs with ON morphology share a more hyperpolarized phenotype, likely due to the shared alteration of On BC input to both of these genotypes.

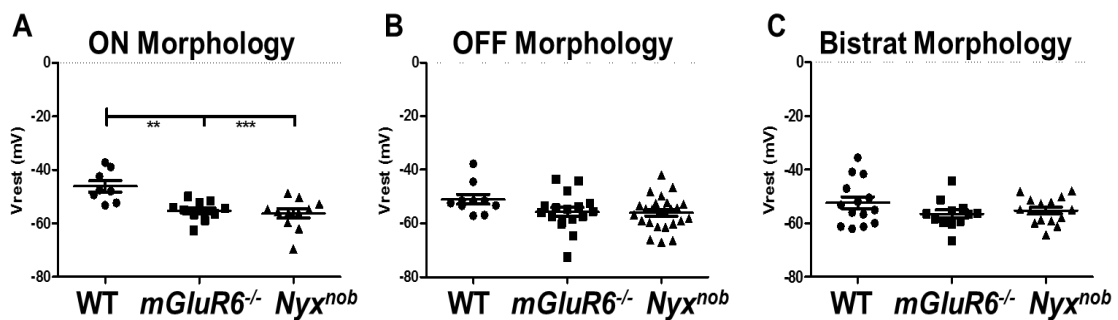


Figure 15. WT, *mGluR6^{-/-}* and *Nyx^{nob}* RGC V_{rest} . A. ON morphology *mGluR6^{-/-}* and *Nyx^{nob}* RGC V_{rest} are more hyperpolarized compared to WT RGCs although *mGluR6^{-/-}* and *Nyx^{nob}* ON morphology V_{rest} are similar (Dunns post hoc: ** $P < 0.01$; *** $P < 0.001$). B. OFF morphology *mGluR6^{-/-}*, *Nyx^{nob}* and WT RGC V_{rest} are similar. C. Bistratified morphology *mGluR6^{-/-}*, *Nyx^{nob}* and WT RGC V_{rest} are similar.

mGluR6^{-/-} ON morphology RGC spontaneous activity is lower than Nyx^{nob}

The spontaneous activity of neurons is a function of both intrinsic properties and tonic synaptic inputs. Therefore, I examined whether *mGluR6^{-/-}* RGCs are generally less excitable than *Nyx^{nob}* RGCs. Including all RGC types, WT, *mGluR6^{-/-}* and *Nyx^{nob}* RGC spontaneous activity levels were similar (One-way ANOVA: $P > 0.05$; data not shown). However, the mechanism of spontaneous activity is known to differ in ON and OFF morphology RGCs (Margolis & Detwiler, 2007), so I next compared spontaneous activity within RGC morphological classes. Within OFF and Bistratified morphology RGCs, spontaneous activity was similar across WT, *mGluR6^{-/-}* and *Nyx^{nob}* RGCs (Kruskal-Wallis with Dunns post hoc: $P > 0.05$; Figure 16B, C). In contrast, the spontaneous activity of *mGluR6^{-/-}* ON morphology RGCs was significantly lower compared to *Nyx^{nob}* RGCs (Kruskal-Wallis with Dunns post hoc: $P < 0.05$; Figure 16A) and in fact, the majority of *mGluR6^{-/-}* ON morphology RGCs had little or no spontaneous activity, although both *mGluR6^{-/-}* and *Nyx^{nob}* were statistically similar to WT RGCs (Figure 16A; Kruskal-Wallis with Dunns post hoc: $P > 0.05$). The results suggest that the general excitatory input to ON morphology *mGluR6^{-/-}* RGCs is significantly lower than *Nyx^{nob}*.

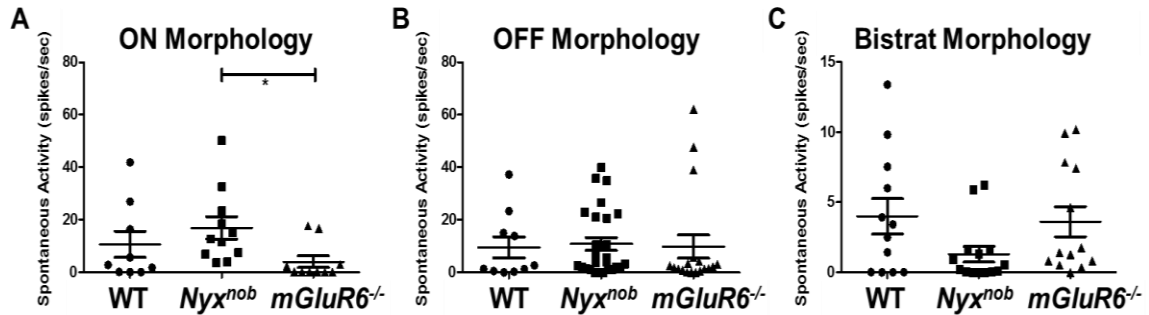


Figure 16. WT, *mGluR6^{-/-}* and *Nyx^{nob}* RGC spontaneous activity. ON morphology *mGluR6^{-/-}* RGC spontaneous activity was significantly decreased compared to *Nyx^{nob}* RGCs while *mGluR6^{-/-}* and *Nyx^{nob}* are similar to WT RGCs (Kruskal-Wallis with Dunns post hoc: * $P < 0.05$). B. OFF morphology *mGluR6^{-/-}*, *Nyx^{nob}* and WT RGC spontaneous activity are similar. C. Bistratified morphology *mGluR6^{-/-}*, *Nyx^{nob}* and WT RGC spontaneous activity are similar.

Neither mGluR6^{-/-} nor Nyx^{nob} RGCs have a correlation between V_{rest} and the presence or absence of rhythmic spiking activity

If the excitatory input is different between *Nyx^{nob}* and *mGluR6^{-/-}* RGCs, it also could be reflected in the V_{rest} of the RGCs. I compared the relationship between the presence/absence of rhythmic spiking or membrane oscillations and V_{rest} within *Nyx^{nob}* and *mGluR6^{-/-}* RGCs in specific morphological classes. A more hyperpolarized V_{rest} in RGCs that do not have rhythmic spiking would indicate that for the same presynaptic input it is more difficult to achieve spike threshold.

Only 4% of *Nyx^{nob}* RGCs lack any type of rhythmicity, either spiking or membrane oscillations (Figure 13B). There were so few non-rhythmic RGCs across all *Nyx^{nob}* morphological classes, that all classes were combined for comparison of V_{rest} . *Nyx^{nob}* non-rhythmic RGC V_{rest} was similar to *Nyx^{nob}* rhythmic RGCs (t-test: $P = 0.65$; data not shown). Of the 96% of *Nyx^{nob}* RGCs with rhythmicity, V_{rest} was similar between RGCs with rhythmic spiking and RGCs with only membrane oscillations across all morphological classes (t-test: OFF morphology $P = 0.95$; Bistratified morphology $P = 0.16$; data not shown). *Nyx^{nob}* ON morphology class could not be analyzed because the number of values within each group was too low ($n=1$).

Sixty percent of *mGluR6^{-/-}* RGCs lack any type of rhythmicity, either spiking or membrane oscillations (Figure 13B). *mGluR6^{-/-}* non-rhythmic RGC V_{rest} was similar to *mGluR6^{-/-}* rhythmic RGCs across all morphological classes (t-test: OFF morphology $P = 0.1.0$; Bistratified morphology $P = 0.21$; ON morphology $P = 0.33$; data not shown). There were so few *mGluR6^{-/-}* RGCs with rhythmic spiking or only membrane oscillations, that all morphological classes were combined for the following comparison. Of the 40% of *mGluR6^{-/-}* RGCs with rhythmicity, V_{rest} was similar between RGCs with rhythmic spiking and RGCs with only membrane oscillations (t-test: $P = 0.17$; data not shown). These results indicate that the presence or absence of rhythmic spiking activity in *Nyx^{nob}* and *mGluR6^{-/-}* RGCs is independent of V_{rest} .

A decrease in spontaneous activity can account for Nyx^{nob} RGCs that do not exhibit rhythmic spiking, but not for $mGluR6^{-/-}$ RGCs

I examined the relationship between the presence/absence of rhythmic spiking or membrane oscillations and spontaneous activity within Nyx^{nob} and $mGluR6^{-/-}$ RGCs in specific morphological classes (Figure 17). Different intrinsic mechanisms (in OFF morphology RGCs) or different synaptic inputs (in either ON or OFF morphology RGCs) could alter RGC spontaneous activity. For example, if RGCs that do not spike rhythmically have decreased spontaneous activity compared to RGCs that do spike rhythmically, one could presume that the non-rhythmic spiking RGCs cannot exhibit sufficient spiking activity to result in rhythmic spiking, but could maintain membrane oscillations. Therefore, differences in spontaneous activity between rhythmic spiking and membrane oscillatory RGCs could account for the dichotomy between rhythmic spiking/non-rhythmic spiking Nyx^{nob} and $mGluR6^{-/-}$ RGCs.

Of the 96% of Nyx^{nob} RGCs with rhythmicity, OFF and Bistratified morphology Nyx^{nob} RGCs with only membrane oscillations exhibited lower spontaneous activity compared to OFF and Bistratified morphology Nyx^{nob} RGCs with rhythmic spiking (Figure 17Aii, 7Aiii; Mann-Whitney: OFF morphology Nyx^{nob} rhythmic vs. non-rhythmic: $P = 0.0001$; Bistratified morphology Nyx^{nob} rhythmic vs. non-rhythmic: $P = 0.02$). The horizontal black lines on the graphs in Figure 17 represent the minimum spontaneous activity level where RGCs exhibited

rhythmic spiking; none of the RGCs below this line exhibited rhythmic spiking, though some exhibited rhythmic membrane oscillations. All *Nyx^{nob}* ON morphology RGCs with rhythmicity exhibited rhythmic spiking activity and have spontaneous activity levels above rhythmic spike threshold (black line; Figure 17Ai). These results suggest that the population of *Nyx^{nob}* RGCs that exhibit membrane oscillations but do not spike rhythmically, lack the rhythmic spiking because their spontaneous activity level is too low (Figure 17A).

Sixty percent of *mGluR6^{-/-}* RGCs lack any type of rhythmicity, either spiking or membrane oscillations (Figure 13B). The spontaneous activity of all morphological classes of *mGluR6^{-/-}* RGCs without rhythmicity was similar to those with rhythmicity (Mann-Whitney: not rhythmic v. rhythmic: ON morphology *mGluR6^{-/-}*: $P = 0.23$; OFF morphology *mGluR6^{-/-}*: $P = 0.09$; Bistratified morphology *mGluR6^{-/-}*: $P = 0.93$). This demonstrates that in *mGluR6^{-/-}* RGCs the presence or absence of rhythmicity does not depend on spontaneous activity. There were so few *mGluR6^{-/-}* RGCs with rhythmic spiking or only membrane oscillations, that all morphological classes were combined for the following comparison. Of the 40% of *mGluR6^{-/-}* RGCs with some type of rhythmicity (Figure 13B), *mGluR6^{-/-}* RGC spontaneous activity was similar between RGCs with rhythmic spiking and RGCs with only membrane oscillations (t-test: $P = 0.14$). In summary, these results suggest that *Nyx^{nob}* RGCs with lower spontaneous activity can account for the RGCs that exhibit only membrane oscillations versus rhythmic spiking (Figure 17A). However, *mGluR6^{-/-}* RGC spontaneous activity

cannot account for the difference in RGCs that exhibit rhythmic activity versus no rhythmic activity or the difference in RGCs that exhibit only membrane oscillations versus rhythmic spiking (Figure 17B).

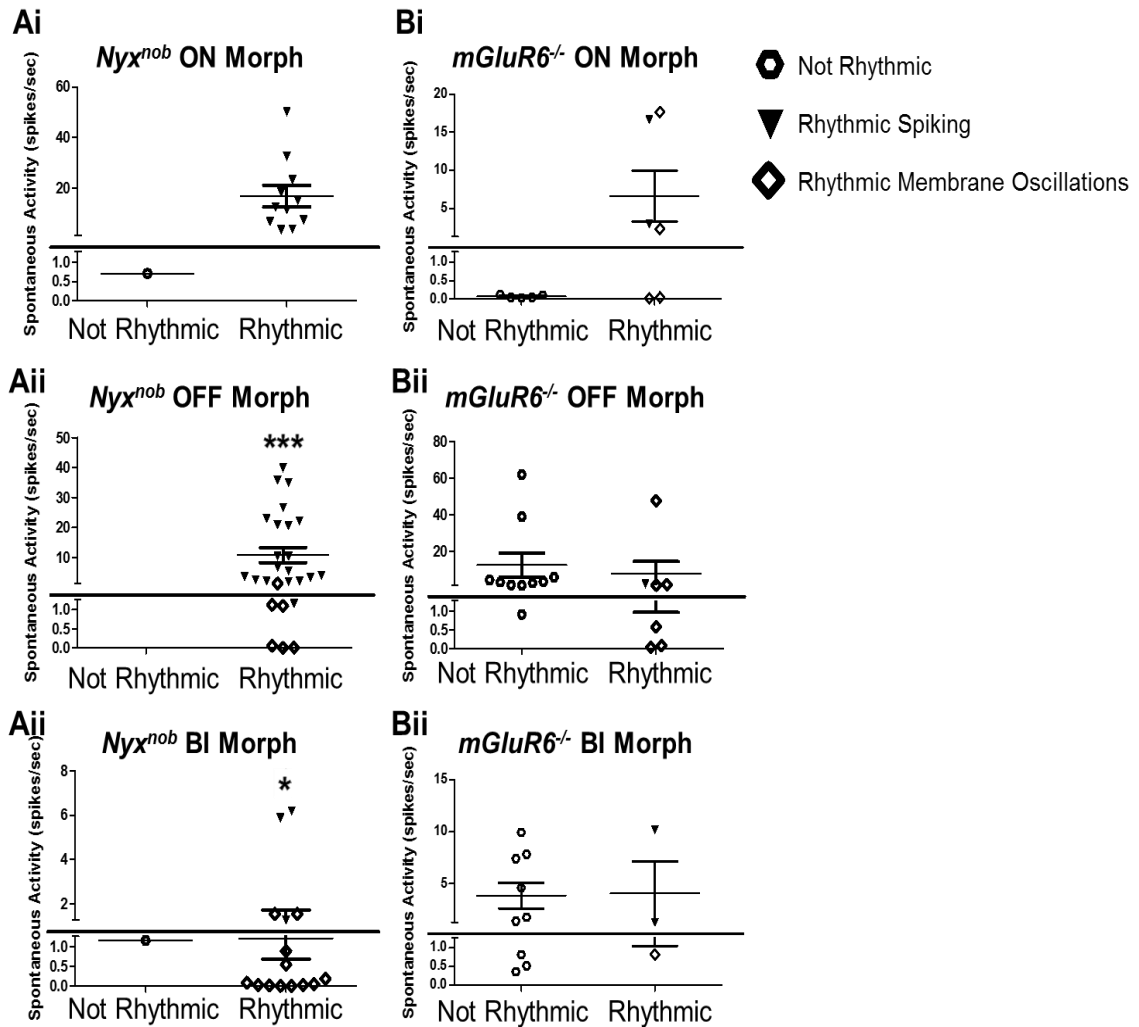


Figure 17. *Nyx^{nob}* RGC spontaneous activity is decreased in membrane oscillation only RGCs compared to rhythmic spiking RGCs. There is no correlation in spontaneous activity and rhythmicity in *mGluR6^{-/-}* RGCs Ai. Scatterplot of *Nyx^{nob}* ON morphology RGCs without rhythmicity and with

rhythmicity. Aii. Scatterplot of *Nyx^{nob}* OFF morphology RGCs without rhythmicity and with rhythmicity. Rhythmic membrane oscillatory RGCs exhibit decreased spontaneous activity compared to rhythmic spiking RGCs. Aiii. Scatterplot of *Nyx^{nob}* Bistratified morphology RGCs without rhythmicity and with rhythmicity. Rhythmic membrane oscillatory RGCs exhibit decreased spontaneous activity compared to rhythmic spiking RGCs. Bi. Scatterplot of *mGluR6^{-/-}* ON morphology RGCs without rhythmicity and with rhythmicity. There is no difference in spontaneous activity. Bii. Scatterplot of *mGluR6^{-/-}* OFF morphology RGCs without rhythmicity and with rhythmicity. There is no difference in spontaneous activity. Biii. Scatterplot of *mGluR6^{-/-}* Bistratified morphology RGCs without rhythmicity and with rhythmicity. There is no difference in spontaneous activity. Horizontal line denotes spontaneous activity rate where rhythmic spiking activity can be accurately measured via a FFT analysis. Data points below horizontal line exhibit too few spikes to exhibit rhythmic spiking via FFT analysis. (Mann-Whitney: * $P < 0.05$; *** $P < 0.001$).

Discussion

All morphological and functional light-response classes of *Nyx^{nob}* RGCs (Off, dOn/Off and NR) have 2-5 Hz rhythmic spiking. In contrast, only NR *mGluR6^{-/-}* RGCs have rhythmic spiking (Figure 14Bii; Figure 18). Within the *mGluR6^{-/-}* NR RGCs, rhythmic spiking is not related to morphological class as

ON, OFF, and Bistratified RGCs exhibit NR light-responses (Figure 14Aii; Figure 18). This demonstrates that the rhythmic spiking in *mGluR6*^{-/-} RGCs is related to an absence of visual function within the On pathway, but is not confined by it as only 5/11 NR RGCs had rhythmic spiking. This suggests that in *mGluR6*^{-/-} RGCs, the absence of both On and Off pathway-mediated light responses are necessary for a RGC to spike rhythmically, since *mGluR6*^{-/-} RGCs that maintained Off pathway-mediated light inputs (Off, dON, dON/OFF light responses) did not exhibit rhythmic spiking. *Nyx*^{nob} RGC rhythmic spiking is not unique to the same pathway as *mGluR6*^{-/-} RGCs, as *Nyx*^{nob} rhythmic spiking is found in all morphological and functional light response classes. These data show that On BC defects affect downstream visual function across all morphological classes.

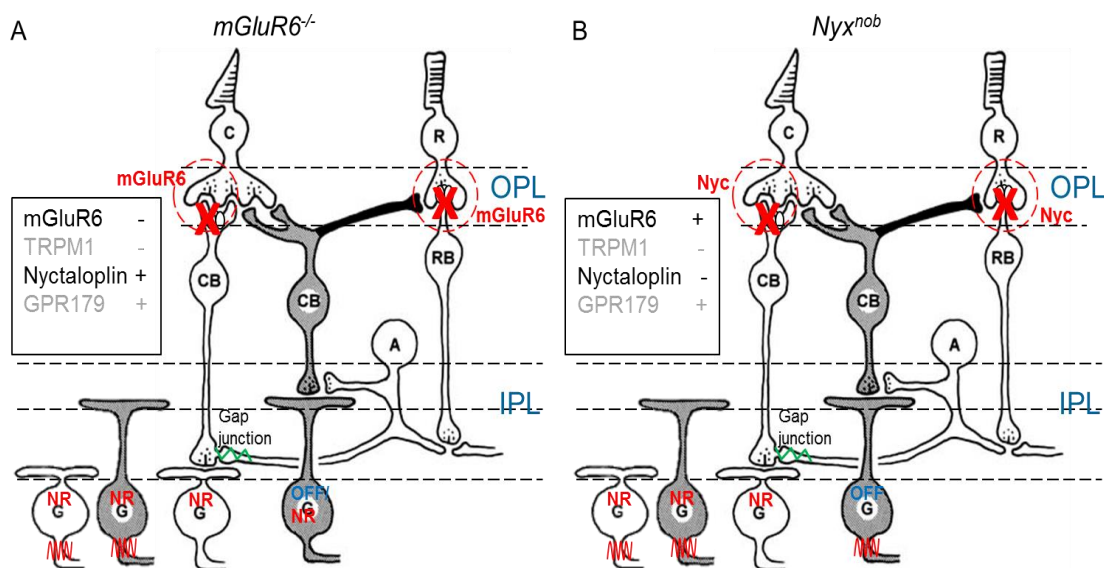


Figure 18. Summary schematic of rhythmic RGCs in *mGluR6*^{-/-} and *Nyx*^{nob}. Text boxes show the presence and absence of rod BC proteins in each of the mutants. The red waveforms on the RGCs represent cells with rhythmic activity.

For simplicity, only ON and OFF morphology RGCs are shown. A. In *mGluR6*^{-/-} retina, all morphological classes exhibit a population of RGCs with rhythmicity, either rhythmic spiking or rhythmic membrane oscillations. However, only *mGluR6*^{-/-} RGCs non-responsive to light exhibit rhythmicity. There is no relationship between *mGluR6*^{-/-} RGC V_{rest} or spontaneous activity rate and the presence/absence of rhythmicity. B. In *Nyx*^{nob} retina, all morphological classes exhibit a population of RGCs with rhythmicity, either rhythmic spiking or rhythmic membrane oscillations. In contrast to *mGluR6*^{-/-} RGCs, all *Nyx*^{nob} RGC light response classes exhibit cells with rhythmicity. There is no relationship between *Nyx*^{nob} RGC V_{rest} and the presence/absence of rhythmicity. However, *Nyx*^{nob} RGCs with lower spontaneous activity account for the RGCs that exhibit only membrane oscillations versus rhythmic spiking.

I examined whether membrane properties of *mGluR6*^{-/-} and *Nyx*^{nob} RGCs were or were not responsible for the general difference in *mGluR6*^{-/-} and *Nyx*^{nob} RGCs rhythmic/non-rhythmic spiking. V_{rest} was similar between *Nyx*^{nob} and *mGluR6*^{-/-} RGCs within all morphological classes. This suggests a similarity in the intrinsic properties of the RGCs in that the leak channels that maintain V_{rest} of *mGluR6*^{-/-} or *Nyx*^{nob} RGCs are retained. It also suggests that both *Nyx*^{nob} and *mGluR6*^{-/-} RGCs were at similar resting states relative to their spike threshold, so neither genotype would elicit a spike more or less easily than the other based on

changes in V_{rest} . However, V_{rest} of both $mGluR6^{-/-}$ and Nyx^{nob} ON morphology RGCs were more hyperpolarized compared to WT ON morphology RGCs. This was likely due to the shared lack of excitatory tonic input from the On pathway in $mGluR6^{-/-}$ and Nyx^{nob} retinas.

Even though V_{rest} was similar in Nyx^{nob} and $mGluR6^{-/-}$ RGCs, it is possible that spontaneous activity was altered. A difference in spontaneous activity could result from alterations in intrinsic mechanisms of Nyx^{nob} and $mGluR6^{-/-}$ RGCs (for OFF morphology RGCs) or excitatory synaptic inputs (for ON and OFF morphology RGCs). I found that ON morphology $mGluR6^{-/-}$ RGC spontaneous activity was decreased compared to Nyx^{nob} . Therefore, it is possible that a decrease in $mGluR6^{-/-}$ ON morphology spontaneous activity could account for the general trend for ON morphology Nyx^{nob} RGCs to exhibit rhythmic spiking and $mGluR6^{-/-}$ RGCs to lack rhythmic spiking. However, spontaneous activity rate could not account for the difference in rhythmic spiking in $mGluR6^{-/-}$ and Nyx^{nob} OFF or Bistratified RGCs.

The difference in spontaneous activity between Nyx^{nob} and $mGluR6^{-/-}$ ON morphology RGCs indicates one of two situations: 1) an increase in Nyx^{nob} ON morphology RGCs tonic excitatory input (or alternatively a decrease in tonic inhibitory input) or 2) a decrease in $mGluR6^{-/-}$ ON morphology RGCs tonic excitatory input (or alternatively an increase in tonic inhibitory input). An alteration in signaling within the On pathway is not surprising because of the absence of signaling within the On BCs. However, an alteration of inputs to only

one of the mutants' RGCs is initially surprising, given that BCs in both mutants fail to signal. However, recordings from *Nyx^{nob}* and *mGluR6^{-/-}* rod BCs in Chapter IV will elucidate some unexpected differences between these genotypes. In addition, it is interesting that the spontaneous activity of *Nyx^{nob}* and *mGluR6^{-/-}* Bistratified RGCs do not show a similar phenotype to ON morphology RGCs since they should receive similar inputs from the On pathway. This suggests that the inputs/intrinsic mechanisms of OFF sublamina RGCs heavily influence Bistratified RGCs spontaneous activity.

To determine if an association was present between rhythmic spiking, rhythmic membrane oscillations and non-rhythmic RGCs, I compared V_{rest} and spontaneous activity of RGCs within each genotype and morphological class. V_{rest} in rhythmic spiking and non-rhythmic spiking RGCs were similar in both *mGluR6^{-/-}* and *Nyx^{nob}* RGCs. Therefore, alterations in V_{rest} could not account for the difference in rhythmic spiking and non-rhythmic spiking RGCs.

Spontaneous activity was lower in *Nyx^{nob}* RGCs which exhibit only membrane oscillations than those that spike rhythmically, suggesting that the few *Nyx^{nob}* RGCs that only exhibit rhythmic membrane oscillations do so because they have very low spontaneous activity. In contrast, in *mGluR6^{-/-}* RGCs, the presence/absence of rhythmicity or rhythmic spiking versus membrane oscillations do not depend on spontaneous activity level. It remains unclear why *mGluR6^{-/-}* RGCs exhibit rhythmic spiking as opposed to membrane oscillations and further experiments are needed to elucidate this.

Forty percent of *mGluR6*^{-/-} RGCs have 2-5 Hz oscillations. There were no prior reports of *mGluR6*^{-/-} RGCs with rhythmic spiking nor membrane oscillations (Renteria et al., 2006). While previous publications have not reported rhythmic spiking in *mGluR6*^{-/-} RGCs, they measured extracellular RGC spikes with a MEA, which records tens to hundreds of RGCs at the same time (Renteria et al., 2006). Since the proportion of *mGluR6*^{-/-} RGCs with rhythmic spikes was very low (12.5%) it is plausible that the rhythmic spiking RGCs were not noticed or not included in the previously reported data sets (Renteria et al., 2006). In addition, I report fewer *Nyx*^{nob} RGCs with rhythmic spiking (61%) than the 80% reported previously in MEA recordings (Demas et al., 2006). My data are the first *in vitro* whole-cell patch clamp recordings from *mGluR6*^{-/-} and *Nyx*^{nob} RGCs and therefore, the discrepancy between my data and previous publications may be due to the difference in recording techniques.

The *mGluR6*^{-/-} RGC population increased 3-fold in rhythmicity from 12.5 to 40% when measuring rhythmic spiking compared to membrane oscillations, while the *Nyx*^{nob} RGC population increased 4-fold in rhythmicity from 61% to 96%. This means that *Nyx*^{nob} RGCs increased in the number of RGCs with rhythmicity even more than *mGluR6*^{-/-} when comparing rhythmic spiking to membrane oscillations. My results demonstrate that the increase in *Nyx*^{nob} RGC rhythmic spiking compared to membrane oscillations was due to the individual RGCs spontaneous activity rate. However, spontaneous activity rate could not account for the difference in rhythmic spiking/non-rhythmic spiking of *mGluR6*^{-/-} RGCs.

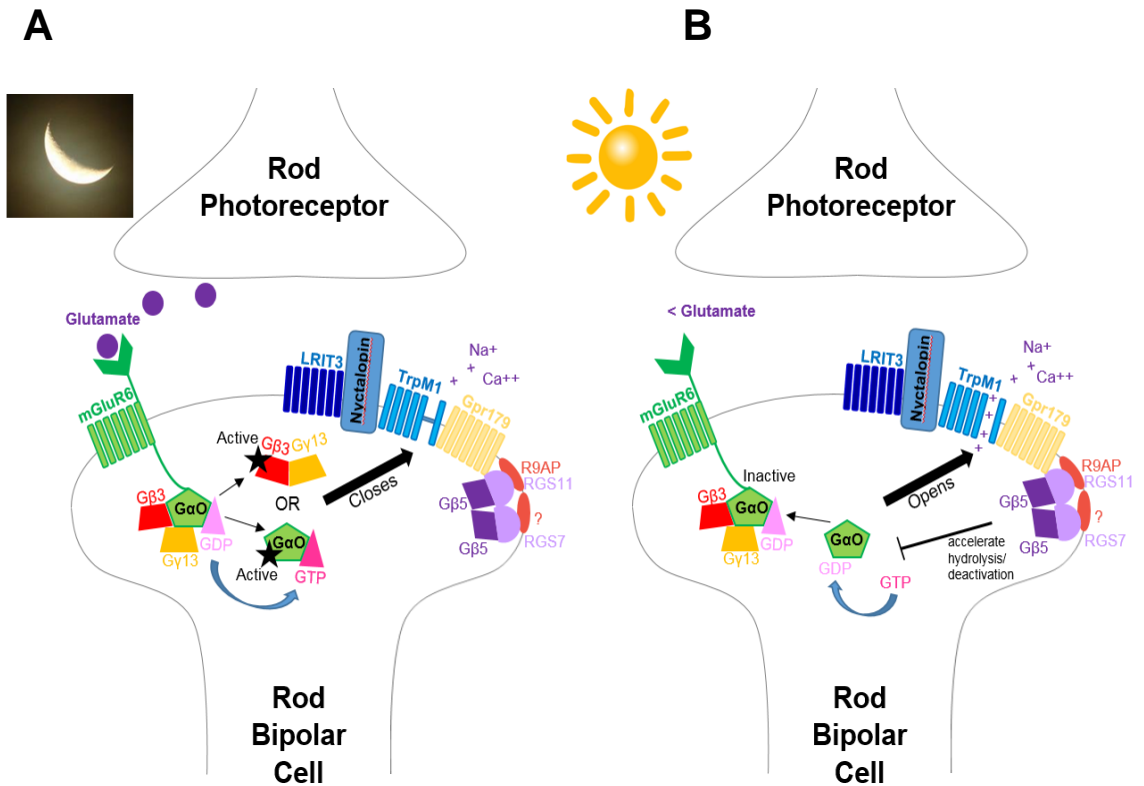
Since none of the properties I have examined in *mGluR6*^{-/-} RGCs appear to explain the difference in rhythmic spiking and non-rhythmic spiking RGCs across all RGC classes, there must be another source of the alteration. In the next chapter, I explore the possibility that these phenotypic differences result from differential alterations in the upstream rod BCs. Rod BCs provide input into both On and Off pathways and therefore could be responsible for the downstream effects seen in all RGC classes.

CHAPTER IV

COMPARISON OF *Nyx^{nob}* AND *mGluR6^{-/-}* ROD BCS

Introduction

The complete mGluR6 G-protein coupled cascade is not yet determined, however the current hypothesis is that in the dark glutamate binds mGluR6, which activates a trimeric G-protein complex (Vardi et al., 1993; Nawy 1999; Dhingra et al., 2000) leading to the closure of the TRPM1 channel (Replication of Figure 7 below). Nyctalopin, a leucine rich repeat protein, is critical for the proper trafficking or localization of TRPM1 (Gregg et al., 2003; Pearring et al., 2011).



Replication of Figure 7. A. In the dark glutamate is released from rods and binds mGluR6. mGluR6 activates a trimeric G-protein complex, G₀ (Vardi et al., 1993; Nawy 1999; Dhingra et al., 2000). The trimeric G-proteins are activated when GDP is exchanged for GTP on Gα₀, which dissociates into Gα₀-GTP (Vardi et al., 1993; Nawy 1999; Dhingra et al., 2000) and the dimer Gβ₃/Gγ₁₃ (Dhingra et al., 2012; Huang et al., 2003). The activated G-protein complex leads to the closure of the non-selective cation channel, TRPM1, and relative hyperpolarization of the rod BC, either through interaction with Gα₀-GTP and/or Gβ₃/Gγ₁₃ or another intermediate effector not yet identified. B. In the light glutamate release is decreased and no longer binds mGluR6. Hydrolysis of GTP into guanine dinucleotide (GDP) forms the inactive state of Gα₀ (Gα₀-GDP; Hooks et al., 2003)

which recombines with G β 3 and G γ 13 to form the trimeric G-protein complex. RGS7 and RGS11, regulator of G-protein signaling (RGS) proteins (Cao et al., 2012; Shim et al., 2012), form heterodimers with G β 5 (Rao et al., 2007). These heterodimers are GTPase-activating protein (GAP) complexes, which accelerate the hydrolysis of GTP to GDP by G α_0 , (Hooks et al., 2003; Rao et al., 2007), resulting in accelerated deactivation of the G-protein and culminates in the opening of TRPM1 and depolarization of the BC (Audo et al., 2009; Li et al., 2009; Morgans et al., 2009, 2010; Shen et al., 2009; Koike et al., 2010; Peachey et al., 2012a). R9AP is a membrane anchor protein for RGS11 and critical for its proper localization in the membrane at the dendritic tips (Jeffrey et al., 2010); nyctalopin, a leucine-rich repeat protein is critical for proper trafficking or localization of TRPM1 (Gregg et al., 2003; Pearing et al., 2011); GPR179 is required for proper dendritic tip localization of RGS7 and RGS11 (Orlandi et al., 2012) and LRIT3 is critical for rod BC light-mediated response (Zeitz et al., 2013; Neuille et al., 2014).

In all identified cCSNB mutants, the no b-wave (nob) ERG phenotype is associated with mutations in the mGluR6 receptor, elements of the G-protein cascade (G α_0 , G β 5, RGS7/RGS11), nyctalopin or TRPM1. There are currently twelve no b-wave mutants that have been identified (Pardue & Peachey, 2014; Zeitz et al., 2013).

Among them *Nyx^{nob}* and *mGluR6^{-/-}* mice have similar no b-wave ERG phenotypes (Masu et al., 1995; Pardue et al., 1998), however they differ in the downstream signaling within their RGCs. Namely, almost all *Nyx^{nob}* RGCs exhibit unique 2-5 Hz rhythmic spiking in their spontaneous activity (Demas et al., 2006; Chapter III). In contrast, *mGluR6^{-/-}* RGCs have spontaneous activity, but rarely have rhythmic spiking (Renteria et al., 2006; Chapter III). While the observation is robust, the mechanism that results in the presence or absence of oscillations in these two mutants is unclear.

There are additional differences between *Nyx^{nob}* and *mGluR6^{-/-}*. Specifically, *mGluR6^{-/-}* On cone BCs have ectopic expression of mGluR7 at their dendritic tips (Tagawa et al., 1999; Tsukamoto et al., 2007), while this has not been explored in *Nyx^{nob}* On cone BCs (Pardue et al., 1998; Pardue et al., 2001; Ball et al., 2003). In the *mGluR6^{-/-}* mGluR6 expression is eliminated. This also leads to the absence of TRPM1 expression as well as a few other mGluR6 G-protein cascade-mediating proteins (Table 2). In the *Nyx^{nob}* retina, where nyctalopin expression is absent, TRPM1 channel expression is absent on the dendritic tips (Table 2). One similarity between *mGluR6^{-/-}* and *Nyx^{nob}* rod BCs is that they lack expression of TRPM1 channels on their dendritic tips (Table 2; Cao et al., 2011; Pearring et al., 2011; Xu et al., 2011).

	mGluR6	TRPM1	Nyctalopin	Gpr179	RGS7	RGS11	G γ 13	G β 5	G β 3	G α_0
Nyx^{nob}	+	-	-	+	+	+	?	+	?	?
mGluR6^{-/-}	-	-	+	+	-	-	+	-	+	+

Table 2. Presence or absence of properly localized proteins in *Nyx^{nob}* and *mGluR6^{-/-}* rod BCs (Ball et al., 2003; Cao et al., 2011; Xu et al., 2011; Pearing et al., 2011; Gregg lab, unpublished observations).

Two mouse models of retinitis pigmentosa, *rd1* and *rd10*, where rods and then cones degenerate, exhibit rhythmic spontaneous spiking activity of RGCs (Blanks et al., 1974; Carter-Dawson et al., 1978; Marc et al., 2007; Ye & Goo 2007 (*rd1*); Margolis et al., 2008 (*rd1*); Stasheff, 2008 (*rd1*); Borowska et al., 2011(*rd1*); Stasheff et al., 2011 (*rd1* & *rd10*); Menzler & Zeck, 2011 (*rd1*); Trenholm et al., 2012 (*rd1*); Menzler et al., 2014 (*rd1* & *rd10*)). In the *rd* retina, the following two mechanisms have been proposed to account for the oscillations: 1) The network of gap junction-coupled All ACs and On cone BCs are the synaptic drive which underlies the RGC bursting (Borowska et al., 2011; Menzler & Zeck, 2011; Trenholm et al., 2012) and 2) Oscillations in the *rd1* retina reflect intrinsic bursting of Alls that are directly relayed to the RGCs rather than emerging from the gap-junction-coupled network (Choi et al., 2014). This intrinsic rhythmic property of All ACs is unmasked by hyperpolarization of *rd1* All ACs when synaptic input is reduced due to photoreceptor degeneration (Choi et al., 2014). While there are differences between *rd* and cCSNB models, which were

reported in Chapter III, it is possible that they share similar underlying mechanisms, which result in RGC oscillations.

Spontaneous activity in RGCs is influenced by synaptic input from the rod BC pathway. The RGC oscillations occur in the spontaneous activity of all *Nyx^{nob}* RGC classes. The only common element in the RGCs upstream input are rod BCs, via All ACs. The question is why the All AC becomes hyperpolarized in rd1 and most likely in *Nyx^{nob}*. My hypothesis is that there is a change in the resting output of the *Nyx^{nob}* rod BCs. Since rod BCs provide excitatory synaptic inputs to All ACs (Famiglietti & Kolb, 1975; Dacheux & Raviola, 1986), a difference in the rod BC membrane properties (between *mGluR6^{-/-}* and *Nyx^{nob}*) could alter their glutamate release and produce a change in the resting membrane potential of the All and a difference in the All AC output to the rest of the retinal circuit. To test this hypothesis, I compared the resting membrane properties of *Nyx^{nob}* to *mGluR6^{-/-}* rod BCs, which share an absence of light-evoked responses, but do not share RGC oscillatory responses (Chapter III).

I examined basic membrane properties of rod BCs in WT, *Nyx^{nob}* and *mGluR6^{-/-}* mice to determine if there were correlations between the intrinsic properties of *Nyx^{nob}* and *mGluR6^{-/-}* rod BCs and the downstream differences in rhythmic RGC spontaneous activity. In most neurons I measured V_{rest} , as well as the characteristics of different types of potassium currents in WT, *Nyx^{nob}* and *mGluR6^{-/-}* rod BCs. I also measured the input conductance of rod BCs in the three mouse strains, because input conductance can be used as a relative

estimate of the number of open channels. In rod BCs at rest and when glutamate occupancy is high (in the dark) the leak channels, which are potassium channels that maintain V_{rest} , are open. Therefore, changes in input conductance directly evaluate this property of the cell's membrane.

I focused on voltage dependent potassium channels (Kv) because potassium channels generate the leak currents that provide hyperpolarizing contributions to the resting membrane potential in many neurons (V_{rest} ; Hodgkin & Horowicz, 1959), although contributions from tonic excitatory and inhibitory inputs also play a role (Kuffler, et al., 1957; Frishman & Levine, 1983; Margolis & Detwiler, 2007). Also, I focused on voltage dependent potassium channels (Kv) because of the known expression of Kv1.1, 1.2, 1.3 and 11.1 in rod BCs (Kaneko et al., 1989; Karschin and Wassle 1990; Klumpp et al., 1995a; Pinto & Klumpp, 1998; Hu & Pan, 2002; Cordeiro et al., 2011; Larsen et al., 2010). My results show that V_{rest} in *Nyx^{nob}* rod BCs is more depolarized relative to WT and *mGluR6^{-/-}* rod BCs. The *Nyx^{nob}* rod BCs also have a smaller potassium conductance compared to *mGluR6^{-/-}* and WT rod BCs.

Materials and Methods

Rod BC Whole Cell Patch Clamp Protocols

Current Clamp

The resting membrane potential (V_{rest}) for each rod BC was measured in whole cell patch clamp current clamp mode using glass pipettes filled with K-gluconate intracellular solution (containing in mM: 120 K-gluconate, 1 $CaCl_2$, 1 $MgCl_2$, 10 Na-HEPES, 11 EGTA, 4 ATP, 1 GTP and 1% sulforhodamine). Rod BC V_{rest} was recorded with a holding current of 0 pA and the mean potential was taken across the first second of recording. V_{rest} was measured under dark- and light-adapted conditions.

Capsaicin Pressure Application

The TRPM1 channel agonist, Capsaicin (10 μ M), was applied by pressure application using a Picospritzer II (Parker Instrumentation) onto the center of the recorded rod BC soma followed by the rod BC dendritic tips. Puffs were applied with the following durations (in order): 25 msec, 50 msec, 100 msec, and 200 msec at both the cell soma and dendritic tips. Capsaicin was purchased from Tocris Bioscience.

Voltage Clamp Protocols

Current/Voltage (I/V)

For each rod BC, an I/V protocol was recorded in voltage clamp mode under light-adapted conditions using K-gluconate intracellular solution (described above) to maintain normal ion concentrations within the cell. Alternatively, a Cs-gluconate-TEA intracellular solution (containing in mM: 20 CsCl, 107 CsOH, 107 D-Gluconic Acid, 10 Na⁺ HEPES, 10 BAPTA, 10 TEA and 1% sulforhodamine) was used to block potassium currents in the cell. The membrane potential of each rod BC was held at either -85mV or -55mV and voltage steps were applied from -115 to +35 mV in 10mV increments. Depolarizing voltage steps from very negative holding potentials (-85mV) activate both transient and delayed-rectifying potassium currents, while voltage steps from more positive holding potentials (-55mV) completely inactivate all transient channels while leaving delayed-rectifying currents intact (Walz, 2000). Each step lasted four seconds and the membrane potential was returned to the starting potential, either -85mV or -55mV. The response to the voltage step was analyzed at: its peak amplitude, at the beginning of each step (defined as the peak between the capacitive artifact and .3 seconds) and at the steady-state mean amplitude, at the end of each step (defined as the mean between time 3.9 and 4 seconds; Clampfit 10.2 software). The responses were plotted as I/V curves, which were compared across genotypes for responses with the different intracellular solutions to isolate Cs-

TEA-sensitive K⁺ currents and for responses at the two holding potentials (-55mV and -85mV) to isolate transient K⁺ currents (Walz, 2000; Prism 5.04 software).

Input Conductance

Rod BC input conductance was measured under dark-adapted conditions and evaluated by calculating the slope conductance from the steady-state K-Gluconate I/V protocols between the two data points which incorporate V_{rest} of the rod BCs (-55mV and -35mV). The slopes were compared between WT and *Nyx^{nob}* and WT and *mGluR6^{-/-}*. A significant difference in slope measured by a linear regression ($P < 0.05$) indicates a significant difference in input conductance.

Statistical Analysis

One-way ANOVA with Bonferroni post hoc, Kruskal-Wallis with Dunns post hoc, Two-way ANOVA with Bonferroni post hoc, Mann-Whitney or unpaired t-tests were used as the statistical analyses. Post hoc P values are reported. Analyses were performed in Prism 5.04.

Results

Nyx^{nob} Rod BC Resting Membrane Potential Is Depolarized Compared to WT and mGluR6^{-/-}

Within each genotype the V_{rest} of *Nyx^{nob}*, *mGluR6^{-/-}* and WT rod BCs under light- and dark-adapted conditions were the same (Figure 19; Two-way ANOVA with Bonferroni post hoc: dark v light: WT; *Nyx^{nob}*; *mGluR6^{-/-}*: $P > 0.05$ for all). As expected this result suggests that adaptation level does not influence V_{rest} . My WT rod BC V_{rest} mean of -49.82mV was very similar to a previous report of -49.5mV (Borowska et al., 2011). The mean V_{rest} of *Nyx^{nob}* rod BCs in the light-adapted retinal slice was significantly more depolarized compared to WT and *mGluR6^{-/-}* rod BCs (Figure 19A; *Nyx^{nob}* -46.27mV \pm 1.16; WT -49.82mV \pm 1.55; *mGluR6^{-/-}* -53.13mV \pm 1.48; Kruskal-Wallis with Dunns post hoc: WT v. *Nyx^{nob}*: $P < 0.05$; *Nyx^{nob}* v. *mGluR6^{-/-}*: $P < 0.001$). In contrast, the mean V_{rest} of WT and *mGluR6^{-/-}* rod BC were similar (Kruskal-Wallis with Dunns post hoc: WT v. *mGluR6^{-/-}*: $P > 0.05$). I found the same results under dark-adapted conditions. Again, mean V_{rest} of *Nyx^{nob}* rod BCs was significantly more depolarized than WT and *mGluR6^{-/-}* rod BCs (Figure 19B; *Nyx^{nob}* -43.20mV \pm 1.36; WT -50.82mV \pm 1.24; *mGluR6^{-/-}* -51.43mV \pm 0.92; Kruskal-Wallis with Dunns post hoc: WT v. *Nyx^{nob}* $P < 0.001$; *Nyx^{nob}* v. *mGluR6^{-/-}*: $P < 0.001$) and WT and *mGluR6^{-/-}* rod BCs were similar (Kruskal-Wallis with Dunns post hoc: WT v. *mGluR6^{-/-}*: $P > 0.05$).

This difference in V_{rest} between Nyx^{nob} and $mGluR6^{-/-}$ suggests a change in the mechanism that sets the resting membrane potential in Nyx^{nob} rod BCs.

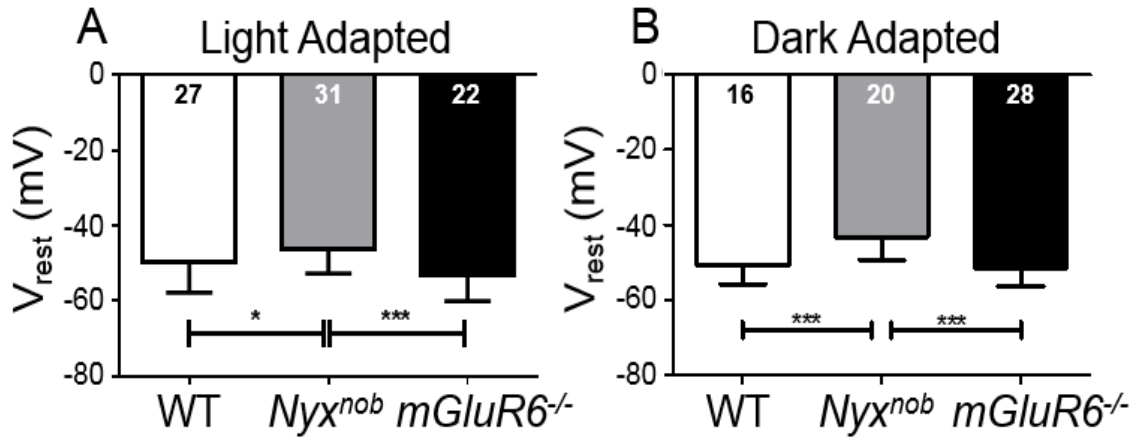


Figure 19. Nyx^{nob} rod BC V_{rest} is more depolarized than WT and $mGluR6^{-/-}$. A. Histogram compares the average V_{rest} (\pm SEM) of WT, Nyx^{nob} , and $mGluR6^{-/-}$ rod BCs under light-adapted conditions. Nyx^{nob} rod BC V_{rest} is significantly more depolarized than WT or $mGluR6^{-/-}$ rod BCs. V_{rest} from WT and $mGluR6^{-/-}$ rod BCs are the same. B. Histogram compares the average V_{rest} (\pm SEM) of WT, Nyx^{nob} , and $mGluR6^{-/-}$ rod BCs under dark-adapted conditions. Nyx^{nob} rod BC V_{rest} is significantly more depolarized than WT or $mGluR6^{-/-}$ rod BCs. V_{rest} from WT and $mGluR6^{-/-}$ rod BCs are the same. There are no significant differences for any of the genotypes between light and dark-adapted conditions. The number of rod BCs in each experimental group is shown within each bar of the histograms (Kruskal-Wallis with Dunns post hoc; * $P < 0.05$; *** $P < 0.001$).

Nyx^{nob} Rod BCs Do Not Exhibit Functional TRPM1 Channels

A more depolarized V_{rest} in *Nyx^{nob}* rod BCs could result from a difference in tonic input (opened TRPM1 channels) or in constitutively closed potassium channels. A contribution from TRPM1 channels is unlikely given its mislocalization to the soma of the *Nyx^{nob}* rod BCs and that TRPM1 is likely confined within an intracellular compartment (Pearing et al., 2011). To be certain the *Nyx^{nob}* mislocalized TRPM1 cannot mediate current, I examined whether the TRPM1 channels could be gated by stimulation at either the dendrites or somata in *Nyx^{nob}* compared to WT rod BCs. I tried to directly gate the TRPM1 channel using exogenous application (puffs) of the TRPM1 channel agonist, capsaicin (10 μ M). In WT rod BCs, dendritic focused capsaicin puffs elicited robust responses at all puff durations tested (Figure 20 Ai). In *Nyx^{nob}* rod BCs, dendritic focused capsaicin puffs only elicited very small current responses to long duration puffs. I have reported previously that these responses are likely mediated via an unknown capsaicin-mediated channel that I also have recorded in *Trpm1^{-/-}* rod BCs (Ray et al., 2014; Chapter V, Figure 26). In WT rod BCs, soma focused capsaicin puffs elicited responses only with long duration puffs (200msec; Figure 20Bi). The WT soma focused puffs resulted in an increased time-to-peak of response compared to dendritic focused puffs (t-test: 50msec puffs: soma v. dendrite: $P = 0.03$; soma TTP: 0.56 ± 0.09 ; dendrite TTP: 0.30 ± 0.05 ; all other puff durations follow the same trend; data not shown). This increase in response time-to-peak likely represents diffusion of the agonist to

TRPM1 channels located at the dendritic tips. In *Nyx^{nob}* rod BCs, soma focused capsaicin puffs only elicited very small currents at all puff durations, similar to the small currents seen with *Nyx^{nob}* and *Trpm1^{-/-}* dendritic focused puffs (Chapter IV, Figure 26), which are likely mediated by an unknown channel (Ray et al., 2014). These results demonstrate that mislocalized TRPM1 protein found in *Nyx^{nob}* rod BCs is not expressed in the membrane and support the idea that these TRPM1 channels are not functional (Pearing et al., 2011). Most importantly, these results eliminate a role for constitutively open TRPM1 channels in the depolarized V_{rest} in *Nyx^{nob}* rod BCs.

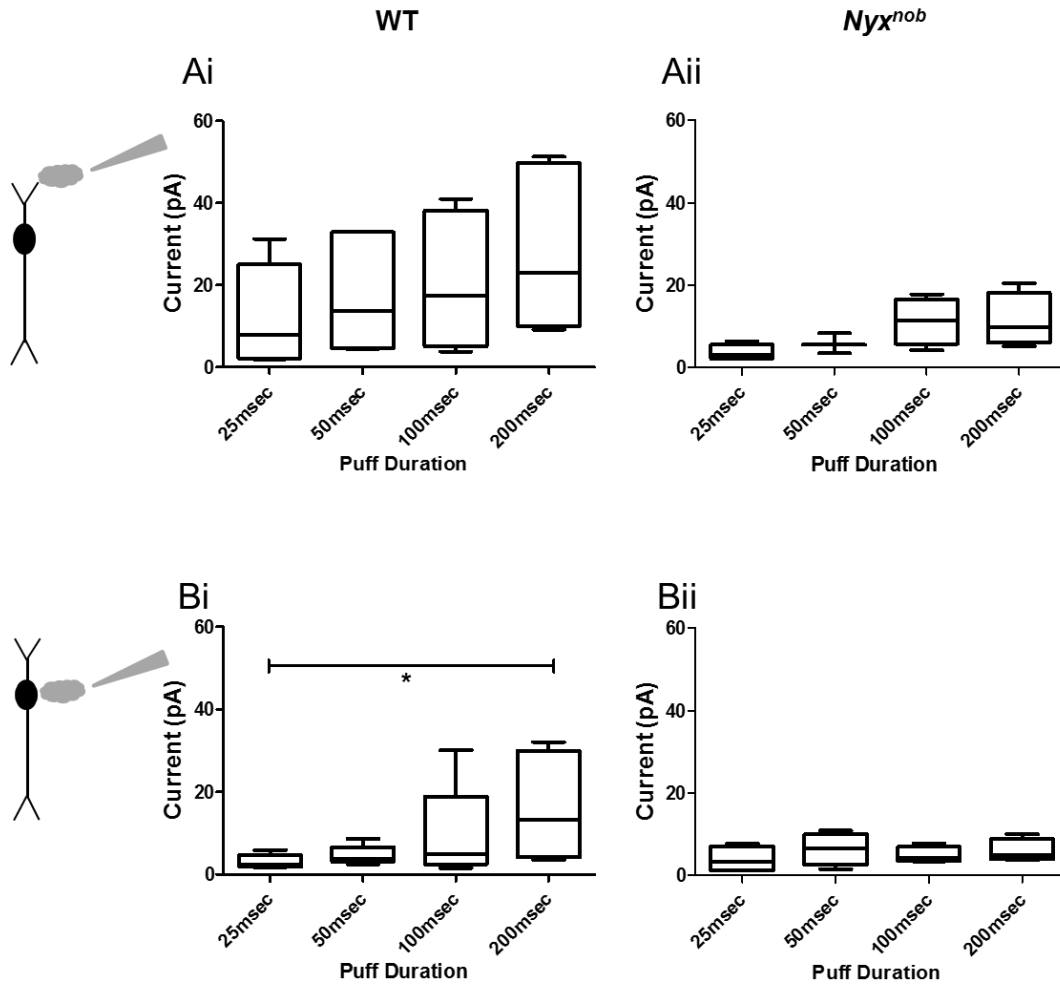


Figure 20. *Nyx^{nob}* rod BCs do not exhibit TRPM1-mediated currents at dendritic tips nor soma. Ai. Dendritic focused Capsaicin evoked robust TRPM1-mediated currents in WT rod BCs with all puff durations (25 msec, 50msec, 100msec, and 200msec). Aii. Dendritic focused Capsaicin did not evoke TRPM1-mediated currents in *Nyx^{nob}* rod BCs at any puff duration. Bi. Soma focused Capsaicin evoked TRPM1-mediated currents in WT rod BCs with longer 200msec puffs, but not with short 25 msec puffs (Mann-Whitney: * $P < 0.05$). This response to long duration puff is likely due to diffusion of the capsaicin from the soma to the

dendrites. Bii. Soma focused Capsaicin did not evoke TRPM1-mediated currents in *Nyx^{nob}* rod BCs at any puff duration.

Nyx^{nob} Rod BCs Have Smaller Potassium Currents than WT and mGluR6^{-/-}

Closure or elimination of potassium channels that represent the leak current in rod BCs could cause a more depolarized V_{rest} in *Nyx^{nob}* rod BCs. To characterize potassium channels in rod BCs, I measured the current/voltage (I/V) relationship under control conditions with the potassium conductance intact and compared them to when intracellular Cs/TEA blocked potassium conductance across the three genotypes.

With the potassium conductance intact, the I/V curves of WT *mGluR6^{-/-}*, and *Nyx^{nob}* rod BCs were outwardly rectifying (Figure 21Ai). Outwardly rectifying currents are characteristic of voltage-gated potassium currents and are defined by the characteristic in which more current passes out of the cell than into the cell (Klumpp et al., 1995a; Walz et al., 2002; Hu & Pan, 2002). For rod BCs across genotype, each voltage step evoked a current response that had a transient peak as well as a steady-state component (Figure 21Ai). The peak outward current of *Nyx^{nob}* rod BCs was significantly smaller than WT or *mGluR6^{-/-}* rod BCs at positive step potentials above -5mV (Figure 21Aiii; Two-way ANOVA with Bonferroni post hoc: $P < 0.001$; all values $\geq -5\text{mV}$ are $P < 0.05$). As a consequence, the slope of the linear region of the I/V curve for *Nyx^{nob}* rod BCs

was significantly smaller than WT or *mGluR6*^{-/-}, while WT and *mGluR6*^{-/-} slopes did not differ (linear regression-comparison of slopes: *Nyx*^{nob} v. WT: $P = 0.005$; *Nyx*^{nob} v. *mGluR6*^{-/-}: $P = 0.00002$; WT v. *mGluR6*^{-/-}: $P > 0.05$).

Similarly, the steady-state component of *Nyx*^{nob} rod BC response was significantly smaller than WT and *mGluR6*^{-/-} rod BCs at positive step potentials above -5mV (Figure 21Aiii; Two-way ANOVA with Bonferroni post hoc: $P < 0.0001$; $\geq -5\text{mV}$, $P < 0.05$). The slope of the linear region of the steady-state measure of *Nyx*^{nob} rod BCs I/V curve also differed significantly from WT and *mGluR6*^{-/-} (linear regression-comparison of slopes: *Nyx*^{nob} v. WT: $P = 0.0137$; *Nyx*^{nob} v. *mGluR6*^{-/-}: $P < 0.0001$). Both the peak and the steady-state I/V curves of *mGluR6*^{-/-} and WT rod BC overlapped (Figure 21Aiii, 21Aiiii). The smaller transient peak and steady-state potassium channel conductance in *Nyx*^{nob} rod BCs, compared to *mGluR6*^{-/-} and WT indicates a smaller potassium conductance, consistent with a more depolarized V_{rest} in *Nyx*^{nob} rod BCs.

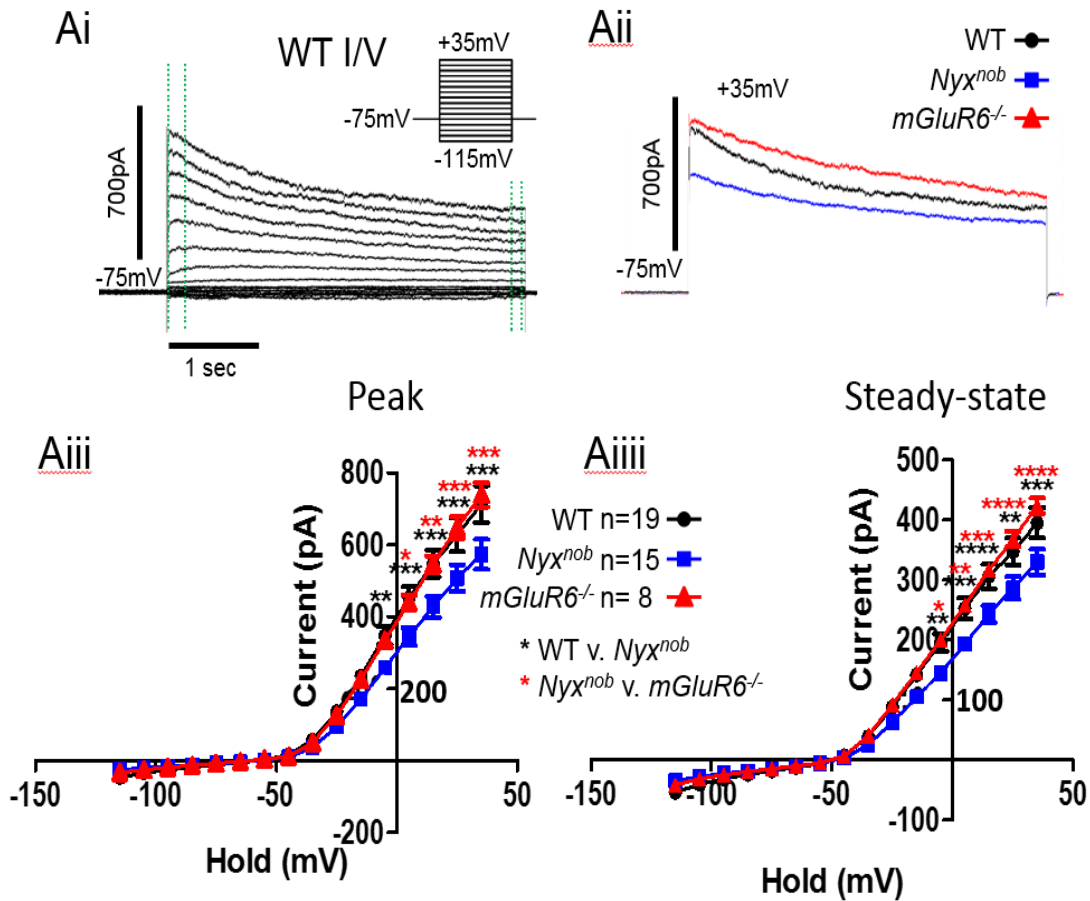


Figure 21. Transient peak and steady-state potassium current components were decreased in amplitude in *Nyx^{nob}* rod BCs compared to WT or *mGluR6^{-/-}*. Ai. Representative current responses evoked by voltage steps in a WT rod BC. Green dotted lines represent the two regions of the response used to measure peak amplitude and steady-state currents. The upper right corner displays the voltage steps that evoked the responses. Aii. Representative responses from I/V protocol recordings at +35mV step for WT, *Nyx^{nob}*, and *mGluR6^{-/-}* rod BCs. Aiii. Mean population data (\pm SEM) of peak amplitude plotted as a function of voltage step for WT, *Nyx^{nob}*, and *mGluR6^{-/-}* rod BCs. The peak outward current of *Nyx^{nob}*

rod BCs was significantly smaller than WT and *mGluR6*^{-/-} rod BCs at positive step potentials above -5mV (Two-way ANOVA with Bonferroni post hoc: $P < .001$; all values $\geq -5\text{mV}$ are $P < 0.05$). WT and *mGluR6*^{-/-} rod BC I/Vs were similar. Aiiii. Mean population data (\pm SEM) of steady-state current plotted as a function of step potential for WT, *Nyx*^{nob}, and *mGluR6*^{-/-} rod BCs. The steady-state component of *Nyx*^{nob} rod BCs was significantly smaller than WT and *mGluR6*^{-/-} rod BCs at positive step potentials above -5mV (Two-way ANOVA with Bonferroni post hoc: $P < .0001$; all values $\geq -5\text{mV}$ are $P < 0.05$). WT and *mGluR6*^{-/-} rod BC I/Vs were similar (* $P < 0.05$; ** $P < 0.01$; *** $P < 0.001$; **** $P < 0.0001$).

To confirm that these changes in the current were the result of potassium channels, I intracellularly blocked both Cesium (Cs) and TEA-sensitive potassium channels. In rod BCs across all genotypes the elimination of Cs/TEA-sensitive potassium conductance significantly reduced the outward peak and steady-state currents at positive holding potentials (Figure 22; Table 3; CS/TEA vs. K peak: Two-way ANOVA with Bonferroni post hoc: Table 3; CS/TEA vs. K steady-state: Two-way ANOVA with Bonferroni post hoc: Table 3). Since calcium channels are intact, a small transient inward calcium current can be seen as a dip in the I/V curve between -55mV and -35mV (Figure 22Aii). The elimination of the Cs/TEA-sensitive potassium channel mediated response resulted in similar

peak and steady-state rod BC responses across genotypes (Figure 22Aiii, Aiiii; Two-way ANOVA with Bonferroni post hoc: all comparisons $P > 0.05$). These results demonstrate that *Nyx^{nob}* rod BCs have a smaller Cs/TEA-sensitive potassium conductance compared to WT and *mGluR6^{-/-}* rod BCs.

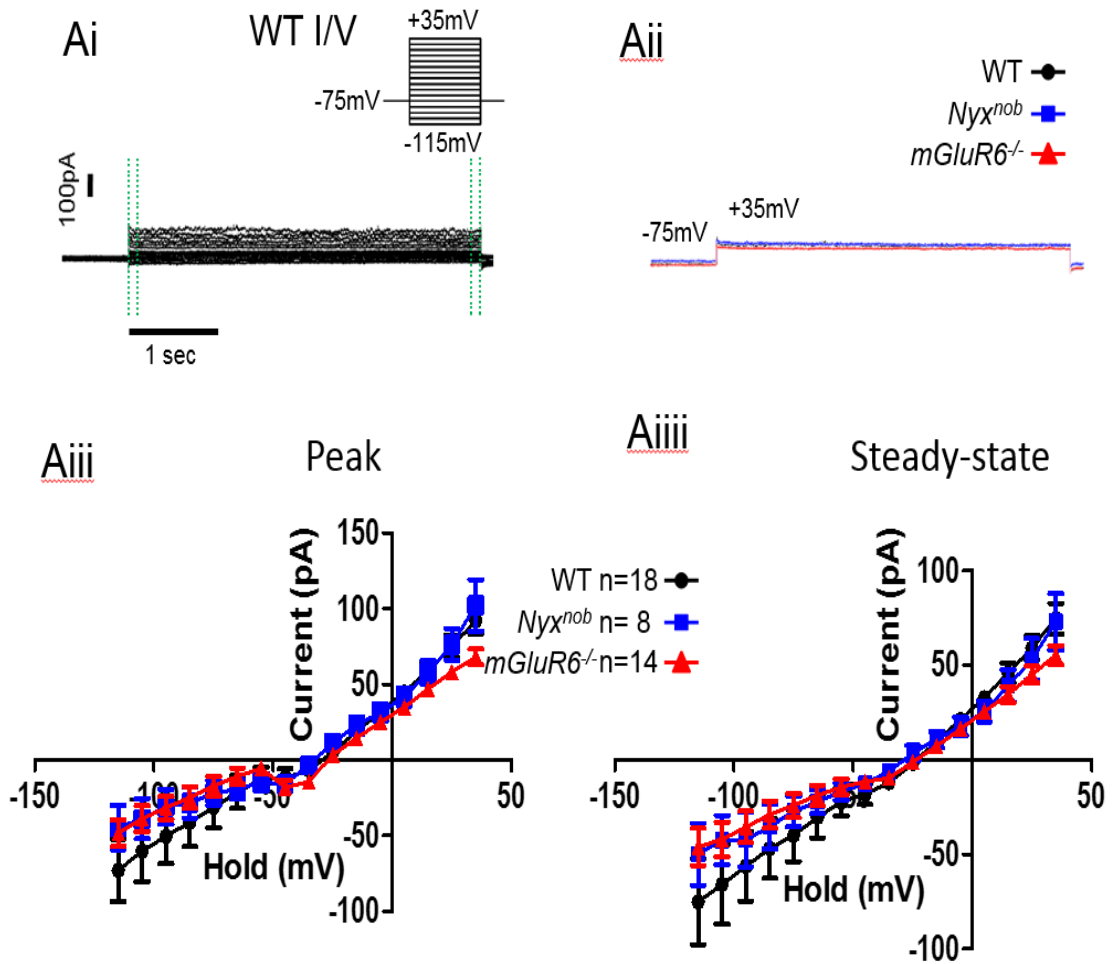


Figure 22. Transient peak and steady-state components of the Cs/TEA-insensitive currents were similar in WT, *Nyx^{nob}* and *mGluR6^{-/-}* rod BCs. Ai. A representative I/V protocol recording from a WT rod BC. Green dotted lines represent the two regions of recordings used to measure peak amplitude and steady-state currents. The upper right corner displays the voltage stimulus provided to the rod BCs. Aii. Representative traces from I/V protocol recordings at +35mV sweep for WT, *Nyx^{nob}*, and *mGluR6^{-/-}* rod BCs. Aiii. Mean population data (\pm SEM) of peak amplitude plotted as a function of step potential for WT,

Nyx^{nob}, and *mGluR6^{-/-}* rod BCs. The peak outward current of WT, *Nyx^{nob}* and *mGluR6^{-/-}* rod BCs were similar at all step potentials (Two-way ANOVA with Bonferroni post hoc: all comparisons $P > .05$). Aiii. Mean population data (\pm SEM) of steady-state current plotted as a function of step potential for WT, *Nyx^{nob}*, and *mGluR6^{-/-}* rod BCs. The steady-state current of WT, *Nyx^{nob}* and *mGluR6^{-/-}* rod BCs were similar at all step potentials (Two-way ANOVA with Bonferroni post hoc: all comparisons $P > .05$). Note the difference in Y-axis scale for Figure 14Aiii, Aiii and Figure 13Aiii,Aiii.

	-35mV	-25mV	-15mV	-5mV	5mV	15mV	25mV	35mV
CS/TEA v. K Peak WT		P < 0.0001	P < 0.0001	P < 0.0001	P < 0.0001	P < 0.0001	P < 0.0001	P < 0.0001
CS/TEA v. K Peak <i>Nyx^{nob}</i>		P < 0.05	P < 0.0001	P < 0.0001	P < 0.0001	P < 0.0001	P < 0.0001	P < 0.0001
CS/TEA v. K Peak <i>mGluR6^{-/-}</i>	P < 0.0001	P < 0.0001	P < 0.0001	P < 0.0001	P < 0.0001	P < 0.0001	P < 0.0001	P < 0.0001
CS/TEA vs. K steady-state WT	P < 0.05	P < 0.05	P < 0.05	P < 0.05	P < 0.05	P < 0.05	P < 0.05	P < 0.05
CS/TEA vs. K steady-state <i>Nyx^{nob}</i>		P < 0.001	P < 0.001	P < 0.001	P < 0.001	P < 0.001	P < 0.001	P < 0.001
CS/TEA vs. K steady-state <i>mGluR6^{-/-}</i>	P < 0.0001	P < 0.0001	P < 0.0001	P < 0.0001	P < 0.0001	P < 0.0001	P < 0.0001	P < 0.0001

Table 3. In rod BCs of all genotypes the elimination of Cs/TEA-sensitive potassium conductance significantly reduced the outward current in the I/V curves across all peak and steady-state responses at more positive holding potentials. The P values for every statistical comparison is presented. (CS/TEA vs. K peak: Two-way ANOVA with Bonferroni post hoc; CS/TEA vs. K steady-state: Two-way ANOVA with Bonferroni post hoc).

Nyx^{nob} Rod BCs have Smaller Transient Potassium Currents Compared to WT or mGluR6^{-/-}

There are several classes of Cs and TEA-sensitive potassium channels. The shape of the I/V evoked currents in WT rod BCs appears to be a

combination of transient and persistent potassium currents, which likely correspond to two different potassium channel classes. Depolarizing voltage steps from very negative holding potentials (-85mV) activate both transient and delayed-rectifying potassium currents (Walz, 2000), while voltage steps from more positive holding potentials (-55mV) completely inactivate all transient channels, leaving delayed-rectifying currents intact (Walz, 2000). To examine whether one or both of these types of currents were altered in *Nyx^{nob}* rod BCs, I applied depolarizing voltage steps from positive holding potentials (-55mV holding) to inactivate transient type channels and isolate the delayed-rectifier current (persistent currents; Walz et al., 2002). The persistent potassium currents, measured at the steady-state component of the response, were similar across all genotypes (Figure 23Ai, Aii; Two-way ANOVA with Bonferroni post hoc: all comparisons: $P > 0.05$), suggesting that they are unlikely to be related to the difference in V_{rest} .

To isolate the transient component of the current I subtracted the current evoked with $V_{hold} = -55mV$ (when the transient channel was inactivated and only the steady-state remained) from the current evoked with $V_{hold} = -85mV$ (Figure 23Bi, Bii; Walz et al., 2002). The peak of the transient type potassium current was significantly smaller in *Nyx^{nob}* rod BCs compared to WT and *mGluR6^{-/-}* (Figure 23Bi, Bii; Two-way ANOVA with Bonferroni post hoc: *Nyx^{nob}* vs. WT: -5mV: $P < 0.05$; 5mV: $P < 0.01$; 15mV: $P < 0.001$; 35mV: $P < 0.05$; *Nyx^{nob}* vs. *mGluR6^{-/-}*: 15mV and 25mV: $P < 0.05$; 35mV: $P < 0.001$). In contrast, the

transient type potassium current was similar in WT and *mGluR6*^{-/-} rod BCs (Two-way ANOVA with Bonferroni post hoc: WT v. *mGluR6*^{-/-}: $P > 0.05$). In conclusion, differences in both the V_{rest} and I/V curves of *Nyx*^{nob} rod BC compared to WT and *mGluR6*^{-/-} are consistent and suggest that transient type potassium channels are either decreased in number or in their open probability. Both would lead to a more depolarized V_{rest} in *Nyx*^{nob} rod BCs.

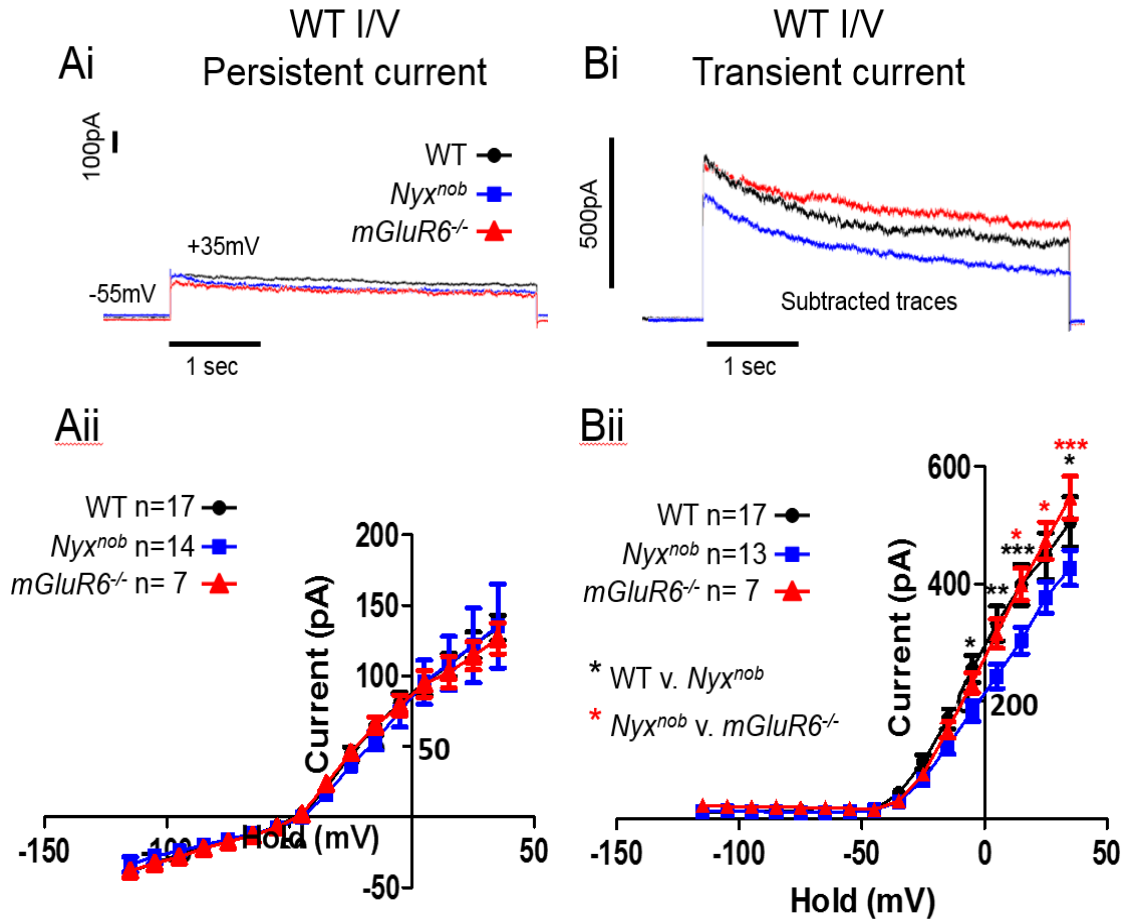


Figure 23. Transient but not persistent currents were decreased in *Nyx^{nob}* rod BCs compared to WT and *mGluR6^{-/-}*. Ai. Representative traces from I/V protocol recordings that isolate persistent currents at +35mV sweeps for WT, *Nyx^{nob}*, and *mGluR6^{-/-}* rod BCs. Bi. Representative traces from I/V protocol recordings that isolate transient currents at +35mV sweeps for WT, *Nyx^{nob}*, and *mGluR6^{-/-}* rod BCs. Aii. Mean population data (\pm SEM) of steady-state current plotted as a function of step potential for WT, *Nyx^{nob}*, and *mGluR6^{-/-}* rod BCs. The steady-state current of WT, *Nyx^{nob}* and *mGluR6^{-/-}* rod BCs were similar at all step potentials (Two-way ANOVA with Bonferroni post hoc: all comparisons $P > .05$).

Bii. Mean population data (\pm SEM) of peak current plotted as a function of step potential for WT, *Nyx^{nob}*, and *mGluR6^{-/-}* rod BCs. The peak current in *Nyx^{nob}* was significantly smaller compared to WT and *mGluR6^{-/-}* rod BCs (Two-way ANOVA with Bonferroni post hoc: *Nyx^{nob}* vs. WT: -5mV: $P < .05$; 5mV: $P < .01$; 15mV: $P < .001$; 35mV: $P < .05$; *Nyx^{nob}* vs. *mGluR6^{-/-}*: 15mV and 25mV: $P < .05$; 35mV: $P < .001$). The peak current was similar in WT and *mGluR6^{-/-}* (Two-way ANOVA with Bonferroni post hoc: WT v. *mGluR6^{-/-}*: $P > .05$; * $P < 0.05$; ** $P < 0.01$; *** $P < 0.001$).

Nyx^{nob}, mGluR6^{-/-} and WT Rod BCs Input Conductance are Similar

Input conductance can be used as a relative estimate of the number of open channels in a cell's membrane. I examined the input conductance by comparing the slope conductance close to V_{rest} (between -55mV and -35mV data points) from I/V curves recorded with K-Gluconate intracellular solution under dark-adapted conditions (Figure 24). I measured input conductance near V_{rest} in order to examine the resting state of rod BCs. I hypothesized that the input conductance of *Nyx^{nob}* rod BCs would be smaller than WT and *mGluR6^{-/-}* rod BCs, as a reflection of fewer open channels in *Nyx^{nob}* rod BC membrane. However, the input conductance of *Nyx^{nob}* rod BCs was similar to WT and *mGluR6^{-/-}* rod BCs, suggesting a similar number of open channels in the membrane (slope conductance: WT: 1.837 nS \pm 0.2375; *Nyx^{nob}*: 1.136 nS \pm

0.2639; *mGluR6*^{-/-}: 1.567 nS ± 0.1604; WT vs *Nyx*^{nob} $P = 0.076$; *Nyx*^{nob} vs *mGluR6*^{-/-}: $P = 0.162$; Figure 24). This result is inconsistent with the V_{rest} and I/V data and the differences between *Nyx*^{nob} and WT or *mGluR6*^{-/-} rod BCs. Future experiments are needed to address this discrepancy.

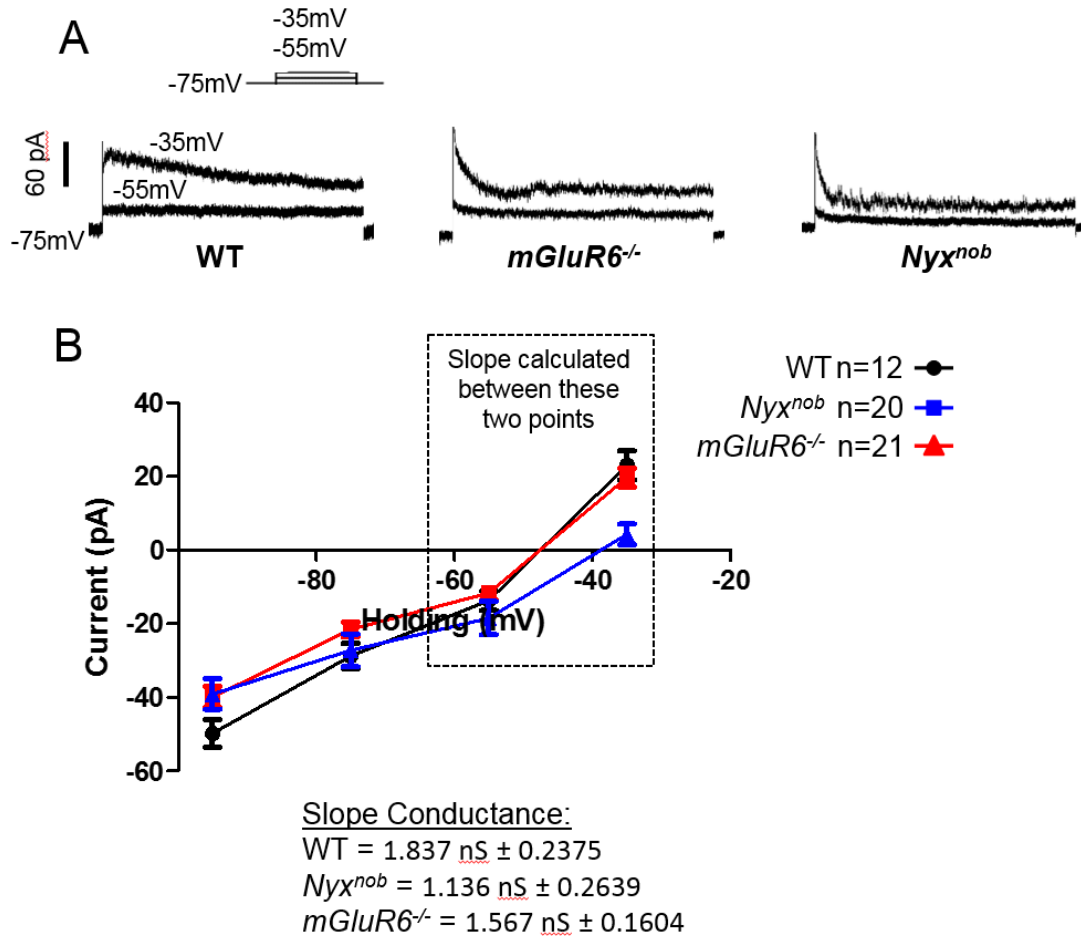


Figure 24. The input conductance of *Nyx^{nob}* rod BCs was similar to WT and *mGluR6^{-/-}* rod BCs. A. WT, *mGluR6^{-/-}*, and *Nyx^{nob}* rod BC recordings from holding potential of -85mV to voltage steps of -55mV and -35mV. B. Mean population data (\pm SEM) of steady-state current plotted as a function of step potential for WT, *Nyx^{nob}*, and *mGluR6^{-/-}* rod BCs recorded with K current intact (K-Gluconate intracellular solution). The input conductance was examined by comparison of the slope conductance close to V_{rest} (slope between -55mV and -35mV) across WT, *Nyx^{nob}* and *mGluR6^{-/-}* rod BCs. The input conductance of *Nyx^{nob}* rod BCs were similar to WT and *mGluR6^{-/-}* rod BCs (slope: WT: 1.837 nS \pm 0.2375;

Nyx^{nob}: 1.136 nS \pm 0.2639; *mGluR6^{-/-}*: 1.567 nS \pm 0.1604; WT vs *Nyx^{nob}*: $P = .0275$; *Nyx^{nob}* vs *mGluR6^{-/-}*: $P = 0.3626$).

Discussion

Nyx^{nob} rod BC V_{rest} was significantly more depolarized than WT and *mGluR6^{-/-}* rod BCs. The depolarization could result from either the opening of TRPM1 channels or the closure of potassium channels. The TRPM1 agonist, capsaicin, did not elicit responses when puffed onto the dendrites nor somata of *Nyx^{nob}* rod BCs, demonstrating that the depolarization is not due to opening of TRPM1 channels in the *Nyx^{nob}* rod BCs (Figure 20).

The voltage clamp recordings demonstrated a difference in an outward rectifying conductance in *Nyx^{nob}* rod BCs compared to WT and *mGluR6^{-/-}* rod BCs (Figure 21). Based on the pharmacological block of Cs/TEA-sensitive potassium currents, the results suggest *Nyx^{nob}* rod BCs exhibit altered potassium conductance (Figures 21, 22). Experiments to isolate candidate outward rectifying potassium channels suggest that transient-type potassium channels are altered in *Nyx^{nob}* rod BCs (Figure 23; Walz et al., 2002). Therefore, the depolarized V_{rest} of *Nyx^{nob}* rod BCs is not due to a change in TRPM1 channel modulation, but to smaller potassium channel conductance, which includes transient-type potassium channels.

Given *Nyx^{nob}* rod BCs have a V_{rest} that is more depolarized and have smaller potassium currents than WT and *mGluR6^{-/-}*, I anticipated a smaller *Nyx^{nob}* rod BC input conductance compared to WT and *mGluR6^{-/-}*. However, my data were not consistent with this hypothesis since their input conductances were statistically similar across genotypes. While there may be a trend for *Nyx^{nob}* rod BCs to have a smaller input conductance compared to WT and *mGluR6^{-/-}* rod BCs (Figure 24), the *P* value did not reach significance. There could be a technical reason that underlies this unexpected result related to the order and duration of the recordings. I measured V_{rest} immediately after initial whole cell break-in of the membrane, whereas the I/V protocol was performed approximately three minutes later. During this time the intracellular solution dialyzes the cell and can alter the cell's ion concentration thereby altering the inherent steady-state properties, which are influenced by the composition and concentration of ions. In future experiments, I will measure input conductance promptly following initial whole cell break-in of the rod BC membrane to determine if this could be the cause of the discrepancy in my results. I anticipate that future experiments will demonstrate a significantly smaller *Nyx^{nob}* rod BC input conductance compared to WT and *mGluR6^{-/-}*.

Nyx^{nob} rod BCs lack expression of the nyctalopin protein, which is critical for TRPM1 membrane localization (Pearing et al., 2011). Given the previously documented role of nyctalopin it was unexpected to find that nyctalopin would also affect potassium conductance. However, it has been reported that cCSNB

mice have decreased expression of other proteins in On BC dendritic tips, specifically the response-modulating proteins G β 5, RGS7, RGS11, R9AP, and GPR179 (Cao et al., 2009; Morgans et al., 2007; Xu et al., 2011; Ray et al., 2014). It is possible that the lack of nyctalopin or other cascade related proteins in *Nyx^{nob}* rod BCs lead to a down-regulation not only of cascade specific proteins, but others located at rod BC dendritic tips, such as potassium channels. In the absence of neuronal activity, channels such as A-type potassium channels, (Hoffman & Johnston, 1998), Kv4.2 (Shah et al., 2010), K_{Ca}2.2, and HCN (Wang et al., 2007) have been shown to be down-regulated (Shah et al., 2010). Activity-dependent regulation of channels is commonly found in neurons (Shah et al., 2010) and one of these mechanism may be at play in *Nyx^{nob}* rod BCs.

Some potassium channels have genetic sequences that cause them to associate with scaffolding proteins that have protein-interaction sequences, such as PDZ domains, which help cluster complexes together (Miller et al., 2000). This provides a mechanism to localize potassium channels to specific regions of the cell. It is possible that specific potassium channels bind to either nyctalopin or another associated scaffolding protein that is absent in *Nyx^{nob}* rod BCs. However, the *Nyx^{nob}* transient-type potassium current is smaller than WT, but not absent, suggesting that nyctalopin is not the only protein required for localization of transient-type potassium channels.

It is of interest to note that none of the genotypes, including WT differed in V_{rest} between light- and dark-adapted states. At first glance this may seem

surprising, however the result is consistent with the effects of adaptation in the retina. Adaptation helps maintain a cell's steady-state activity within the center of the cell's dynamic range, so that the cell can continue to signal increments or decrements in illumination across a working range of background luminance. Given the known process of adaptation in retinal neurons, it is expected that rod BCs would maintain a similar resting membrane state regardless of the adapted background luminance level.

In the current study *mGluR6*^{-/-} rod BCs did not differ from WT in any of the measures of membrane property. In contrast, Xu et al. (2011) claimed that *mGluR6*^{-/-} rod BCs were more hyperpolarized due to a lack of TRPM1 channels in rod BC membrane in a dark-adapted preparation. My dark-adapted results are similar to my light-adapted results and regardless of the adaptation state I found that *mGluR6*^{-/-} rod BCs do not differ from WT. While it is hard to reconcile the difference between the two reports, it is possible that the discrepancy is due to genetic drift between the *mGluR6*^{-/-} or WT colonies. Breeding for more than twenty generations within one or both of the colonies or an undetected spontaneous mutant which became fixed in the colony are possible sources of genetic drift in either of the two laboratory colonies. Given the methodological similarities between the two experiments, it is more likely that the discrepancy in the results is due to genetic drift.

While my data demonstrate that V_{rest} is more depolarized in *Nyx*^{nob} rod BCs and has smaller voltage-gated potassium conductance compared to WT,

there is an inconsistency in the data that remains. The potassium I/V curve (Figure 21) demonstrates a significantly smaller conductance at the more depolarized holding potentials ($\geq -5\text{mV}$), but not at holding potentials close to V_{rest} (-55mV to -35mV). This suggests a voltage mismatch between the control of V_{rest} and the voltage-gated potassium currents examined in the I/V curves (Figure 21). This could be an artifact of scale, as the I/V sweeps that are recorded close to V_{rest} do not drive much outward current and therefore small but real changes in potassium conductance may be present but not statistically significant. It is also possible that two different mechanisms underlie the two effects.

In order to determine if the two results are due to different mechanisms, I plan to record activation and inactivation protocols to get a more defined voltage range of potassium activation/inactivation. I also plan to record rod BC currents with pharmacological antagonists/agonists of potassium channels in the bath and compare the currents to recordings without pharmacological manipulation. Kv1.1, 1.2, and 11.1 are known to be present in rod BCs, while Kv4 currents have not been identified in rod BCs, but exhibit similar kinetics as the currents recorded here (Kaneko et al., 1989; Karschin and Wassle 1990; Klumpp et al., 1995a; Pinto & Klumpp, 1998; Hu & Pan, 2002; Cordeiro et al., 2011; Larsen et al., 2010; Bogin, 2004). The Kv1.1 potassium channel, known to be expressed in rod BCs, exhibits the most similar kinetics to the currents I recorded. However, I plan to utilize dendrotoxin, which blocks Kv1.1 and Kv1.2 channels, heteropodatoxin or stromatoxin which blocks Kv4 channels, and clozapine which gates Kv11

channels at potentials near V_{rest} and at more depolarized potentials to determine if a specific class or classes of potassium channel are responsible for the difference at V_{rest} and/or the difference in voltage-gated potassium conductance.

I examined basic properties of *mGluR6*^{-/-} and *Nyx*^{nob} rod BCs in anticipation that altered rod BC properties may correlate with downstream differences in *mGluR6*^{-/-} and *Nyx*^{nob} RGC rhythmic spiking. I discovered that *Nyx*^{nob} rod BCs have a V_{rest} that is more depolarized due to smaller potassium conductance compared to WT and *mGluR6*^{-/-}. It has been demonstrated in *rd1* and WT retina that oscillations in All ACs result from a more hyperpolarized All AC V_{rest} compared to normal All AC V_{rest} (Choi et al., 2014). Therefore, I propose that the alterations in *Nyx*^{nob} rod BCs result in the cessation of glutamate release (possibly due to a compensatory mechanism to keep the perpetually depolarized cell from constantly releasing glutamate) and subsequent hyperpolarization of All ACs downstream, unmasking the All ACs oscillatory properties, which have been shown to drive the oscillations in *rd* RGCs (Choi et al., 2014).

The difference in *Nyx*^{nob} and *mGluR6*^{-/-} RGC oscillations could be related to the absence of different elements of the G-protein cascade. Specifically, more mGluR6 G-protein cascade elements are absent in *mGluR6*^{-/-} than *Nyx*^{nob} rod BCs (RGS7: Gregg lab, unpublished observation; RGS11: Cao et al., 2012; Shim et al., 2012; Gβ5: Rao et al., 2007). However, it is unclear how elements of the G-protein cascade would affect V_{rest} . This difference cannot be related to the TRPM1 channel, because it is absent in both *Nyx*^{nob} and *mGluR6*^{-/-} rod BCs.

Future experiments will examine whether RGC oscillations might be driven by these changes in potassium conductance and whether there is altered glutamate release from BCs and/or altered membrane properties in All ACs, which could influence the stability of the downstream circuit and possibly permit network oscillations.

The All AC and RGC oscillations in *rd* retina range from 3-15 Hz oscillations (Borowska et al., 2011; Margolis & Detwiler 2011; Menzler & Zeck 2011; Trenholm et al., 2012; Yee et al. 2012; Margolis et al., 2014), and I propose a similar mechanism is responsible for the 3-5 Hz oscillations found in *Nyx^{nob}* RGCs (Demas et al., 2006). Choi et al. (2014) showed that modification of All AC's V_{rest} altered the oscillatory frequency (the more hyperpolarized V_{rest} (ex. -56mV), the lower the oscillatory frequency (3.5-4Hz), while the more depolarized V_{rest} (ex. -48mV), the higher the oscillatory frequency (~6 Hz). Therefore, it is possible that *rd* and *Nyx^{nob}* utilize the same oscillatory mechanism, but that the V_{rest} of *Nyx^{nob}* All ACs is shifted slightly more hyperpolarized than *rd* All ACs resulting in the range of oscillatory potentials found across *Nyx^{nob}* and *rd* RGCs.

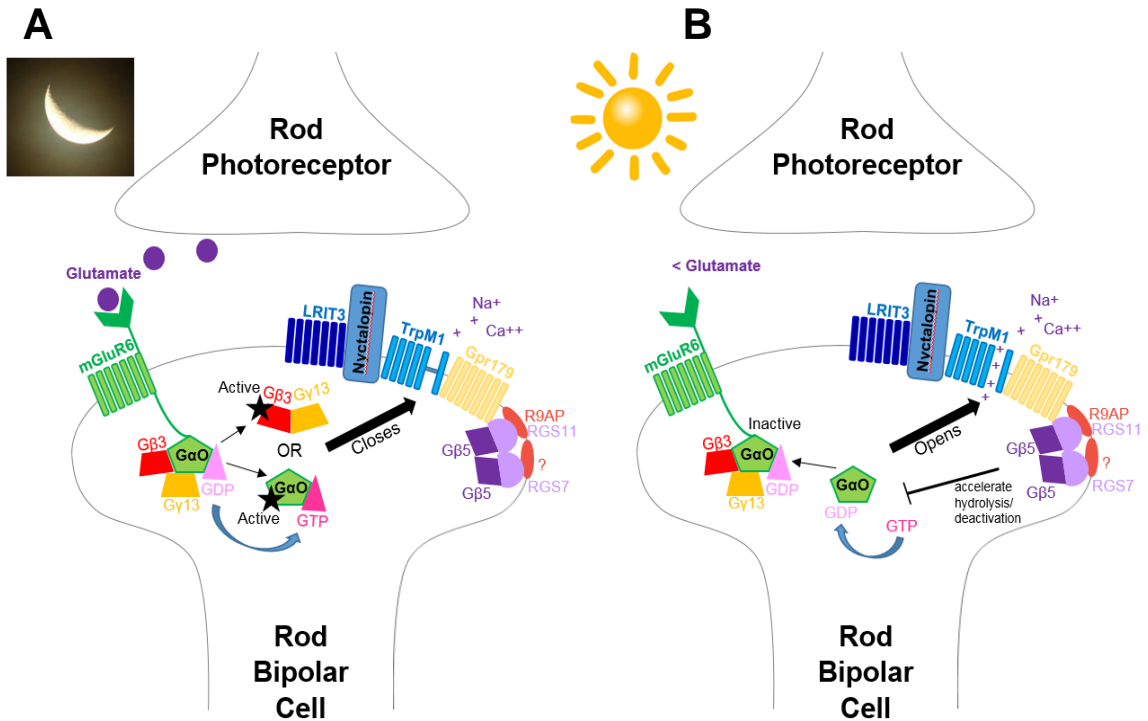
CHAPTER V

CRITICAL ROLE OF GPR179 IN ROD BC RESPONSE

Introduction

The mGluR6-mediated modulation of TRPM1 is known to require GPR179 (Audo et al., 2012; Peachey et al., 2012b). GPR179 is a seven transmembrane G-protein coupled receptor whose expression is eliminated in the *Gpr179^{nob5}* mouse mutant because of a transposable element insertion into the *Gpr179* gene. This mouse mutant and mutations in the human gene are inherited in an autosomal recessive manner and cause a no b-wave ERG phenotype (Peachey et al., 2012b). GPR179 interacts with and is required for RGS7 and RGS11 localization to the On BC dendritic tips (Orlandi et al., 2012; Replication of Figure 7 below). Since *Gpr179^{nob5}* not only lacks expression of GPR179, but also the proper localization of RGS7 and RGS11, I compared properties of rod BCs from *Gpr179^{nob5}* to *RGS7^{-/-}/RGS11^{-/-}* mice, which have normal GPR179 expression, in order to determine the role of GPR179 in isolation from RGS7/RGS11 (Ray et al., 2014). Ray et al. (2014) showed that mGluR6, nyctalopin and TRPM1 protein

expression and outer plexiform layer (OPL) localization are independent of GPR179 expression and that GPR179 and TRPM1 proteins interact.



Replication of Figure 7. A. In the dark glutamate is released from rods and binds mGluR6. mGluR6 activates a trimeric G-protein complex, G $_0$ (Vardi et al., 1993; Nawy 1999; Dhingra et al., 2000). The trimeric G-proteins are activated when GDP is exchanged for GTP on G α_0 , which dissociates into G α_0 -GTP (Vardi et al., 1993; Nawy 1999; Dhingra et al., 2000) and the dimer G β_3 /G γ_{13} (Dhingra et al., 2012; Huang et al., 2003). The activated G-protein complex leads to the closure of the non-selective cation channel, TRPM1, and relative hyperpolarization of the rod BC, either through interaction with G α_0 -GTP and/or G β_3 /G γ_{13} or another

intermediate effector not yet identified. B. In the light glutamate release is decreased and no longer binds mGluR6. Hydrolysis of GTP into guanine dinucleotide (GDP) forms the inactive state of $G\alpha_0$ ($G\alpha_0$ -GDP; Hooks et al., 2003) which recombines with $G\beta_3$ and $G\gamma_{13}$ to form the trimeric G-protein complex. RGS7 and RGS11, regulator of G-protein signaling (RGS) proteins (Cao et al., 2012; Shim et al., 2012), form heterodimers with $G\beta_5$ (Rao et al., 2007). These heterodimers are GTPase-activating protein (GAP) complexes, which accelerate the hydrolysis of GTP to GDP by $G\alpha_0$, (Hooks et al., 2003; Rao et al., 2007), resulting in accelerated deactivation of the G-protein and culminates in the opening of TRPM1 and depolarization of the BC (Audo et al., 2009; Li et al., 2009; Morgans et al., 2009, 2010; Shen et al., 2009; Koike et al., 2010; Peachey et al., 2012a). R9AP is a membrane anchor protein for RGS11 and critical for its proper localization in the membrane at the dendritic tips (Jeffrey et al., 2010); nyctalopin, a leucine-rich repeat protein is critical for proper trafficking or localization of TRPM1 (Gregg et al., 2003; Pearing et al., 2011); GPR179 is required for proper dendritic tip localization of RGS7 and RGS11 (Orlandi et al., 2012) and LRIT3 is critical for rod BC light-mediated response (Zeitz et al., 2013; Neuille et al., 2014).

Initial comparisons of the ERG responses of WT and *Gpr179^{nob5}* showed a significant reduction in the *Gpr179^{nob5}* b-wave and as a result *Gpr179^{nob5}* was

defined as a no b-wave phenotype (Peachey et al., 2012b). *RGS7^{-/-}/RGS11^{-/-}* mice also show a no b-wave phenotype to short light flashes (10msec), but a small light-evoked response can be evoked from a longer ERG stimulus duration (20sec), as well as from individual rod BCs, when a sustained stimulus is used (Cao et al., 2012). Given the differential responses of *RGS7^{-/-}/RGS11^{-/-}* mice in ERG and *in vitro* rod BC recordings I compared *Gpr179^{nob5}*, *RGS7^{-/-}/RGS11^{-/-}*, *Trpm1^{-/-}* and WT mice via *in vitro* rod BC recordings to gain further insight into the role of GPR179 in the rod BC light response.

Materials and Methods

Whole-cell patch-clamp recording

To block inhibitory inputs, Ames solution in the bath was supplemented with the following: 1 μ M strychnine, 100 μ M picrotoxin, and 50 μ M 6-tetrahydropyridin-4-yl methylphosphinic acid (TPMPA). L-AP4 (4 μ M) was added to the bath solution to saturate mGluR6 receptors. The mGluR6 receptor antagonist α -cyclopropyl-4-phosphonophenylglycine (CPPG) was dissolved in Ames medium to a working concentration of 0.6 mM or 3mM. CPPG was applied by pressure application using a Picospritzer II (Parker Instrumentation) onto the rod BC dendritic tips in the OPL. In separate experiments, capsaicin (10 μ M), a TRPM1 agonist, was puffed onto the rod BC dendrites to gate the opening of the

TRPM1 channel. Reagents were purchased from Sigma-Aldrich, except for L-AP4, CPPG, and capsaicin, which were purchased from Tocris Bioscience.

Voltage-clamp protocols

Rod BCs were voltage clamped at +50mV (Nawy, 2004; Shen et al., 2009). CPPG was puffed at rod BC dendrites for 200 ms and 1 s. For capsaicin experiments 1 s puffs were applied. Three to five responses were recorded from each cell and then averaged. Off-line, a 20 Hz eight-pole Bessel low-pass filter was applied to the data. Variance and standing current were measured across the first 1.5 s of the recording for each rod BC. Off-line analyses of data were performed using Clampfit 10.2.

Statistical Analysis

Prism 5.04 software (GraphPad Software) was used to perform two-way repeated-measures ANOVAs with Bonferroni post hoc, two-way ANOVAs with Bonferroni post hoc, one-way ANOVAs with Bonferroni post hoc, Kruskal-Wallis with Dunns post hoc, Mann-Whitney, or unpaired t-tests as suited for the necessary comparison. Post hoc *P* values are reported. Statistical significance = $P < 0.05$.

Results

Both mGluR6 and TRPM1 proteins are expressed in the OPL of *Gpr179^{nob5}* (Ray et al., 2014) and *RGS7^{-/-}/RGS11^{-/-}* retina (Cao et al., 2012). To

examine the capacity of the cascade to gate the channel, I used a pharmacological manipulation in which all synaptic inputs are blocked and retinal slices are bathed in 4 μ M L-AP4 to maximally activate the mGluR6 cascade and close TRPM1 channels (Nawy, 2004). To examine the properties of the mGluR6 cascade and its ability to open TRPM1 channels, CPPG, an mGluR6 antagonist was exogenously applied (puffed) onto the rod BC dendrites. Its effect is to deactivate mGluR6, similar to the reduction in glutamate occupancy resulting from light onset. To examine the ability of the TRPM1 channel to be directly gated, capsaicin, a TRPM1 channel agonist, was exogenously applied. Because rod BCs were held at +50mV to minimize rundown, both CPPG and capsaicin puffs evoked outward currents (Figures 25, 26).

Small mGluR6-mediated responses can be elicited in rod BCs in the absence of GPR179 and increased stimulation increases response amplitude

Puffs of CPPG (0.6 mM) onto the dendritic terminals of WT rod BCs evoked a robust response whose amplitude was similar regardless of puff duration (200 ms or 1 s duration; Figure 25A; two-way ANOVA with Bonferroni post hoc: $P > 0.05$). As a result, WT responses were combined (Figure 25B). The responses of *Gpr179^{nob5}* and *RGS7^{-/-}/RGS11^{-/-}* rod BCs to 200 ms CPPG puffs were similar but significantly smaller than WT (Figure 25B; two-way ANOVA with Bonferroni post hoc: *Gpr179^{nob5}* vs *RGS7^{-/-}/RGS11^{-/-}*, $P > 0.05$; *Gpr179^{nob5}* vs WT, $P < 0.001$; *RGS7^{-/-}/RGS11^{-/-}* vs WT, $P < 0.001$). In contrast to WT, increasing puff duration to 1 s produced significant increases in both

Gpr179^{nob5} and *RGS7^{-/-}/RGS11^{-/-}* rod BC responses (Figure 25A,B; two-way ANOVA with Bonferroni post hoc: $P < 0.001$ for both comparisons), although again amplitudes were significantly smaller than WT (Figure 25A,B; two-way ANOVA with Bonferroni post hoc: $P < 0.001$ for both comparisons). Increasing the concentration of CPPG to 3 mM had minimal impact on the WT response (Figure 25C,D), indicating that the mGluR6 cascade is maximally activated by 0.6 mM puffs for 200 ms. Increasing CPPG concentration to 3 mM evoked similar responses in *Gpr179^{nob5}* and *RGS7^{-/-}/RGS11^{-/-}* rod BCs independent of puff duration, although responses were always significantly smaller than WT (Figure 25C,D; two-way ANOVA with Bonferroni post hoc: *Gpr179^{nob5}* vs *RGS7^{-/-}/RGS11^{-/-}* 200 ms and 1 s, $P > 0.05$; *Gpr179^{nob5}* vs WT 200 ms and 1 s, $P < 0.001$; *RGS7^{-/-}/RGS11^{-/-}* vs WT 200 ms and 1 s, $P < 0.001$). Together these results suggest that in rod BCs TRPM1 can be gated via mGluR6 even when GPR179 expression is absent. The specific role of GPR179 cannot be determined with the reagents at hand, because the effects on cascade sensitivity could be because of its close interaction with TRPM1. However, the fact that it also is required for localization of the RGS complex confounds a simple conclusion.

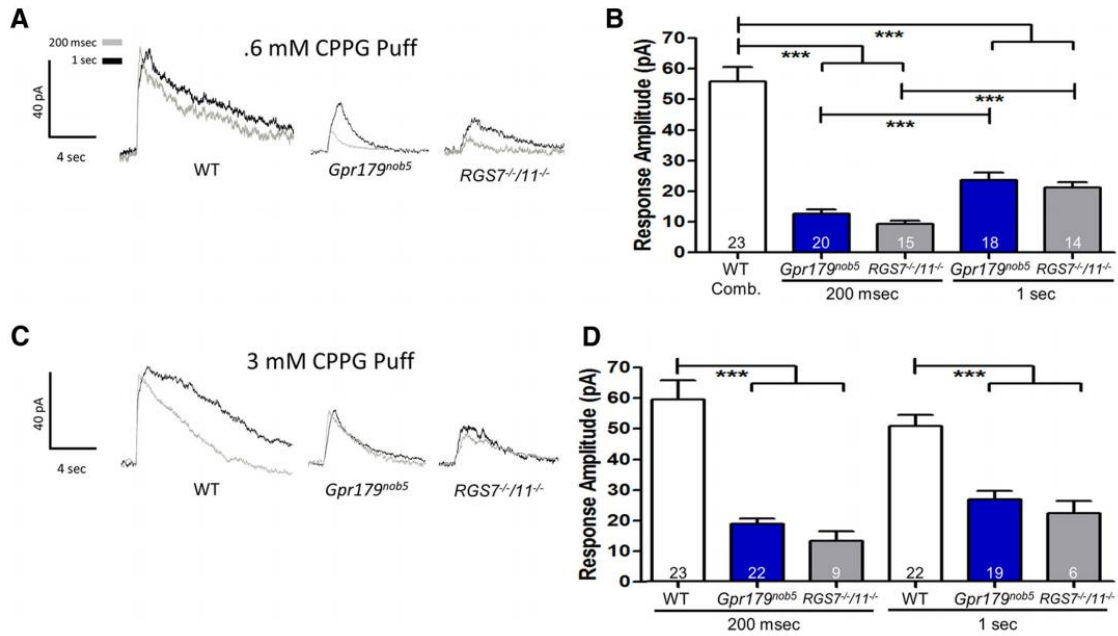


Figure 25. A small amplitude, concentration-dependent CPPG response in *Gpr179^{nob5}* and *RGS7^{-/-}/RGS11^{-/-}* rod BCs. A. Representative voltage-clamp responses of WT, *Gpr179^{nob5}*, and *RGS7^{-/-}/RGS11^{-/-}* rod BCs evoked by puff application of the mGluR6 antagonist, CPPG (0.6mM for 200 ms or 1 s). B. Histogram compares the average peak response amplitudes (\pm SEM) of WT, *Gpr179^{nob5}*, and *RGS7^{-/-}/RGS11^{-/-}* rod BCs. WT responses to 200 ms and 1 s puffs did not differ and were combined. Regardless of duration *Gpr179^{nob5}* and *RGS7^{-/-}/RGS11^{-/-}* response amplitudes were significantly smaller than WT, although response amplitudes of rod BCs from both mutants significantly increase when puff duration increased from 200 ms to 1 s. C. Representative voltage-clamp responses of WT, *Gpr179^{nob5}*, and *RGS7^{-/-}/RGS11^{-/-}* rod BCs evoked by puff application of 3mM CPPG for either 200 ms or 1 s. D. Histogram

compares the average peak response (\pm SEM) amplitudes of WT, *Gpr179^{nob5}*, and *RGS7^{-/-}/RGS11^{-/-}* rod BCs. WT responses did not change with increased concentration or puff duration of CPPG (200ms to 1 s). Regardless of duration *Gpr179^{nob5}* and *RGS7^{-/-}/RGS11^{-/-}* response amplitudes were significantly smaller than WT. The increased puff duration did not produce larger response amplitudes in either *Gpr179^{nob5}* or *RGS7^{-/-}/RGS11^{-/-}* rod BCs, suggesting that they were saturated under these conditions (two-way ANOVA with Bonferroni post hoc; *** $P < 0.001$).

GPR179 is required for normal TRPM1 channel sensitivity in rod BCs

Because TRPM1 is expressed in both *Gpr179^{nob5}* and *RGS7^{-/-}/RGS11^{-/-}* rod BCs, one can assume that the capsaicin-evoked current would be mediated by TRPM1. To test this idea, I compared direct activation of the TRPM1 channel using capsaicin in WT, *RGS7^{-/-}/RGS11^{-/-}*, *Gpr179^{nob5}*, and *Trpm1^{-/-}* rod BCs (Figure 26). As observed previously (Shen et al., 2009), capsaicin-evokes robust responses in WT rod BCs (Figure 26A,B) and the capsaicin-evoked current in *RGS7^{-/-}/RGS11^{-/-}* and WT rod BCs were not significantly different (one-way ANOVA with Bonferroni post hoc: WT vs *RGS7^{-/-}/RGS11^{-/-}*, $P > 0.05$). In contrast, the capsaicin-evoked current in *Gpr179^{nob5}* rod BCs was significantly smaller than either WT or *RGS7^{-/-}/RGS11^{-/-}* rod BCs (one-way ANOVA with Bonferroni post hoc: 1 s, *Gpr179^{nob5}* vs WT, $P < 0.001$; *Gpr179^{nob5}* vs *RGS7^{-/-}/RGS11^{-/-}*, $P <$

0.05). This response also was significantly larger than the capsaicin-evoked current in *Trpm1*^{-/-} rod BCs, which are barely measurable above background noise (one-way ANOVA with Bonferroni post hoc: *Gpr179*^{nob5} vs *Trpm1*^{-/-}, *P* < 0.05). A similar small residual *Trpm1*^{-/-} current of unknown identity has been noted previously (Morgans et al., 2009). These results indicate that it is the presence of GPR179 in both WT and *RGS7*^{-/-}/*RGS11*^{-/-} On BCs that allows the TRPM1 channel to be efficiently gated by capsaicin, whereas its absence leads to a TRPM1 channel whose sensitivity to direct gating is significantly reduced.

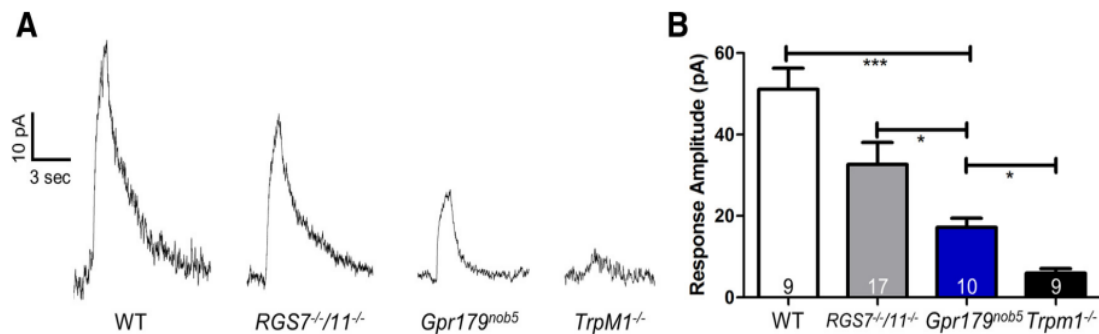


Figure 26. Capsaicin-evoked TRPM1 responses are normal in *RGS7*^{-/-}/*RGS11*^{-/-} and decreased in *Gpr179*^{nob5} rod BCs. A. Representative voltage-clamp responses of WT, *RGS7*^{-/-}/*RGS11*^{-/-}, *Gpr179*^{nob5}, and *Trpm1*^{-/-} rod BCs evoked by a 1 s puff of the TRPM1 channel agonist, capsaicin (10 μ M). B. Histogram compares the average peak response amplitudes (\pm SEM) of WT, *RGS7*^{-/-}/*RGS11*^{-/-}, *Gpr179*^{nob5}, and *Trpm1*^{-/-} rod BCs. *Gpr179*^{nob5} response amplitudes are significantly larger than *Trpm1*^{-/-}, although significantly smaller than either WT or *RGS7*^{-/-}/*RGS11*^{-/-} rod BCs. The responses from *RGS7*^{-/-}/*RGS11*^{-/-} rod BCs are the

same as WT. The number of rod BCs in each experimental group is shown within each bar of the histograms (one-way ANOVA with Bonferroni post hoc, * $P < 0.05$; *** $P < 0.001$).

GPR179 is important for normal TRPM1 channel modulation

Given this result, I examined the open probability of TRPM1 channels and compared the magnitude of the standing outward current and its variance in WT, *Gpr179^{nob5}*, and *RGS7^{-/-}/RGS11^{-/-}* rod BCs. I compared them to *Trpm1^{-/-}* rod BCs, where the channel is absent. Both the standing outward current and current variance of *Gpr179^{nob5}*, *RGS7^{-/-}/RGS11^{-/-}*, and *Trpm1^{-/-}* rod BCs were similar (Figure 27B,C; one-way ANOVA with Bonferroni post hoc: $P > 0.05$) and all were significantly lower than WT (one-way ANOVA with Bonferroni post hoc: standing current: WT vs *Gpr179^{nob5}*, $P < 0.001$; WT vs *RGS7^{-/-}/RGS11^{-/-}*, $P < 0.001$; WT vs *Trpm1^{-/-}*, $P < 0.001$; variance: WT vs *Gpr179^{nob5}*, $P < 0.01$; WT vs *RGS7^{-/-}/RGS11^{-/-}*, $P < 0.05$; WT vs *Trpm1^{-/-}* $P < 0.01$). These data indicate that even though the TRPM1 channel is expressed in *Gpr179^{nob5}* and *RGS7^{-/-}/RGS11^{-/-}* rod BCs it has an extremely low (near 0) open probability, similar to when the TRPM1 channel is absent. These data suggest that GPR179 clusters RGS7 and RGS11 close to the TRPM1 channel and also interacts with TRPM1 to alter the ability of the channel to be gated directly by capsaicin.

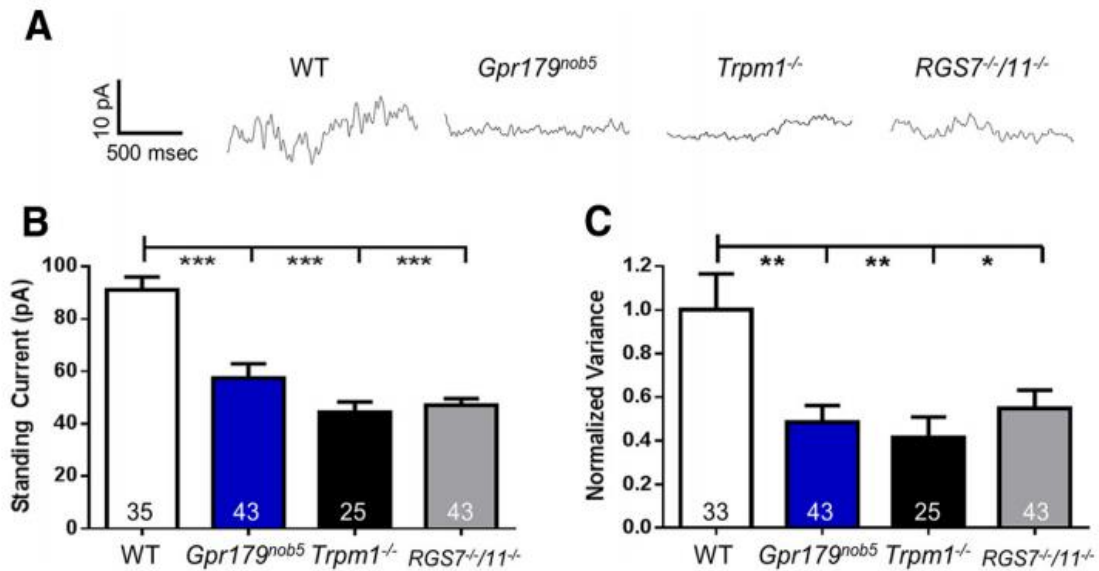


Figure 27. *Gpr179^{nob5}*, *Trpm1^{-/-}*, and *RGS7^{-/-}/RGS11^{-/-}* rod BCs have decreased standing currents and channel open probability. A. Representative traces of spontaneous currents from WT, *Gpr179^{nob5}*, *Trpm1^{-/-}*, and *RGS7^{-/-}/RGS11^{-/-}* rod BCs. Rod BCs were held at +50 mV and 1.5 s sections of each recording were analyzed to yield the data in B and C. Histograms compare average (\pm SEM) (B) standing current and (C) current variance for WT, *Gpr179^{nob5}*, *Trpm1^{-/-}*, and *RGS7^{-/-}/RGS11^{-/-}* rod BCs. Rod BCs from *Gpr179^{nob5}*, *Trpm1^{-/-}*, and *RGS7^{-/-}/RGS11^{-/-}* have similar standing currents (B) and current variance (C) and all are significantly lower than WT (one-way ANOVA with Bonferroni post hoc, * $P < 0.05$; ** $P < 0.01$, *** $P < 0.001$). Combined these data indicate that a channel that remains in *Gpr179^{nob5}* and *RGS7^{-/-}/RGS11^{-/-}* rod BCs has an open probability that is similar to rod BCs where the TRPM1 channel is absent (*Trpm1^{-/-}*). The number of rod BCs in each experimental group is shown within each bar of the histograms.

Discussion

Scotopic visual depends on the modulation of mGluR6, which gates the TRPM1 channel in rod BCs. Critical elements of the mGluR6 G-protein cascade, all expressed on the tips of WT rod BCs, have been identified because they have been found to reduce or eliminate the signaling pathway. While the complete cascade is not yet determined, the current hypothesis is that glutamate binding to mGluR6 (which occurs in the dark) activates a trimeric G-protein complex, G_0 (Vardi et al., 1993; Nawy 1999; Dhingra et al., 2000), which breaks down into the dimer composed of $G\beta_3$ and $G\gamma_{13}$ subunits (Dhingra et al., 2012; Huang et al., 2003) and the $G\alpha$ subunit (Dhingra et al., 2000). This G-protein complex activation leads to closure of the TRPM1 channel. $G\alpha_0$ is bound to guanine trinucleotide (GTP) ($G\alpha_0$ -GTP) in its active state and hydrolysis of GTP into guanine dinucleotide (GDP) forms the inactive state of $G\alpha_0$ ($G\alpha_0$ -GDP; Hooks et al., 2003). Other critical elements of the cascade include RGS7 and RGS11, regulator of G-protein signaling (RGS) proteins (Cao et al., 2012; Shim et al., 2012), which form heterodimers with $G\beta_5$ (Rao et al., 2007). These heterodimers are GTPase-activating protein (GAP) complexes, which accelerate the hydrolysis of GTP to GDP by $G\alpha_0$, (Hooks et al., 2003; Rao et al., 2007), resulting in accelerated deactivation of the G-protein and subsequent TRPM1 channel opening. R9AP is a membrane anchor protein for RGS11 and critical for its proper localization in the membrane at the dendritic tips (Jeffrey et al., 2010); nyctalopin, a leucine-rich repeat protein that is critical for the proper trafficking or

localization of TRPM1 (Gregg et al., 2003; Pearing et al., 2011); GPR179, a seven transmembrane domain protein that is required for proper dendritic tip localization of RGS7 and RGS11; and LRIT3, a leucine-rich repeat protein of unknown function (Zeitz et al., 2013).

Small responses from *Gpr179^{nob5}* rod BCs were elicited using the same pharmacological concentration and duration of CPPG as used by Nawy, 2004. While WT rod BC responses were saturated at this level of pharmacological stimulation, increased concentration and duration of pharmacological application increased the response amplitudes from *Gpr179^{nob5}* rod BCs, though never reaching WT amplitudes (Figure 25). The increased concentration and duration of pharmacological activation of mGluR6 in *Gpr179^{nob5}* rod BCs produce a similar response to *RGS7^{-/-}/RGS11^{-/-}* rod BCs. Although the positive polarity b-wave of the ERG responses from *Gpr179^{nob5}* was previously reported to be missing (Peachey et al., 2012), my *in vitro* rod BC responses prompted a closer examination of the ERG responses. Ray et al. (2014) found a b-wave-like response, albeit small (~15–20 μ V), to low luminance flashes (-3.6, -2.4 log cd s/m²) that was increased with longer flash duration in *Gpr179^{nob5}* but was absent in *Trpm1^{-/-}* mice. The presence of a small ERG b-wave in these mice suggests that mGluR6 and its cascade maintain some capacity to gate the TRPM1 channel, although the sensitivity is significantly reduced. These results are consistent with the no b-wave ERG phenotype in *RGS7^{-/-}/RGS11^{-/-}* mice to short

flash stimuli (Cao et al., 2012), but a small light-evoked response from their rod BCs, to sustained light stimuli.

My current measures do not discriminate between the roles of GPR179 and the RGS complex in gating the TRPM1 channel through the mGluR6 cascade because the RGS complex is mislocalized in the absence of GPR179. However, the presence of GPR179 is required to maximize direct TRPM1 channel gating via capsaicin application, which does not involve the cascade. Capsaicin-mediated gating is altered in *Gpr179^{nob5}* rod BCs, but is retained in *RGS7^{-/-}/RGS11^{-/-}* rod BCs in which GPR179 is expressed normally (Figure 26). This suggests a unique function of GPR179, related to its direct protein:protein interactions with TRPM1 (Ray et al., 2014). Together these electrophysiological, immunohistochemical and biochemical results contribute new information to the ongoing construction of the mGluR6 G-protein cascade that is critical to night vision.

When glutamate binds mGluR6, its trimeric G-proteins are activated and GDP is exchanged for GTP on $G\alpha_0$, producing activated $G\alpha_0$ -GTP and $G\beta\gamma$, which become disassociated. Both components are membrane bound and likely in close proximity to TRPM1. This means that one or possibly both can interact with TRPM1 and are instrumental in channel closure, either directly or via another intermediate effector. Regardless of the identity of this component, the interaction must be transient in nature because even when mGluR6 is maximally activated, either under dark-adapted conditions (Sampath & Rieke, 2004) or in

the presence of L-AP4 (Figure 27), there remains a standing current and nonzero channel open probability referred to as the dark current.

Manipulations that increase the level of the activated $G\alpha_0$ ($G\alpha_0$ -GTP) all decrease either the light response or response to mGluR6 antagonists. These manipulations have included: adding GTP- γ -S to the patch pipette (Sampath and Rieke, 2004; Zhang et al., 2010). GTP- γ -S is a nonhydrolyzable GTP analog that increases the lifetime of the G protein ≥ 100 -fold, thereby leading to a quick decay of the light response due to the additional G-protein activity (Sampath and Rieke, 2004; Zhang et al., 2010); deleting the RGS7/RGS11 complex (Zhang et al., 2010; Cao et al., 2012; Shim et al., 2012), which leads to a decreased amplitude and delay in rod BC depolarizing response, suggesting these complexes play a critical role in accelerating deactivation of the G-protein (GTP hydrolysis) and subsequent TRPM1 channel opening (Zhang et al., 2010; Cao et al., 2012; Shim et al., 2012). However, Shen et al. (2012) found that introduction of active $G\beta\gamma$ but not $G\alpha_0$ blocked the light response, and suggested $G\beta\gamma$ as the active component in TRPM1 channel closure. However, these manipulations cannot distinguish between the $G\alpha_0$ -GTP and $G\beta\gamma$ models because decreasing $G\alpha_0$ -GDP concentrations necessarily increases free $G\beta\gamma$. This is because these proteins form trimeric heterodimers and when $G\alpha_0$ is no longer bound to $G\beta\gamma$, $G\beta\gamma$ is free in the cell and can influence downstream, making it difficult to separate the effects of $G\alpha_0$ -GTP and $G\beta\gamma$ on the TRPM1 channel. Therefore, it

remains undetermined whether $G\alpha_0$ -GTP or $G\beta\gamma$ are the critical component for TRMP1 channel closure.

My results show that the RGS complex is not required for cascade function, because in its absence the TRPM1 channel can be gated by strong mGluR6 cascade stimulation. Rod BCs from both *Gpr179^{nob5}* and *RGS7^{-/-}/RGS11^{-/-}* mice had standing currents and variance that were similar to *Trpm1^{-/-}* rod BCs, indicating the presence of a remaining current of unknown identity, which has been noted previously (Morgans et al., 2009). Further, my results show that in the absence of localized RGS proteins the standing current and channel open probability decrease to background levels, in contrast to what is seen when the cascade is maximally activated (Figure 27). I propose this occurs in *Gpr179^{nob5}* and *RGS7^{-/-}/RGS11^{-/-}* rod BCs because of increased concentrations of both $G\alpha_0$ -GTP and free $G\beta\gamma$, which arise because of the loss of the RGS complex, resulting in complete TRPM1 closure.

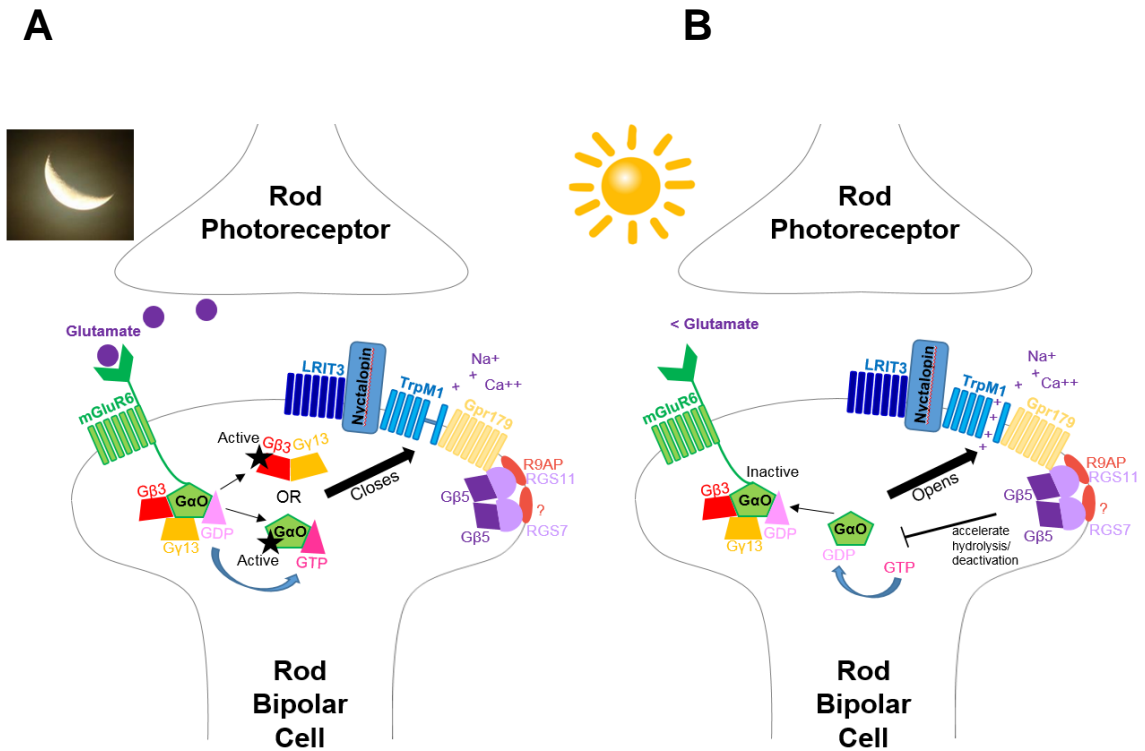
In conclusion, a critical function of GPR179 is to set the state of the TRPM1 channel, allowing it to respond optimally to deactivation of the mGluR6 cascade. Understanding the various states of TRPM1, which I in collaboration with Ray et al. (2014) show are dependent on at least GPR179, at the molecular level may provide important clues as to how TRPM1 is gated by the mGluR6 cascade.

CHAPTER VI

CRITICAL ROLE OF LRIT3 IN ROD BC RESPONSE

Introduction

In the dark glutamate binds mGluR6, which activates a trimeric G-protein complex (Vardi et al., 1993; Nawy 1999; Dhingra et al., 2000) leading to the closure of the TRPM1 channel (Replication of Figure 7 below).



Replication of Figure 7. A. In the dark glutamate is released from rods and binds mGluR6. mGluR6 activates a trimeric G-protein complex, G_0 (Vardi et al., 1993; Nawy 1999; Dhingra et al., 2000). The trimeric G-proteins are activated when GDP is exchanged for GTP on $G\alpha_0$, which dissociates into $G\alpha_0$ -GTP (Vardi et al., 1993; Nawy 1999; Dhingra et al., 2000) and the dimer $G\beta_3/G\gamma_{13}$ (Dhingra et al., 2012; Huang et al., 2003). The activated G-protein complex leads to the closure of the non-selective cation channel, TRPM1, and relative hyperpolarization of the rod BC, either through interaction with $G\alpha_0$ -GTP and/or $G\beta_3/G\gamma_{13}$ or another intermediate effector not yet identified. B. In the light glutamate release is decreased and no longer binds mGluR6. Hydrolysis of GTP into guanine dinucleotide (GDP) forms the inactive state of $G\alpha_0$ ($G\alpha_0$ -GDP; Hooks et al., 2003)

which recombines with G β 3 and G γ 13 to form the trimeric G-protein complex. RGS7 and RGS11, regulator of G-protein signaling (RGS) proteins (Cao et al., 2012; Shim et al., 2012), form heterodimers with G β 5 (Rao et al., 2007). These heterodimers are GTPase-activating protein (GAP) complexes, which accelerate the hydrolysis of GTP to GDP by G α ₀, (Hooks et al., 2003; Rao et al., 2007), resulting in accelerated deactivation of the G-protein and culminates in the opening of TRPM1 and depolarization of the BC (Audo et al., 2009; Li et al., 2009; Morgans et al., 2009, 2010; Shen et al., 2009; Koike et al., 2010; Peachey et al., 2012a). R9AP is a membrane anchor protein for RGS11 and critical for its proper localization in the membrane at the dendritic tips (Jeffrey et al., 2010); nyctalopin, a leucine-rich repeat protein is critical for proper trafficking or localization of TRPM1 (Gregg et al., 2003; Pearing et al., 2011); GPR179 is required for normal TRPM1 channel sensitivity and proper dendritic tip localization of RGS7 and RGS11 (Orlandi et al., 2012; Chapter V) and LRIT3 is critical for rod BC light-mediated response (Zeititz et al., 2013; Neuille et al., 2014).

Recently, cCSNB patients have been identified with mutations in the *LRIT3* gene (Zeititz et al., 2013). *LRIT3* encodes leucine-rich-repeat (LRR), immunoglobulin-like, and transmembrane-domain 3 and is expressed in the brain and eye (Zeititz et al., 2013). Human patients with *LRIT3* mutations exhibit ERG phenotypes consistent with cCSNB (Zeititz et al., 2013). Similar to the ERG

responses of other no b-wave cCSNB mouse models (Masu et al., 1995; Gregg et al., 2003; Shen et al., 2009) *Lrit3^{nob6/nob6}* (Neuille et al., 2014) and *Lrit3^{-/-}* mice (Figure 28) have a normal a-wave but lack a b-wave at all luminance levels, suggesting an absence of rod and On cone BC signaling. *Lrit3^{nob6/nob6}* mice exhibit decreased optomotor responses under scotopic conditions, but have normal fundus autofluorescence and histological structure (Neuille et al., 2014). Unlike other no b-wave mouse mutants, *Lrit3^{nob6/nob6}* mice are reported to have thinned inner nuclear layers, inner plexiform layers, ganglion cell layers and nerve fiber layers (Neuille et al., 2014).

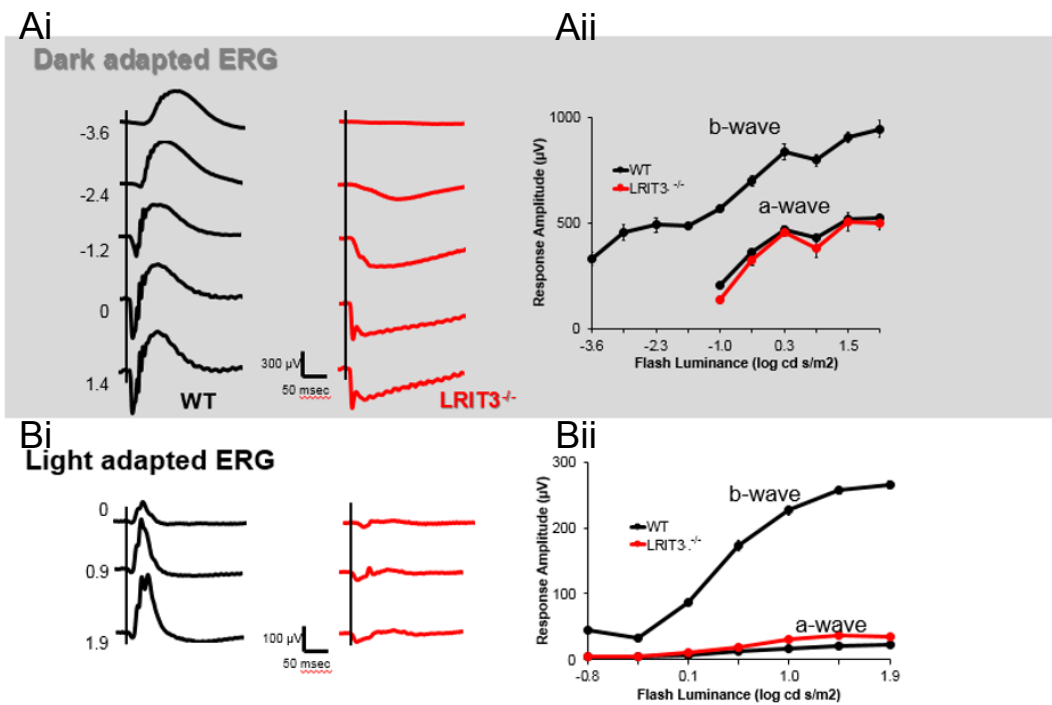


Figure 28. *Lrit3^{-/-}* ERG recordings exhibit the classic cCSNB no b-wave phenotype under dark and light-adapted conditions. Ai, Bi. Representative WT littermate control and *Lrit3^{-/-}* ERG recordings are presented at a variety of flash

luminances. Aii, Bii. Response amplitude for a and b-wave plotted as a function of flash luminance for WT littermate control and *Lrit3*^{-/-} ERGs. *Lrit3*^{-/-} a-waves have normal response amplitudes, while *Lrit3*^{-/-} lacks b-waves under both dark (Aii) and light-adapted (Bii) conditions. J. Noel, M.A. McCall, & R.G. Gregg, unpublished observations.

Consistent with a lack of an ERG b-wave, immunohistochemical and confocal microscopy show that the TRPM1 channel is mislocalized to the cell body and absent from the rod BC dendritic tips (Figure 29B). In contrast, mGluR6 remains properly localized in the OPL and presumably on the rod BC dendritic tips (Figure 29C).

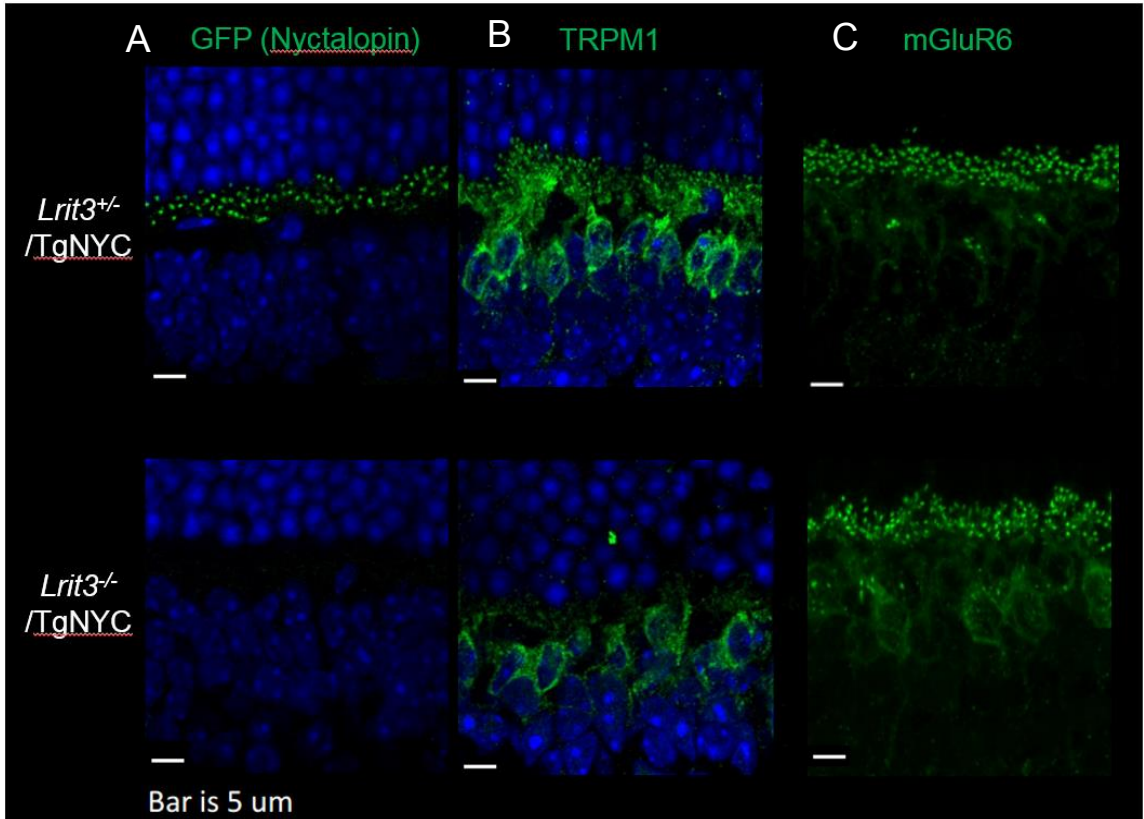


Figure 29. *Lrit3*^{-/-} rod BCs lack expression of nyctalopin, have mislocalized TRPM1, and normal expression of mGluR6. Confocal microscopy images from retinal slices of *Lrit3*^{+/+}*TgNyc* and *Lrit3*^{-/-}*TgNyc* mice. Antibodies were used to label GFP (nyctalopin), TRPM1, and mGluR6. A. Nyctalopin expression is absent in *Lrit3*^{-/-}*TgNyc* mice. B. TRPM1 expression is localized only to the cell body and is not present in the dendritic tips in *Lrit3*^{-/-}*TgNyc* mice. C. mGluR6 expression is normal in *Lrit3*^{-/-}*TgNyc* mice. J. Noel, M.A. McCall, & R.G. Gregg, unpublished observations.

In addition, nyctalopin expression is absent in the *Lrit3*^{-/-} rod BCs (Figure 29A). Expression of the RGS complex components Gβ5, RGS7, RGS11 and R9AP localize properly to the dendritic tips of *Lrit3*^{-/-} rod BCs (Figure 30A). In addition, GPR179, which is important for proper TRPM1 channel sensitivity, is expressed normally in *Lrit3*^{-/-} rod BC dendritic tips (Figure 30B).

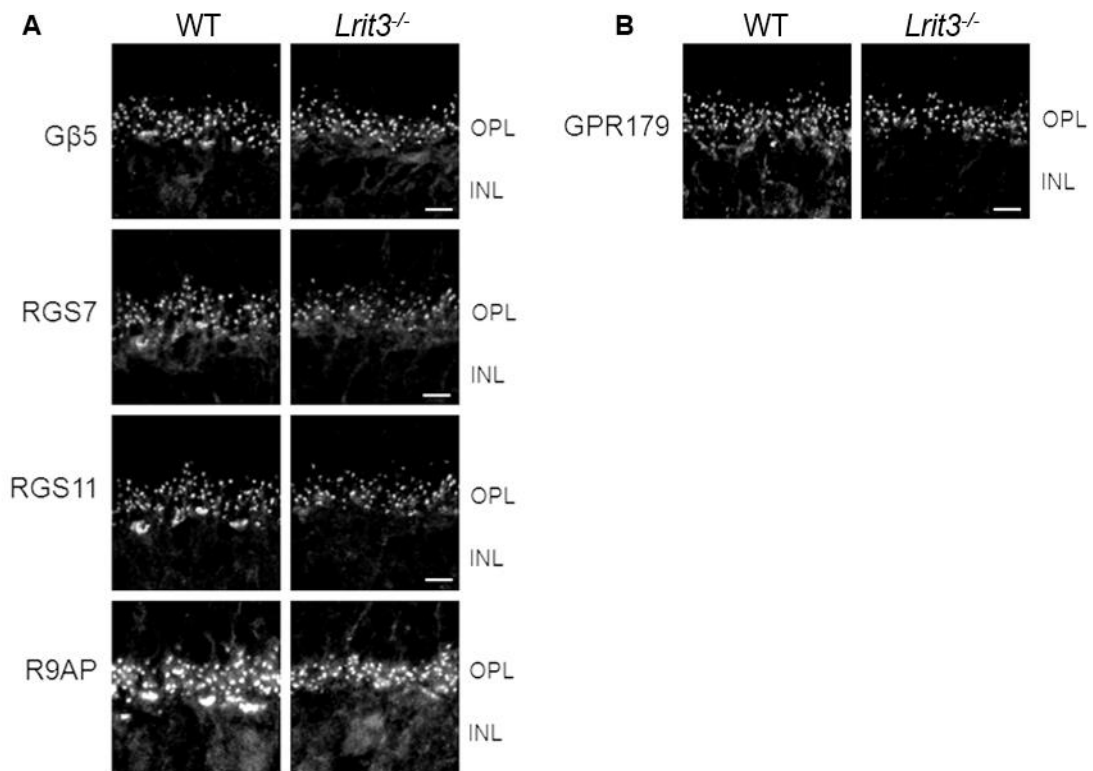


Figure 30. *Lrit3*^{-/-} rod BCs have normal expression of RGS complex proteins and GPR179 in rod BCs. Confocal microscopy images from retinal slices of WT littermate controls and *Lrit3*^{-/-} mice. A. Antibodies were used to label Gβ5, RGS7, RGS11, and R9AP. *Lrit3*^{-/-} rod BCs have normal expression of Gβ5, RGS7, RGS11, and R9AP. B. Antibodies were used to label GPR179. *Lrit3*^{-/-} rod BCs

have normal expression of GPR179. T. Ray & R.G. Gregg, unpublished observations.

Given that the mGluR6 receptor is normally expressed, I performed whole cell patch clamp recordings from *Lrit3*^{-/-} rod BCs to determine whether they exhibit mGluR6-mediated cascade activation or if the TRPM1 channels could be gated directly. Finally, to determine whether the TRPM1 channels are open/closed or fluctuating in the membrane, I examined *Lrit3*^{-/-} rod BC channel noise and standing current and compared them to WT or *Trpm1*^{-/-} rod BCs.

Materials and Methods

Generation of *Lrit3*^{-/-} mice

Lrit3^{-/-} mice were created utilizing zinc finger nucleotides (Blackburn et al., 2013; Gaj et al., 2013) to target a region of LRIT3 exon 2 that encodes a peptide corresponding to the second leucine-rich-repeat domain that is highly conserved across species. Fifteen *Lrit3* lines were created and line G47 was used because it had a 40 bp deletion that introduced a frameshift mutation resulting in a null allele.

Retinal slice preparation and whole-cell, patch-clamp recording

Statistical Analysis

Prism 5.04 software (GraphPad Software) was used to perform two-way repeated-measures ANOVAs with Bonferroni post hoc, two-way ANOVAs with Bonferroni post hoc, one-way ANOVAs with Bonferroni post hoc, Kruskal-Wallis with Dunns post hoc, Mann-Whitney, or unpaired t-tests as suited for the necessary comparison. Post hoc *P* values are reported. Statistical significance = $P < 0.05$. The rest of the methods are the same as Chapter V.

Results

To examine whether mGluR6 and its cascade elements, most of which remain expressed, could gate the TRPM1 channel, I pharmacologically activated the mGluR6 cascade with bath application of L-AP4 (4 μ M) and blocked all synaptic input (Nawy, 2004; Ray et al., 2014; Chapter V). CPPG, an mGluR6 antagonist, was exogenously applied (puffed) onto the rod BC dendrites. This approach mimics the reduction of glutamate in the synapse at light onset. WT littermates were used as controls and *Trpm1*^{-/-} mice were used as a negative control because their rod BCs lack the TRPM1 channel. In the figures that follow, CPPG and capsaicin evoked outward currents because the rod BCs were held at +50mV to minimize rundown (Figures 31, 32).

LRIT3 is required for mGluR6-mediated responses in rod BCs

As I have shown previously, (Ray et al., 2014; Chapter V), 200 msec CPPG puffs onto WT control rod BC dendritic tips evoked large amplitude responses (Figure 31A, B). *Lrit3*^{-/-} and *Trpm1*^{-/-} rod BC responses to 200 msec CPPG puffs were similar to each other and significantly smaller than WT littermate controls (Figure 31A, B; one-way ANOVA with Bonferroni post hoc: *Lrit3*^{-/-} v. *Trpm1*^{-/-}: $P > 0.05$; *Lrit3*^{-/-} v. WT & *Trpm1*^{-/-} v. WT: $P < 0.001$). To determine if *Lrit3*^{-/-} rod BCs could be driven harder to elicit increased response amplitudes, I increased the CPPG puff duration to 1 sec. As expected from the absence of correctly localized TRPM1 channels, *Lrit3*^{-/-} and *Trpm1*^{-/-} rod BC responses to 1 sec CPPG puffs remained significantly smaller than WT littermate controls and similar to each other (Figure 31A, B; one-way ANOVA with Bonferroni post hoc: *Lrit3*^{-/-} v. WT & *Trpm1*^{-/-} v. WT: $P < 0.001$). Finally, the increase in puff duration, from 200 msec to 1 sec, did not increase the response amplitude in *Lrit3*^{-/-} or *Trpm1*^{-/-} rod BCs (*Lrit3*^{-/-} 200 msec v. 1 sec: $P < 0.05$; *Trpm1*^{-/-} 200 msec v. 1 sec: $P > 0.05$) indicating that whatever mechanism generates this current, it is already saturated at the short puff duration. Together my results show that *Lrit3*^{-/-} rod BCs exhibit responses that are not mediated through mislocalized TRPM1 channels similar to my findings in Chapter IV (Figure 20).

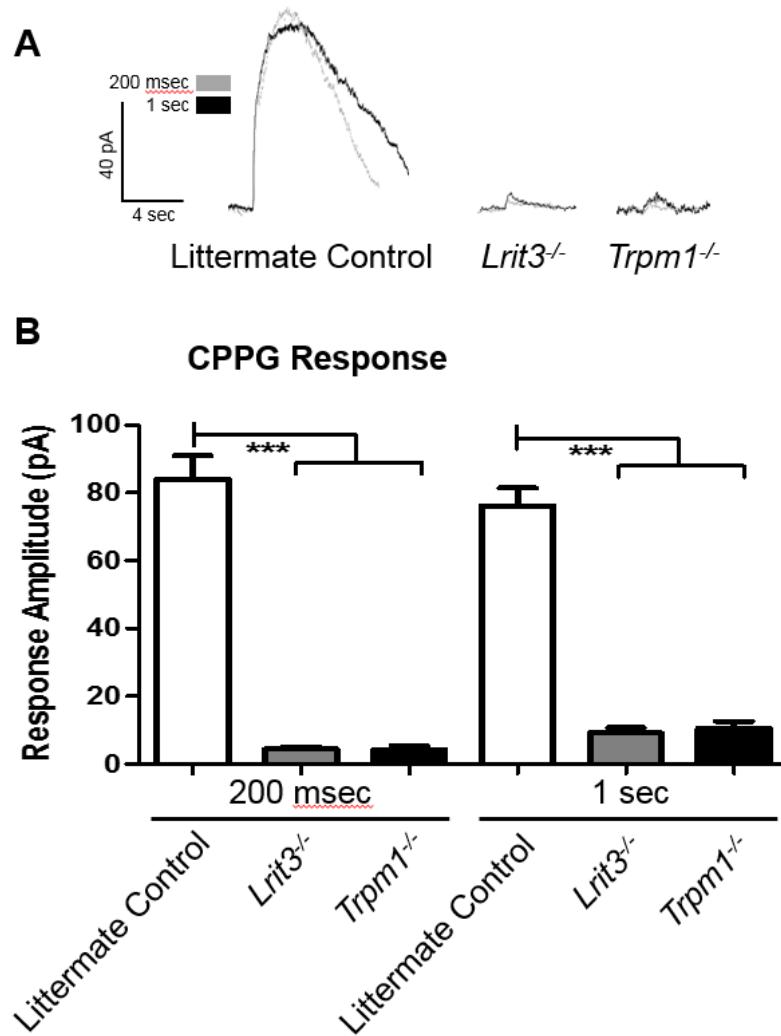


Figure 31. *Lrit3*^{-/-} rod BCs lack a CPPG mediated response at short and long duration stimulation. A. Representative voltage-clamp responses of WT littermate control, *Lrit3*^{-/-}, and *Trpm1*^{-/-} rod BCs evoked by puff application of the mGluR6 antagonist, CPPG for either 200 msec or 1 sec durations. B. Histogram compares the average peak response amplitudes (\pm SEM) of WT littermate control, *Lrit3*^{-/-}, and *Trpm1*^{-/-} rod BCs with 200 msec and 1 sec puff durations. Regardless of duration *Lrit3*^{-/-} and *Trpm1*^{-/-} response amplitudes were significantly

smaller than WT. None of the response amplitudes significantly increase when puff duration increased from 200 msec to 1 sec. (two-way ANOVA with Bonferroni post hoc *** $P < 0.001$).

LRIT3 is required for direct TRPM1 channel modulation in rod BCs

To examine the ability of the TRPM1 channel to be directly gated, I exogenously applied capsaicin, a TRPM1 channel agonist, onto the rod BC dendrites; an approach I described previously (Ray et al., 2014; Chapter V). Since in the LRIT3 mouse mGluR6 and most of the downstream cascade mediating proteins are expressed, this experiment was designed to determine whether the lack of response was due to the absence of functional TRPM1 channels. *Lrit3*^{-/-} and *Trpm1*^{-/-} rod BC responses to 200 msec capsaicin puffs were similar to each other and significantly smaller than WT littermate controls (Figure 32; one-way ANOVA with Bonferroni post hoc: *Lrit3*^{-/-} v. WT & *Trpm1*^{-/-} v. WT: $P < 0.001$) demonstrating that LRIT3 is critical for TRPM1 channel modulation. These data combined with the immunohistochemical analysis of rod BC protein expression (Figure 29) demonstrate that LRIT3 expression is critical for nyctalopin expression and functional TRPM1 channel localization to the dendritic tips.

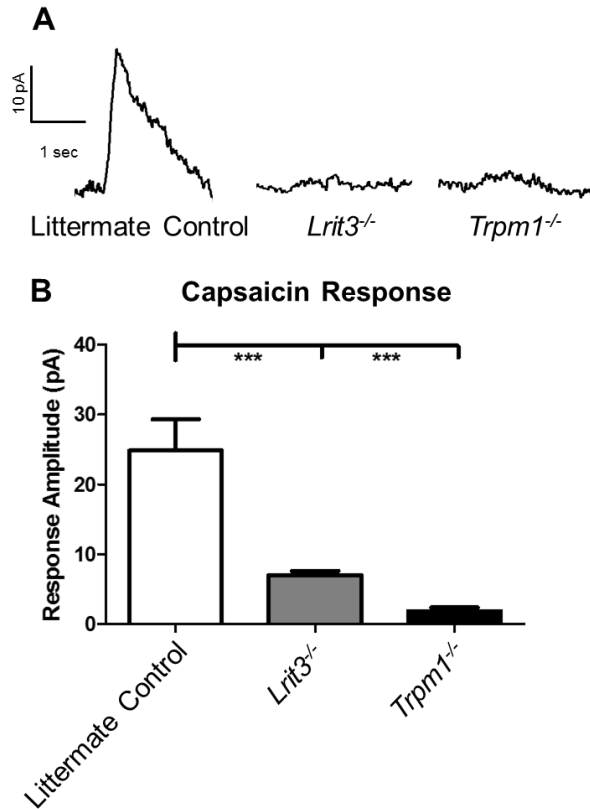


Figure 32. Capsaicin-evoked TRPM1 responses are absent in *Lrit3^{-/-}* rod BCs. **A.** Representative voltage-clamp responses of WT littermate control, *Lrit3^{-/-}*, and *Trpm1^{-/-}* rod BCs evoked by a 200 msec puff of the TRPM1 channel agonist, capsaicin. **B.** Histogram compares the average peak response amplitudes (\pm SEM) of WT littermate control, *Lrit3^{-/-}*, and *Trpm1^{-/-}* rod BCs. *Lrit3^{-/-}* response amplitudes are similar to *Trpm1^{-/-}* rod BCs, while both *Lrit3^{-/-}* and *Trpm1^{-/-}* rod BC amplitudes are significantly smaller than WT rod BCs. The number of rod BCs in each experimental group is shown within each bar of the histograms (one-way ANOVA with Bonferroni post hoc, *** $P < 0.001$).

In the absence of LRIT3, TRPM1 channels are either constitutively closed or absent in rod BCs

In order to determine whether the lack of TRPM1 gating by capsaicin was due to a change in the open probability of TRPM1 channels or the absence of TRPM1 channels, I examined the magnitude of the standing outward current and its variance in WT littermate controls, *Lrit3*^{-/-} and *Trpm1*^{-/-} rod BCs. Both the standing outward current and current variance of *Lrit3*^{-/-} and *Trpm1*^{-/-} rod BCs were similar (Figure 33; one-way ANOVA with Bonferroni post hoc: standing outward current: $P > 0.05$; variance: $P > 0.05$) and both *Lrit3*^{-/-} and *Trpm1*^{-/-} standing outward current and current variance were significantly smaller than WT littermate controls (one-way ANOVA with Bonferroni post hoc: standing current: WT vs *Lrit3*^{-/-}, $P < 0.001$; WT vs *Trpm1*^{-/-}, $P < 0.05$; variance: WT vs *Lrit3*^{-/-}, $P < 0.01$; WT vs *Trpm1*^{-/-}, $P < 0.05$). These data further support my previous results which suggest that although TRPM1 is expressed in *Lrit3*^{-/-} rod BCs, the mislocalized TRPM1 channels are not functional. Also, these results are consistent with my data presented in Chapter IV Figure 20, which show that direct soma capsaicin puffs could not gate mislocalized TRPM1 channels in *Nyx*^{nob} rod BCs. I would anticipate the same results in soma recordings from *Lrit3*^{-/-} rod BCs.

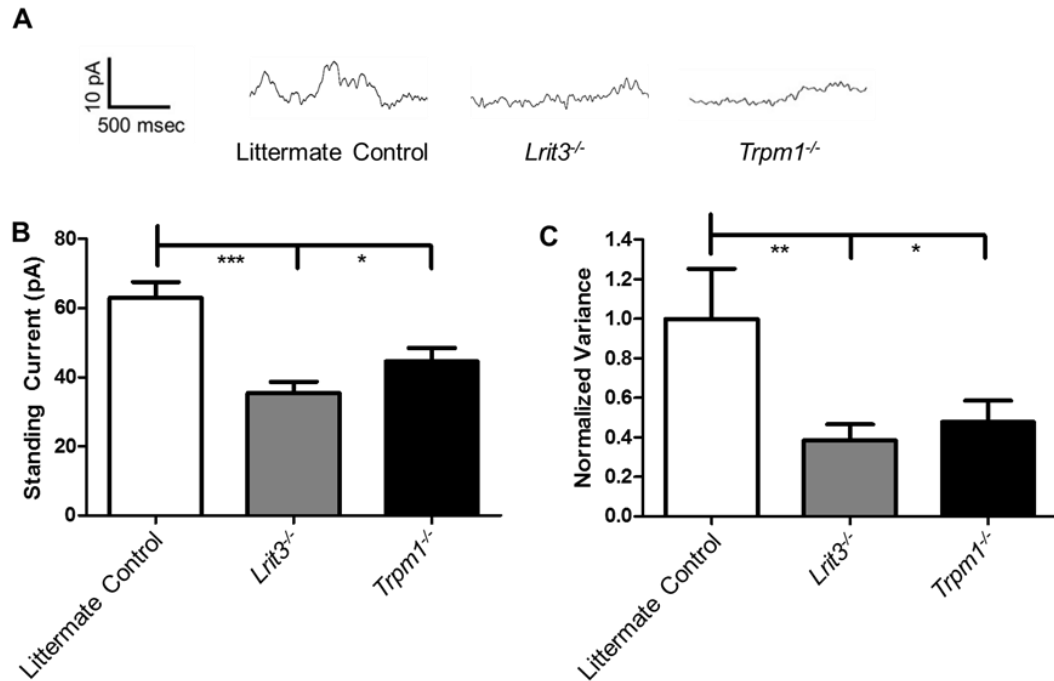


Figure 33. *Lrit3*^{-/-} and *Trpm1*^{-/-} rod BCs have decreased standing currents and channel open probability. A. Representative traces of spontaneous currents from WT littermate controls, *Lrit3*^{-/-} and *Trpm1*^{-/-} rod BCs. Rod BCs were held at +50 mV and 1.5 sec sections of each recording were analyzed to yield the data in B and C. Histograms compare average (\pm SEM) (B) standing current and (C) current variance for WT, *Lrit3*^{-/-} and *Trpm1*^{-/-} rod BCs. *Lrit3*^{-/-} and *Trpm1*^{-/-} rod BCs have similar standing currents (B) and current variance (C) and all are significantly lower than WT (one-way ANOVA with Bonferroni post hoc, * $P < 0.05$; ** $P < 0.01$, *** $P < 0.001$). Combined these data indicate that *Lrit3*^{-/-} rod BCs have an open channel probability that is similar to rod BCs where the TRPM1 channel is absent (*Trpm1*^{-/-}). The number of rod BCs in each experimental group is shown within each bar of the histograms.

Discussion

My results demonstrate that LRIT3 is a new, critical component of the rod BC signaling cascade. In the absence of LRIT3 expression, the mGluR6-mediated cascade, although expressed and properly localized, cannot gate the TRPM1 channel, because the channel cannot be gated, even directly (Figures 31 & 32). In fact, the standing current and noise variance of *Lrit3*^{-/-} rod BCs was similar to *Trpm1*^{-/-} rod BCs suggesting that TRPM1 channels are not present in *Lrit3*^{-/-} rod BC dendritic tips and non-functional at the cell body (Figure 33).

My results in conjunction with the data presented in Figure 29 suggest that LRIT3 is critical for the proper localization and function of rod BC TRPM1 channels. The localization of membrane proteins to the synapse involves cytoskeletal scaffolding proteins, many containing PDZ domains (Feng & Zhang, 2009). Consistent with this idea, the C-terminal region of LRIT3 is highly conserved and may exhibit a PDZ-binding motif (Zeitz et al., 2013). The Neuille et al. (2014) *Lrit3*^{nob6/nob6} mouse had exons 3 and 4 deleted as well as a truncation, leading to the absence of the transmembrane domain and PDZ-binding motif, likely critical for LRIT3 function (Neuille et al., 2014; Zeitz et al., 2013). Several human patients with cCSNB have been found with mutations expected to affect similar regions of the LRIT3 gene (Zeitz et al., 2013). Several human patients with cCSNB have been identified with mutations in exon 4, which is predicted to lead to truncation of the protein and lack of the transmembrane

domain and PDZ-binding motif (Neuille et al., 2014; Zeitz et al., 2013). The *Lrit3*^{-/-} mouse that I used targeted a highly conserved region of exon 2, resulting in a frameshift mutation and a null allele.

Pearring et al. (2011) demonstrated that nyctalopin is necessary for proper localization of TRPM1 channels to the rod BC dendritic tips, but noted that since nyctalopin is an extracellular protein it is likely to require another ancillary transmembrane protein to anchor the TRPM1 channel in the rod BC synapse. Figure 29 demonstrates that in the absence of LRIT3, nyctalopin also is absent. Because we lack an antibody to LRIT3 we do not know if LRIT3 is present in the *Nyx^{nob}* mouse. Therefore, my results in combination with the immunohistochemistry presented in Figure 29 suggest that LRIT3 may be the ancillary transmembrane protein which is critical for the expression of nyctalopin and in combination, both nyctalopin and LRIT3 properly localize TRPM1 to the rod BC dendritic tips.

CHAPTER VII

SUMMARY AND FUTURE DIRECTIONS

The BC is the sole conduit for information flow between the outer retina, where the visual signal is initiated, and the RGCs response, which is the foundation of all higher order visual processing. My dissertation focused on changes in RGCs and rod BCs in a mouse model of the human disease, cCSNB.

The experiments and results presented in Chapter III describe differences between the RGC properties of two models of cCSNB. The *mGluR6*^{-/-} mouse lacks the glutamate receptor that initiates the transduction cascade, which leads to the rod BC signal. The *Nyx*^{nob} mouse lacks the protein nyctalopin, which is required for trafficking or anchoring of the TRPM1 channel, which produces the depolarizing response in the rod BC.

In summary, Chapter III reveals the following conclusions:

1. Almost all *Nyx*^{nob} RGCs exhibited rhythmic spiking while only a few *mGluR6*^{-/-} RGCs exhibit rhythmic spiking.
2. All classes of *Nyx*^{nob} RGCs exhibited rhythmic spiking, while only non-responsive *mGluR6*^{-/-} RGCs exhibit rhythmic spiking.

3. There were no alterations in V_{rest} to account for the differences in *Nyx^{nob}* and *mGluR6^{-/-}* RGCs or in rhythmic and non-rhythmic RGCs within genotypes.
4. A decrease in spontaneous activity level can account for the *Nyx^{nob}* RGCs that lack rhythmic spiking, however spontaneous activity level could not account for the lack of rhythmic spiking in *mGluR6^{-/-}* RGCs.

Further experiments are needed to elucidate the mechanism of rhythmic spiking or lack of rhythmic spiking in *mGluR6^{-/-}* RGCs, as well as the difference in *Nyx^{nob}* and *mGluR6^{-/-}* retinal circuitry that account for the genotypic differences in rhythmicity.

The experiments and results presented in Chapter IV describe differences between the rod BC properties of two mouse models of cCSNB, *mGluR6^{-/-}* and *Nyx^{nob}*.

In summary, Chapter IV revealed the following conclusions:

1. *Nyx^{nob}* rod BC resting membrane potential was depolarized compared to WT and *mGluR6^{-/-}*.
2. *Nyx^{nob}* rod BCs had smaller transient potassium currents than WT and *mGluR6^{-/-}* rod BCs.

My data surprisingly suggest a possible role for nyctalopin or TRPM1 channels in potassium channel conductance and/or localization. It is possible that specific potassium channels bind to either nyctalopin, TRPM1 or another

associated scaffolding protein that is absent in *Nyx^{nob}* rod BCs. However, further studies are needed to elucidate the connection between nyctalopin and potassium channels.

In future experiments, I will identify the altered rod BC potassium channel. I will use pharmacological agonists/antagonists specific to potassium channels and determine if Kv1.1, Kv1.2, Kv11.1, or Kv4 is the potassium channel responsible for the decrease in *Nyx^{nob}* potassium current compared to WT and *mGluR6^{-/-}* rod BCs. An immunohistochemical analysis will follow to validate that there is a decrease in expression of that specific channel in the OPL.

The experiments and results presented in Chapter V describe the rod BCs in the *Gpr179^{nob5}* mouse model of cCSNB. The *Gpr179^{nob5}* mouse lacks the G-protein GPR179. In summary, Chapter V describes the critical role of GPR179 in rod BC signaling with the following conclusions:

1. In the absence of GPR179 a small mGluR6-mediated responses can be elicited in rod BCs and the response can be increased with increased stimulation.
2. GPR179 is required for direct TRPM1 channel modulation in rod BCs.
3. GPR179 sets the sensitivity of the mGluR6 cascade that modulates TRPM1.

A critical function of GPR179 is to set the state of the TRPM1 channel, allowing it to optimally respond to deactivation of the mGluR6 cascade. Future

study at the molecular level may help to elucidate the various states of the TRPM1 channel and clarify how GPR179 modulates the gating of TRPM1.

The experiments and results presented in Chapter VI describe the rod BCs in the *Lrit3*^{-/-} mouse model of cCSNB. The *Lrit3*^{-/-} mouse lacks leucine-rich-repeat, immunoglobulin-like, and transmembrane-domain 3 protein (LRIT3). In summary, Chapter VI describes the critical role of LRIT3 in rod BCs with the following conclusions:

1. LRIT3 is required for mGluR6-mediated responses in rod BCs.
2. LRIT3 is required for direct TRPM1 channel modulation in rod BCs.
3. In the absence of LRIT3 TRPM1 channels are either constitutively closed or absent in rod BCs.
4. LRIT3 is critical for the expression of nyctalopin and TRPM1 channel proteins in rod BCs.

My results in conjunction with the immunohistochemical data presented in Figure 29 suggest that LRIT3 is critical for the proper localization and function of rod BC TRPM1 channels. The C-terminal region of LRIT3 is highly conserved and may exhibit a PDZ-binding motif (Zeitz et al., 2013). PDZ domains are involved in the localization of membrane proteins to the synapse (Feng & Zhang, 2009). I hypothesize that LRIT3 may be the ancillary transmembrane protein which is critical for the expression of nyctalopin and both nyctalopin and LRIT3 properly localize TRPM1 to the rod BC dendritic tips. However, this hypothesis

has not been tested. Future experiments examining protein interactions at the molecular level are needed to determine if my hypothesis is correct.

Implications of my research

My research has increased our understanding of the effects of the disease cCSNB. Not only has my research elucidated cellular effects of cCSNB, but cCSNB mouse models have allowed me to examine the function of specific proteins in retinal neurons and elucidate their function in the normal healthy retina. I have utilized electrophysiological recording techniques to examine functional characteristics of both rod BCs and RGCs. I have also used fluorescent dyes to label these cells and immunohistochemistry and confocal microscopy to recover their morphology. The combination of these techniques result in an increased understanding of how identified cell classes function in the diseased and healthy retina.

cCSNB has been thought to occur due to a plethora of different mutations which result in the same phenotype. However, my dissertation project has shown profound functional differences in the retinas of several cCSNB mouse models, *Nyx^{nob}*, *mGluR6^{-/-}*, *Gpr179^{nob5}* and *Lrit3^{-/-}*. Potential treatment of cCSNB depends on foundational understanding of the disease mechanism and my dissertation research adds to this important literature.

Several retinal diseases such as retinitis pigmentosa and cCSNB have promising treatments in development utilizing gene therapy and retinal prosthetics. In order for many of these treatment techniques to be applied, an understanding of the healthy retinal circuit is critical. The ideal treatment would return the diseased retinal circuitry to the healthy circuitry state. Therefore, one must understand how healthy retinal circuitry functions. By examining models of cCSNB which lack specific proteins in a class of retinal neuron (rod BC) I have gained an understanding of the function these proteins in the healthy neuron. Therefore, my research has added to the greater understanding of how healthy retinal neurons process information, and how the rescue of these proteins may be important for future disease treatment.

REFERENCES

- Ackert JM, Farajian R, Volgyi B, Bloomfield SA (2009) GABA blockade unmasks an OFF response in ON direction selective ganglion cells in the mammalian retina. *The Journal of physiology* 587:4481-4495.
- Ariel M, Daw NW (1982) Effects of cholinergic drugs on receptive field properties of rabbit retinal ganglion cells. *The Journal of physiology* 324:135-160.
- Ashmore JF, Copenhagen DR (1980) Different postsynaptic events in two types of retinal bipolar cell. *Nature* 288:84-86.
- Audo I, Bujakowska K, Orhan E, Poloschek CM, Defoort-Dhellemmes S, Drumare I, Kohl S, Luu TD, Lecompte O, Zrenner E, Lancelot ME, Antonio A, Germain A, Michiels C, Audier C, Letexier M, Saraiva JP, Leroy BP, Munier FL, Mohand-Said S, Lorenz B, Friedburg C, Preising M, Kellner U, Renner AB, Moskova-Doumanova V, Berger W, Wissinger B, Hamel CP, Schorderet DF, De Baere E, Sharon D, Banin E, Jacobson SG, Bonneau D, Zanlonghi X, Le Meur G, Casteels I, Koenekoop R, Long VW, Meire F, Prescott K, de Ravel T, Simmons I, Nguyen H, Dollfus H, Poch O, Leveillard T, Nguyen-Ba-Charvet K, Sahel JA, Bhattacharya SS, Zeitz C (2012) Whole-exome sequencing identifies mutations in GPR179 leading to autosomal-recessive complete congenital stationary night blindness. *American journal of human genetics* 90:321-330.
- Audo I, Kohl S, Leroy BP, Munier FL, Guillonneau X, Mohand-Said S, Bujakowska K, Nandrot EF, Lorenz B, Preising M, Kellner U, Renner AB, Bernd A, Antonio A, Moskova-Doumanova V, Lancelot ME, Poloschek CM, Drumare I, Defoort-Dhellemmes S, Wissinger B, Leveillard T, Hamel CP, Schorderet DF, De Baere E, Berger W, Jacobson SG, Zrenner E, Sahel JA, Bhattacharya SS, Zeitz C (2009) TRPM1 is mutated in patients with autosomal-recessive complete congenital stationary night blindness. *American journal of human genetics* 85:720-729.
- Awatramani GB, Slaughter MM (2000) Origin of transient and sustained responses in ganglion cells of the retina. *The Journal of neuroscience: the official journal of the Society for Neuroscience* 20:7087-7095.
- Bailey DW (1977) Genetic drift: the problem and its possible solution by frozen-embryo storage. *Ciba Foundation symposium* 291-303.
- Bansal A, Singer JH, Hwang BJ, Xu W, Beaudet A, Feller MB (2000) Mice lacking specific nicotinic acetylcholine receptor subunits exhibit dramatically altered spontaneous activity patterns and reveal a limited role for retinal waves in forming ON and OFF circuits in the inner retina. *The*

- Journal of neuroscience: the official journal of the Society for Neuroscience 20:7672-7681.
- Bellone RR, Brooks SA, Sandmeyer L, Murphy BA, Forsyth G, Archer S, Bailey E, Grahn B (2008) Differential gene expression of TRPM1, the potential cause of congenital stationary night blindness and coat spotting patterns (LP) in the Appaloosa horse (*Equus caballus*). *Genetics* 179:1861-1870.
- Bhave G, Nadin BM, Brasier DJ, Glauner KS, Shah RD, Heinemann SF, Karim F, Gereau RWt (2003) Membrane topology of a metabotropic glutamate receptor. *The Journal of biological chemistry* 278:30294-30301.
- Blackburn PR, Campbell JM, Clark KJ, Ekker SC (2013) The CRISPR system--keeping zebrafish gene targeting fresh. *Zebrafish* 10:116-118.
- Blanks JC, Adinolfi AM, Lolley RN (1974) Photoreceptor degeneration and synaptogenesis in retinal-degenerative (rd) mice. *The Journal of comparative neurology* 156:95-106.
- Bloomfield SA, Xin D (1997) A comparison of receptive-field and tracer-coupling size of amacrine and ganglion cells in the rabbit retina. *Visual neuroscience* 14:1153-1165.
- Bormann J, Feigenspan A (1995) GABAC receptors. *Trends in neurosciences* 18:515-519.
- Borowska J, Trenholm S, Awatramani GB (2011) An intrinsic neural oscillator in the degenerating mouse retina. *The Journal of neuroscience: the official journal of the Society for Neuroscience* 31:5000-5012.
- Cadetti L, Tranchina D, Thoreson WB (2005) A comparison of release kinetics and glutamate receptor properties in shaping rod-cone differences in EPSC kinetics in the salamander retina. *The Journal of physiology* 569:773-788.
- Cao Y, Pahlberg J, Sarria I, Kamasawa N, Sampath AP, Martemyanov KA (2012) Regulators of G protein signaling RGS7 and RGS11 determine the onset of the light response in ON bipolar neurons. *Proceedings of the National Academy of Sciences of the United States of America* 109:7905-7910.
- Carter-Dawson LD, LaVail MM, Sidman RL (1978) Differential effect of the rd mutation on rods and cones in the mouse retina. *Investigative ophthalmology & visual science* 17:489-498.
- Catsicas M, Bonness V, Becker D, Mobbs P (1998) Spontaneous Ca²⁺ transients and their transmission in the developing chick retina. *Current biology : CB* 8:283-286.
- Chavez AE, Grimes WN, Diamond JS (2010) Mechanisms underlying lateral GABAergic feedback onto rod bipolar cells in rat retina. *The Journal of neuroscience: the official journal of the Society for Neuroscience* 30:2330-2339.
- Chavez AE, Singer JH, Diamond JS (2006) Fast neurotransmitter release triggered by Ca influx through AMPA-type glutamate receptors. *Nature* 443:705-708.
- Choi H, Zhang L, Cembrowski MS, Sabottke CF, Markowitz AL, Butts DA, Kath WL, Singer JH, Rieke H (2014) Intrinsic bursting of All amacrine cells

- underlies oscillations in the rd1 mouse retina. *Journal of neurophysiology* 112:1491-1504.
- Cohen ED (1998) Interactions of inhibition and excitation in the light-evoked currents of X type retinal ganglion cells. *Journal of neurophysiology* 80:2975-2990.
- Cook PB, McReynolds JS (1998) Lateral inhibition in the inner retina is important for spatial tuning of ganglion cells. *Nature neuroscience* 1:714-719.
- Cook PB, McReynolds JS (1998) Modulation of sustained and transient lateral inhibitory mechanisms in the mudpuppy retina during light adaptation. *Journal of neurophysiology* 79:197-204.
- Cordeiro S, Guseva D, Wulfsen I, Bauer CK (2011) Expression pattern of Kv11 (Ether a-go-go-related gene; erg) K⁺ channels in the mouse retina. *PLoS one* 6:e29490.
- Dacey DM, Packer OS (2003) Colour coding in the primate retina: diverse cell types and cone-specific circuitry. *Current opinion in neurobiology* 13:421-427.
- Dacheux RF, Raviola E (1986) The rod pathway in the rabbit retina: a depolarizing bipolar and amacrine cell. *The Journal of neuroscience: the official journal of the Society for Neuroscience* 6:331-345.
- Demas J, Eglén SJ, Wong RO (2003) Developmental loss of synchronous spontaneous activity in the mouse retina is independent of visual experience. *The Journal of neuroscience: the official journal of the Society for Neuroscience* 23:2851-2860.
- Demas J, Sagdullaev BT, Green E, Jaubert-Miazza L, McCall MA, Gregg RG, Wong RO, Guido W (2006) Failure to maintain eye-specific segregation in nob, a mutant with abnormally patterned retinal activity. *Neuron* 50:247-259.
- DeVries SH (2000) Bipolar cells use kainate and AMPA receptors to filter visual information into separate channels. *Neuron* 28:847-856.
- Dhingra A, Jiang M, Wang TL, Lyubarsky A, Savchenko A, Bar-Yehuda T, Sterling P, Birnbaumer L, Vardi N (2002) Light response of retinal ON bipolar cells requires a specific splice variant of Galphao. *The Journal of neuroscience: the official journal of the Society for Neuroscience* 22:4878-4884.
- Dhingra A, Lyubarsky A, Jiang M, Pugh EN, Jr., Birnbaumer L, Sterling P, Vardi N (2000) The light response of ON bipolar neurons requires G α o. *The Journal of neuroscience: the official journal of the Society for Neuroscience* 20:9053-9058.
- Dhingra A, Ramakrishnan H, Neinstein A, Fina ME, Xu Y, Li J, Chung DC, Lyubarsky A, Vardi N (2012) Gbeta3 is required for normal light ON responses and synaptic maintenance. *The Journal of neuroscience: the official journal of the Society for Neuroscience* 32:11343-11355.
- Dong CJ, Picaud SA, Werblin FS (1994) GABA transporters and GABAC-like receptors on catfish cone- but not rod-driven horizontal cells. *The Journal of neuroscience: the official journal of the Society for Neuroscience*

14:2648-2658.

- Dong CJ, Werblin FS (1998) Temporal contrast enhancement via GABAC feedback at bipolar terminals in the tiger salamander retina. *Journal of neurophysiology* 79:2171-2180.
- Dowling JE (1970) Organization of vertebrate retinas. *Investigative ophthalmology* 9:655-680.
- Dowling JE, Boycott BB (1966) Organization of the primate retina: electron microscopy. *Proceedings of the Royal Society of London Series B, Containing papers of a Biological character Royal Society* 166:80-111.
- Eggers ED, Lukasiewicz PD (2006) GABA(A), GABA(C) and glycine receptor-mediated inhibition differentially affects light-evoked signalling from mouse retinal rod bipolar cells. *The Journal of physiology* 572:215-225.
- Eggers ED, Lukasiewicz PD (2006) Receptor and transmitter release properties set the time course of retinal inhibition. *The Journal of neuroscience: the official journal of the Society for Neuroscience* 26:9413-9425.
- Eggers ED, Lukasiewicz PD (2010) Interneuron circuits tune inhibition in retinal bipolar cells. *Journal of neurophysiology* 103:25-37.
- Eggers ED, Lukasiewicz PD (2011) Multiple pathways of inhibition shape bipolar cell responses in the retina. *Visual neuroscience* 28:95-108.
- Eggers ED, McCall MA, Lukasiewicz PD (2007) Presynaptic inhibition differentially shapes transmission in distinct circuits in the mouse retina. *The Journal of physiology* 582:569-582.
- Eglen SJ (1999) The role of retinal waves and synaptic normalization in retinogeniculate development. *Philosophical transactions of the Royal Society of London Series B, Biological sciences* 354:497-506.
- Enroth-Cugell C, Robson JG (1966) The contrast sensitivity of retinal ganglion cells of the cat. *The Journal of physiology* 187:517-552.
- Euler T, Masland RH (2000) Light-evoked responses of bipolar cells in a mammalian retina. *Journal of neurophysiology* 83:1817-1829.
- Famiglietti EV, Jr., Kolb H (1975) A bistratified amacrine cell and synaptic circuitry in the inner plexiform layer of the retina. *Brain research* 84:293-300.
- Farajian R, Pan F, Akopian A, Volgyi B, Bloomfield SA (2011) Masked excitatory crosstalk between the ON and OFF visual pathways in the mammalian retina. *The Journal of physiology* 589:4473-4489.
- Feigenspan A, Bormann J (1994) Differential pharmacology of GABAA and GABAC receptors on rat retinal bipolar cells. *European journal of pharmacology* 288:97-104.
- Feigenspan A, Wassle H, Bormann J (1993) Pharmacology of GABA receptor Cl⁻ channels in rat retinal bipolar cells. *Nature* 361:159-162.
- Feigenspan A, Weiler R (2004) Electrophysiological properties of mouse horizontal cell GABAA receptors. *Journal of neurophysiology* 92:2789-2801.
- Fisher SK, Boycott BB (1974) Synaptic connections made by horizontal cells within the outer plexiform layer of the retina of the cat and the rabbit.

- Proceedings of the Royal Society of London Series B, Containing papers of a Biological character Royal Society 186:317-331.
- Fletcher EL, Wassle H (1999) Indoleamine-accumulating amacrine cells are presynaptic to rod bipolar cells through GABA(C) receptors. *The Journal of comparative neurology* 413:155-167.
- Freeman DK, Heine WF, Passaglia CL (2008) The maintained discharge of rat retinal ganglion cells. *Visual neuroscience* 25:535-548.
- Frishman LJ, Levine MW (1983) Statistics of the maintained discharge of cat retinal ganglion cells. *The Journal of physiology* 339:475-494.
- Gaj T, Gersbach CA, Barbas CF, 3rd (2013) ZFN, TALEN, and CRISPR/Cas-based methods for genome engineering. *Trends in biotechnology* 31:397-405.
- Galli L, Maffei L (1988) Spontaneous impulse activity of rat retinal ganglion cells in prenatal life. *Science* 242:90-91.
- Geffen MN, de Vries SE, Meister M (2007) Retinal ganglion cells can rapidly change polarity from Off to On. *PLoS biology* 5:e65.
- Ghosh KK, Bujan S, Haverkamp S, Feigenspan A, Wassle H (2004) Types of bipolar cells in the mouse retina. *The Journal of comparative neurology* 469:70-82.
- Gleason E (2012) The influences of metabotropic receptor activation on cellular signaling and synaptic function in amacrine cells. *Visual neuroscience* 29:31-39.
- Gregg RG, Kamermans M, Klooster J, Lukasiewicz PD, Peachey NS, Vessey KA, McCall MA (2007) Nyctalopin expression in retinal bipolar cells restores visual function in a mouse model of complete X-linked congenital stationary night blindness. *Journal of neurophysiology* 98:3023-3033.
- Gregg RG, Mukhopadhyay S, Candille SI, Ball SL, Pardue MT, McCall MA, Peachey NS (2003) Identification of the gene and the mutation responsible for the mouse nob phenotype. *Investigative ophthalmology & visual science* 44:378-384.
- Grimes WN, Zhang J, Graydon CW, Kachar B, Diamond JS (2010) Retinal parallel processors: more than 100 independent microcircuits operate within a single interneuron. *Neuron* 65:873-885.
- Grunert U, Wassle H (1990) GABA-like immunoreactivity in the macaque monkey retina: a light and electron microscopic study. *The Journal of comparative neurology* 297:509-524.
- Grunert U, Wassle H (1993) Immunocytochemical localization of glycine receptors in the mammalian retina. *The Journal of comparative neurology* 335:523-537.
- Hartline HK (1948) Retinal action potentials of photoreceptor cells and the discharge of nerve impulses in their axones. *Federation proceedings* 7:51.
- Hodgkin AL, Horowicz P (1959) The influence of potassium and chloride ions on the membrane potential of single muscle fibres. *The Journal of physiology* 148:127-160.
- Hodgkin AL, Katz B (1949) The effect of sodium ions on the electrical activity of

- giant axon of the squid. *The Journal of physiology* 108:37-77.
- Hoffman DA, Johnston D (1998) Downregulation of transient K⁺ channels in dendrites of hippocampal CA1 pyramidal neurons by activation of PKA and PKC. *The Journal of neuroscience: the official journal of the Society for Neuroscience* 18:3521-3528.
- Hooks SB, Waldo GL, Corbitt J, Bodor ET, Krumins AM, Harden TK (2003) RGS6, RGS7, RGS9, and RGS11 stimulate GTPase activity of Gi family G-proteins with differential selectivity and maximal activity. *The Journal of biological chemistry* 278:10087-10093.
- Hosoi N, Arai I, Tachibana M (2005) Group III metabotropic glutamate receptors and exocytosed protons inhibit L-type calcium currents in cones but not in rods. *The Journal of neuroscience: the official journal of the Society for Neuroscience* 25:4062-4072.
- Hu HJ, Pan ZH (2002) Differential expression of K⁺ currents in mammalian retinal bipolar cells. *Visual neuroscience* 19:163-173.
- Huang L, Max M, Margolskee RF, Su H, Masland RH, Euler T (2003) G protein subunit G gamma 13 is coexpressed with G alpha o, G beta 3, and G beta 4 in retinal ON bipolar cells. *The Journal of comparative neurology* 455:1-10.
- Ichinose T, Shields CR, Lukasiewicz PD (2005) Sodium channels in transient retinal bipolar cells enhance visual responses in ganglion cells. *The Journal of neuroscience: the official journal of the Society for Neuroscience* 25:1856-1865.
- Ivanova E, Muller F (2006) Retinal bipolar cell types differ in their inventory of ion channels. *Visual neuroscience* 23:143-154.
- Ivanova E, Muller U, Wässle H (2006) Characterization of the glycinergic input to bipolar cells of the mouse retina. *The European journal of neuroscience* 23:350-364.
- Jeffrey BG, Morgans CW, Puthussery T, Wensel TG, Burke NS, Brown RL, Duvoisin RM (2010) R9AP stabilizes RGS11-G beta5 and accelerates the early light response of ON-bipolar cells. *Visual neuroscience* 27:9-17.
- Jeon CJ, Strettoi E, Masland RH (1998) The major cell populations of the mouse retina. *The Journal of neuroscience: the official journal of the Society for Neuroscience* 18:8936-8946.
- Kameneva T, Meffin H, Burkitt AN (2011) Modelling intrinsic electrophysiological properties of ON and OFF retinal ganglion cells. *Journal of computational neuroscience* 31:547-561.
- Kaneko A, Pinto LH, Tachibana M (1989) Transient calcium current of retinal bipolar cells of the mouse. *The Journal of physiology* 410:613-629.
- Karschin A, Wässle H (1990) Voltage- and transmitter-gated currents in isolated rod bipolar cells of rat retina. *Journal of neurophysiology* 63:860-876.
- Klumpp DJ, Song EJ, Ito S, Sheng MH, Jan LY, Pinto LH (1995) The Shaker-like potassium channels of the mouse rod bipolar cell and their contributions to the membrane current. *The Journal of neuroscience: the official journal of the Society for Neuroscience* 15:5004-5013.

- Klumpp DJ, Song EJ, Pinto LH (1995) Identification and localization of K⁺ channels in the mouse retina. *Visual neuroscience* 12:1177-1190.
- Koike C, Obara T, Uriu Y, Numata T, Sanuki R, Miyata K, Koyasu T, Ueno S, Funabiki K, Tani A, Ueda H, Kondo M, Mori Y, Tachibana M, Furukawa T (2010) TRPM1 is a component of the retinal ON bipolar cell transduction channel in the mGluR6 cascade. *Proceedings of the National Academy of Sciences of the United States of America* 107:332-337.
- Kolb H, Famiglietti EV (1974) Rod and cone pathways in the inner plexiform layer of cat retina. *Science* 186:47-49.
- Kolb H, Jones J (1984) Synaptic organization of the outer plexiform layer of the turtle retina: an electron microscope study of serial sections. *Journal of neurocytology* 13:567-591.
- Koulen P, Brandstatter JH, Kroger S, Enz R, Bormann J, Wassle H (1997) Immunocytochemical localization of the GABA(C) receptor rho subunits in the cat, goldfish, and chicken retina. *The Journal of comparative neurology* 380:520-532.
- Kuffler SW (1953) Discharge patterns and functional organization of mammalian retina. *Journal of neurophysiology* 16:37-68.
- Kuffler SW, Fitzhugh R, Barlow HB (1957) Maintained activity in the cat's retina in light and darkness. *The Journal of general physiology* 40:683-702.
- Larsen AP, Bentzen BH, Grunnet M (2010) Differential effects of Kv11.1 activators on Kv11.1a, Kv11.1b and Kv11.1a/Kv11.1b channels. *British journal of pharmacology* 161:614-628.
- Li Z, Sergouniotis PI, Michaelides M, Mackay DS, Wright GA, Devery S, Moore AT, Holder GE, Robson AG, Webster AR (2009) Recessive mutations of the gene TRPM1 abrogate ON bipolar cell function and cause complete congenital stationary night blindness in humans. *American journal of human genetics* 85:711-719.
- Lukasiewicz PD, McReynolds JS (1985) Synaptic transmission at N-methyl-D-aspartate receptors in the proximal retina of the mudpuppy. *The Journal of physiology* 367:99-115.
- Lukasiewicz PD, Werblin FS (1994) A novel GABA receptor modulates synaptic transmission from bipolar to ganglion and amacrine cells in the tiger salamander retina. *The Journal of neuroscience: the official journal of the Society for Neuroscience* 14:1213-1223.
- MacNeil MA, Masland RH (1998) Extreme diversity among amacrine cells: implications for function. *Neuron* 20:971-982.
- Maddox DM, Vessey KA, Yarbrough GL, Invergo BM, Cantrell DR, Inayat S, Balannik V, Hicks WL, Hawes NL, Byers S, Smith RS, Hurd R, Howell D, Gregg RG, Chang B, Naggert JK, Troy JB, Pinto LH, Nishina PM, McCall MA (2008) Allelic variance between GRM6 mutants, Grm6nob3 and Grm6nob4 results in differences in retinal ganglion cell visual responses. *The Journal of physiology* 586:4409-4424.
- Manookin MB, Beaudoin DL, Ernst ZR, Flagel LJ, Demb JB (2008) Disinhibition combines with excitation to extend the operating range of the OFF visual

- pathway in daylight. *The Journal of neuroscience: the official journal of the Society for Neuroscience* 28:4136-4150.
- Manookin MB, Weick M, Stafford BK, Demb JB (2010) NMDA receptor contributions to visual contrast coding. *Neuron* 67:280-293.
- Marc RE, Kalloniatis M, Jones BW (2005) Excitation mapping with the organic cation AGB2+. *Vision research* 45:3454-3468.
- Marc RE, Murry RF, Basinger SF (1995) Pattern recognition of amino acid signatures in retinal neurons. *The Journal of neuroscience: the official journal of the Society for Neuroscience* 15:5106-5129.
- Margolis DJ, Detwiler PB (2007) Different mechanisms generate maintained activity in ON and OFF retinal ganglion cells. *The Journal of neuroscience: the official journal of the Society for Neuroscience* 27:5994-6005.
- Margolis DJ, Detwiler PB (2011) Cellular origin of spontaneous ganglion cell spike activity in animal models of retinitis pigmentosa. *Journal of ophthalmology* 2011.
- Margolis DJ, Gartland AJ, Singer JH, Detwiler PB (2014) Network oscillations drive correlated spiking of ON and OFF ganglion cells in the rd1 mouse model of retinal degeneration. *PloS one* 9:e86253.
- Masu M, Iwakabe H, Tagawa Y, Miyoshi T, Yamashita M, Fukuda Y, Sasaki H, Hiroi K, Nakamura Y, Shigemoto R, et al. (1995) Specific deficit of the ON response in visual transmission by targeted disruption of the mGluR6 gene. *Cell* 80:757-765.
- McCall MA, Gregg RG (2008) Comparisons of structural and functional abnormalities in mouse b-wave mutants. *The Journal of physiology* 586:4385-4392.
- McCall MA, Lukasiewicz PD, Gregg RG, Peachey NS (2002) Elimination of the rho1 subunit abolishes GABA(C) receptor expression and alters visual processing in the mouse retina. *The Journal of neuroscience: the official journal of the Society for Neuroscience* 22:4163-4174.
- Meister M, Wong RO, Baylor DA, Shatz CJ (1991) Synchronous bursts of action potentials in ganglion cells of the developing mammalian retina. *Science* 252:939-943.
- Menger N, Pow DV, Wassle H (1998) Glycinergic amacrine cells of the rat retina. *The Journal of comparative neurology* 401:34-46.
- Menger N, Wassle H (2000) Morphological and physiological properties of the A17 amacrine cell of the rat retina. *Visual neuroscience* 17:769-780.
- Mennerick S, Matthews G (1996) Ultrafast exocytosis elicited by calcium current in synaptic terminals of retinal bipolar neurons. *Neuron* 17:1241-1249.
- Menzler J, Channappa L, Zeck G (2014) Rhythmic ganglion cell activity in bleached and blind adult mouse retinas. *PloS one* 9:e106047.
- Menzler J, Zeck G (2011) Network oscillations in rod-degenerated mouse retinas. *The Journal of neuroscience: the official journal of the Society for Neuroscience* 31:2280-2291.
- Miller C (2000) An overview of the potassium channel family. *Genome biology* 1:REVIEWS0004.

- Miyake Y, Yagasaki K, Horiguchi M, Kawase Y, Kanda T (1986) Congenital stationary night blindness with negative electroretinogram. A new classification. *Archives of ophthalmology* 104:1013-1020.
- Molnar A, Hsueh HA, Roska B, Werblin FS (2009) Crossover inhibition in the retina: circuitry that compensates for nonlinear rectifying synaptic transmission. *Journal of computational neuroscience* 27:569-590.
- Morgans CW, Brown RL, Duvoisin RM (2010) TRPM1: the endpoint of the mGluR6 signal transduction cascade in retinal ON-bipolar cells. *BioEssays : news and reviews in molecular, cellular and developmental biology* 32:609-614.
- Morgans CW, Weiwei L, Wensel TG, Brown RL, Perez-Leon JA, Bearnot B, Duvoisin RM (2007) Gbeta5-RGS complexes co-localize with mGluR6 in retinal ON-bipolar cells. *The European journal of neuroscience* 26:2899-2905.
- Morgans CW, Zhang J, Jeffrey BG, Nelson SM, Burke NS, Duvoisin RM, Brown RL (2009) TRPM1 is required for the depolarizing light response in retinal ON-bipolar cells. *Proceedings of the National Academy of Sciences of the United States of America* 106:19174-19178.
- Muller F, Wassle H, Voigt T (1988) Pharmacological modulation of the rod pathway in the cat retina. *Journal of neurophysiology* 59:1657-1672.
- Murphy GJ, Rieke F (2006) Network variability limits stimulus-evoked spike timing precision in retinal ganglion cells. *Neuron* 52:511-524.
- Nakajima Y, Iwakabe H, Akazawa C, Nawa H, Shigemoto R, Mizuno N, Nakanishi S (1993) Molecular characterization of a novel retinal metabotropic glutamate receptor mGluR6 with a high agonist selectivity for L-2-amino-4-phosphonobutyrate. *The Journal of biological chemistry* 268:11868-11873.
- Nawy S (1999) The metabotropic receptor mGluR6 may signal through G(o), but not phosphodiesterase, in retinal bipolar cells. *The Journal of neuroscience: the official journal of the Society for Neuroscience* 19:2938-2944.
- Nawy S (2004) Desensitization of the mGluR6 transduction current in tiger salamander On bipolar cells. *The Journal of physiology* 558:137-146.
- Neuille M, El Shamieh S, Orhan E, Michiels C, Antonio A, Lancelot ME, Condroyer C, Bujakowska K, Poch O, Sahel JA, Audo I, Zeitz C (2014) Lrit3 deficient mouse (nob6): a novel model of complete congenital stationary night blindness (cCSNB). *PloS one* 9:e90342.
- Nikonov SS, Kholodenko R, Lem J, Pugh EN, Jr. (2006) Physiological features of the S- and M-cone photoreceptors of wild-type mice from single-cell recordings. *The Journal of general physiology* 127:359-374.
- Nirenberg S, Meister M (1997) The light response of retinal ganglion cells is truncated by a displaced amacrine circuit. *Neuron* 18:637-650.
- Nobles RD, Zhang C, Muller U, Betz H, McCall MA (2012) Selective glycine receptor alpha2 subunit control of crossover inhibition between the on and off retinal pathways. *The Journal of neuroscience: the official journal of the*

- Society for Neuroscience 32:3321-3332.
- Nomura A, Shigemoto R, Nakamura Y, Okamoto N, Mizuno N, Nakanishi S (1994) Developmentally regulated postsynaptic localization of a metabotropic glutamate receptor in rat rod bipolar cells. *Cell* 77:361-369.
- Orlandi C, Posokhova E, Masuho I, Ray TA, Hasan N, Gregg RG, Martemyanov KA (2012) GPR158/179 regulate G protein signaling by controlling localization and activity of the RGS7 complexes. *The Journal of cell biology* 197:711-719.
- Palmer MJ (2010) Characterisation of bipolar cell synaptic transmission in goldfish retina using paired recordings. *The Journal of physiology* 588:1489-1498.
- Pang JJ, Abd-El-Barr MM, Gao F, Bramblett DE, Paul DL, Wu SM (2007) Relative contributions of rod and cone bipolar cell inputs to All amacrine cell light responses in the mouse retina. *The Journal of physiology* 580:397-410.
- Pang JJ, Gao F, Wu SM (2003) Light-evoked excitatory and inhibitory synaptic inputs to ON and OFF alpha ganglion cells in the mouse retina. *The Journal of neuroscience: the official journal of the Society for Neuroscience* 23:6063-6073.
- Pang JJ, Gao F, Wu SM (2004) Light-evoked current responses in rod bipolar cells, cone depolarizing bipolar cells and All amacrine cells in dark-adapted mouse retina. *The Journal of physiology* 558:897-912.
- Pang JJ, Gao F, Wu SM (2007) Cross-talk between ON and OFF channels in the salamander retina: indirect bipolar cell inputs to ON-OFF ganglion cells. *Vision research* 47:384-392.
- Pardue MT, McCall MA, LaVail MM, Gregg RG, Peachey NS (1998) A naturally occurring mouse model of X-linked congenital stationary night blindness. *Investigative ophthalmology & visual science* 39:2443-2449.
- Pardue MT, Peachey NS (2014) Mouse b-wave mutants. *Documenta ophthalmologica Advances in ophthalmology* 128:77-89.
- Peachey NS, Pearing JN, Bojang P, Jr., Hirschtritt ME, Sturgill-Short G, Ray TA, Furukawa T, Koike C, Goldberg AF, Shen Y, McCall MA, Nawy S, Nishina PM, Gregg RG (2012) Depolarizing bipolar cell dysfunction due to a Trpm1 point mutation. *Journal of neurophysiology* 108:2442-2451.
- Peachey NS, Ray TA, Florijn R, Rowe LB, Sjoerdsma T, Contreras-Alcantara S, Baba K, Tosini G, Pozdeyev N, Iuvone PM, Bojang P, Jr., Pearing JN, Simonsz HJ, van Genderen M, Birch DG, Traboulsi EI, Dorfman A, Lopez I, Ren H, Goldberg AF, Nishina PM, Lachapelle P, McCall MA, Koenekoop RK, Bergen AA, Kamermans M, Gregg RG (2012) GPR179 is required for depolarizing bipolar cell function and is mutated in autosomal-recessive complete congenital stationary night blindness. *American journal of human genetics* 90:331-339.
- Pearing JN, Bojang P, Jr., Shen Y, Koike C, Furukawa T, Nawy S, Gregg RG (2011) A role for nyctalopin, a small leucine-rich repeat protein, in localizing the TRP melastatin 1 channel to retinal depolarizing bipolar cell

- dendrites. *The Journal of neuroscience: the official journal of the Society for Neuroscience* 31:10060-10066.
- Picaud S, Pattnaik B, Hicks D, Forster V, Fontaine V, Sahel J, Dreyfus H (1998) GABAA and GABAC receptors in adult porcine cones: evidence from a photoreceptor-glia co-culture model. *The Journal of physiology* 513 (Pt 1):33-42.
- Pignatelli V, Strettoi E (2004) Bipolar cells of the mouse retina: a gene gun, morphological study. *The Journal of comparative neurology* 476:254-266.
- Pin JP, Acher F (2002) The metabotropic glutamate receptors: structure, activation mechanism and pharmacology. *Current drug targets CNS and neurological disorders* 1:297-317.
- Pin JP, Galvez T, Prezeau L (2003) Evolution, structure, and activation mechanism of family 3/C G-protein-coupled receptors. *Pharmacology & therapeutics* 98:325-354.
- Pinto LH, Klumpp DJ (1998) Localization of potassium channels in the retina. *Progress in retinal and eye research* 17:207-230.
- Pinto LH, Vitaterna MH, Shimomura K, Siepka SM, Balannik V, McDearmon EL, Omura C, Lumayag S, Invergo BM, Glawe B, Cantrell DR, Inayat S, Olvera MA, Vessey KA, McCall MA, Maddox D, Morgans CW, Young B, Pletcher MT, Mullins RF, Troy JB, Takahashi JS (2007) Generation, identification and functional characterization of the nob4 mutation of Grm6 in the mouse. *Visual neuroscience* 24:111-123.
- Poopalasundaram S, Erskine L, Cheetham ME, Hardcastle AJ (2005) Focus on molecules: nyctalopin. *Experimental eye research* 81:627-628.
- Pourcho RG (1996) Neurotransmitters in the retina. *Current eye research* 15:797-803.
- Pourcho RG, Goebel DJ (1983) Neuronal subpopulations in cat retina which accumulate the GABA agonist, (3H)muscimol: a combined Golgi and autoradiographic study. *The Journal of comparative neurology* 219:25-35.
- Quraishi S, Gayet J, Morgans CW, Duvoisin RM (2007) Distribution of group-III metabotropic glutamate receptors in the retina. *The Journal of comparative neurology* 501:931-943.
- Rae C, Hare N, Bubb WA, McEwan SR, Broer A, McQuillan JA, Balcar VJ, Conigrave AD, Broer S (2003) Inhibition of glutamine transport depletes glutamate and GABA neurotransmitter pools: further evidence for metabolic compartmentation. *Journal of neurochemistry* 85:503-514.
- Rao A, Dallman R, Henderson S, Chen CK (2007) Gbeta5 is required for normal light responses and morphology of retinal ON-bipolar cells. *The Journal of neuroscience: the official journal of the Society for Neuroscience* 27:14199-14204.
- Ray TA, Heath KM, Hasan N, Noel JM, Samuels IS, Martemyanov KA, Peachey NS, McCall MA, Gregg RG (2014) GPR179 is required for high sensitivity of the mGluR6 signaling cascade in depolarizing bipolar cells. *The Journal of neuroscience: the official journal of the Society for Neuroscience* 34:6334-6343.

- Renteria RC, Tian N, Cang J, Nakanishi S, Stryker MP, Copenhagen DR (2006) Intrinsic ON responses of the retinal OFF pathway are suppressed by the ON pathway. *The Journal of neuroscience: the official journal of the Society for Neuroscience* 26:11857-11869.
- Rieke F, Baylor DA (1998) Origin of reproducibility in the responses of retinal rods to single photons. *Biophysical journal* 75:1836-1857.
- Rodieck RW, Stone J (1965) Analysis of receptive fields of cat retinal ganglion cells. *Journal of neurophysiology* 28:832-849.
- Rodieck RW, Stone J (1965) Response of cat retinal ganglion cells to moving visual patterns. *Journal of neurophysiology* 28:819-832.
- Roska B, Molnar A, Werblin FS (2006) Parallel processing in retinal ganglion cells: how integration of space-time patterns of excitation and inhibition form the spiking output. *Journal of neurophysiology* 95:3810-3822.
- Roska B, Nemeth E, Werblin FS (1998) Response to change is facilitated by a three-neuron disinhibitory pathway in the tiger salamander retina. *The Journal of neuroscience: the official journal of the Society for Neuroscience* 18:3451-3459.
- Roska B, Werblin F (2001) Vertical interactions across ten parallel, stacked representations in the mammalian retina. *Nature* 410:583-587.
- Sagdullaev BT, McCall MA (2005) Stimulus size and intensity alter fundamental receptive-field properties of mouse retinal ganglion cells in vivo. *Visual neuroscience* 22:649-659.
- Sagdullaev BT, McCall MA, Lukasiewicz PD (2006) Presynaptic inhibition modulates spillover, creating distinct dynamic response ranges of sensory output. *Neuron* 50:923-935.
- Sampath AP, Rieke F (2004) Selective transmission of single photon responses by saturation at the rod-to-rod bipolar synapse. *Neuron* 41:431-443.
- Sanchez-Ramos C, Guerrera MC, Bonnin-Arias C, Calavia MG, Laura R, Germana A, Vega JA (2012) Expression of TRPV4 in the zebrafish retina during development. *Microscopy research and technique* 75:743-748.
- Shah MM, Hammond RS, Hoffman DA (2010) Dendritic ion channel trafficking and plasticity. *Trends in neurosciences* 33:307-316.
- Shatz CJ, Stryker MP (1988) Prenatal tetrodotoxin infusion blocks segregation of retinogeniculate afferents. *Science* 242:87-89.
- Shen Y, Heimel JA, Kamermans M, Peachey NS, Gregg RG, Nawy S (2009) A transient receptor potential-like channel mediates synaptic transmission in rod bipolar cells. *The Journal of neuroscience: the official journal of the Society for Neuroscience* 29:6088-6093.
- Shen Y, Rampino MA, Carroll RC, Nawy S (2012) G-protein-mediated inhibition of the Trp channel TRPM1 requires the Gbetagamma dimer. *Proceedings of the National Academy of Sciences of the United States of America* 109:8752-8757.
- Shields CR, Tran MN, Wong RO, Lukasiewicz PD (2000) Distinct ionotropic GABA receptors mediate presynaptic and postsynaptic inhibition in retinal bipolar cells. *The Journal of neuroscience: the official journal of the*

- Society for Neuroscience 20:2673-2682.
- Shim H, Wang CT, Chen YL, Chau VQ, Fu KG, Yang J, McQuiston AR, Fisher RA, Chen CK (2012) Defective retinal depolarizing bipolar cells in regulators of G protein signaling (RGS) 7 and 11 double null mice. *The Journal of biological chemistry* 287:14873-14879.
- Singer JH, Diamond JS (2003) Sustained Ca²⁺ entry elicits transient postsynaptic currents at a retinal ribbon synapse. *The Journal of neuroscience: the official journal of the Society for Neuroscience* 23:10923-10933.
- Slaughter MM, Miller RF (1981) 2-amino-4-phosphonobutyric acid: a new pharmacological tool for retina research. *Science* 211:182-185.
- Slaughter MM, Miller RF (1983) The role of excitatory amino acid transmitters in the mudpuppy retina: an analysis with kainic acid and N-methyl aspartate. *The Journal of neuroscience: the official journal of the Society for Neuroscience* 3:1701-1711.
- Snellman J, Zenisek D, Nawy S (2009) Switching between transient and sustained signalling at the rod bipolar-All amacrine cell synapse of the mouse retina. *The Journal of physiology* 587:2443-2455.
- Stasheff SF (2008) Emergence of sustained spontaneous hyperactivity and temporary preservation of OFF responses in ganglion cells of the retinal degeneration (rd1) mouse. *Journal of neurophysiology* 99:1408-1421.
- Stasheff SF, Shankar M, Andrews MP (2011) Developmental time course distinguishes changes in spontaneous and light-evoked retinal ganglion cell activity in rd1 and rd10 mice. *Journal of neurophysiology* 105:3002-3009.
- Strettoi E, Raviola E, Dacheux RF (1992) Synaptic connections of the narrow-field, bistratified rod amacrine cell (All) in the rabbit retina. *The Journal of comparative neurology* 325:152-168.
- Sugihara H, Inoue T, Nakanishi S, Fukuda Y (1997) A late ON response remains in visual response of the mGluR6-deficient mouse. *Neuroscience letters* 233:137-140.
- Sun W, Li N, He S (2002) Large-scale morphological survey of mouse retinal ganglion cells. *The Journal of comparative neurology* 451:115-126.
- Syed MM, Lee S, Zheng J, Zhou ZJ (2004) Stage-dependent dynamics and modulation of spontaneous waves in the developing rabbit retina. *The Journal of physiology* 560:533-549.
- Thoreson WB, Witkovsky P (1999) Glutamate receptors and circuits in the vertebrate retina. *Progress in retinal and eye research* 18:765-810.
- Tian N, Hwang TN, Copenhagen DR (1998) Analysis of excitatory and inhibitory spontaneous synaptic activity in mouse retinal ganglion cells. *Journal of neurophysiology* 80:1327-1340.
- Torborg CL, Feller MB (2005) Spontaneous patterned retinal activity and the refinement of retinal projections. *Progress in neurobiology* 76:213-235.
- Toychiev AH, Ivanova E, Yee CW, Sagdullaev BT (2013) Block of gap junctions eliminates aberrant activity and restores light responses during retinal

- degeneration. *The Journal of neuroscience: the official journal of the Society for Neuroscience* 33:13972-13977.
- Toychiev AH, Yee CW, Sagdullaev BT (2013) Correlated spontaneous activity persists in adult retina and is suppressed by inhibitory inputs. *PloS one* 8:e77658.
- Trenholm S, Borowska J, Zhang J, Hoggarth A, Johnson K, Barnes S, Lewis TJ, Awatramani GB (2012) Intrinsic oscillatory activity arising within the electrically coupled All amacrine-ON cone bipolar cell network is driven by voltage-gated Na⁺ channels. *The Journal of physiology* 590:2501-2517.
- Trifonov IU (1968) [Study of synaptic transmission between photoreceptor and horizontal cell by electric stimulations of the retina]. *Biofizika* 13:809-817.
- van Genderen MM, Bijveld MM, Claassen YB, Florijn RJ, Pearing JN, Meire FM, McCall MA, Riemsdag FC, Gregg RG, Bergen AA, Kamermans M (2009) Mutations in TRPM1 are a common cause of complete congenital stationary night blindness. *American journal of human genetics* 85:730-736.
- van Wyk M, Wassle H, Taylor WR (2009) Receptive field properties of ON- and OFF-ganglion cells in the mouse retina. *Visual neuroscience* 26:297-308.
- Vaney DI (1991) Many diverse types of retinal neurons show tracer coupling when injected with biocytin or Neurobiotin. *Neuroscience letters* 125:187-190.
- Vardi N (1998) Alpha subunit of Go localizes in the dendritic tips of ON bipolar cells. *The Journal of comparative neurology* 395:43-52.
- Vardi N, Matesic DF, Manning DR, Liebman PA, Sterling P (1993) Identification of a G-protein in depolarizing rod bipolar cells. *Visual neuroscience* 10:473-478.
- Veruki ML, Hartveit E (2002) All (Rod) amacrine cells form a network of electrically coupled interneurons in the mammalian retina. *Neuron* 33:935-946.
- Veruki ML, Hartveit E (2002) Electrical synapses mediate signal transmission in the rod pathway of the mammalian retina. *The Journal of neuroscience: the official journal of the Society for Neuroscience* 22:10558-10566.
- Volgyi B, Deans MR, Paul DL, Bloomfield SA (2004) Convergence and segregation of the multiple rod pathways in mammalian retina. *The Journal of neuroscience: the official journal of the Society for Neuroscience* 24:11182-11192.
- Walz W, Boulton AA, Baker GB (2002) Patch-clamp analysis: advanced techniques. Totowa, N.J.: Humana Press.
- Wan QF, Heidelberger R (2011) Synaptic release at mammalian bipolar cell terminals. *Visual neuroscience* 28:109-119.
- Wang M, Ramos BP, Paspalas CD, Shu Y, Simen A, Duque A, Vijayraghavan S, Brennan A, Dudley A, Nou E, Mazer JA, McCormick DA, Arnsten AF (2007) Alpha2A-adrenoceptors strengthen working memory networks by inhibiting cAMP-HCN channel signaling in prefrontal cortex. *Cell* 129:397-410.

- Wassle H (2004) Parallel processing in the mammalian retina. *Nature reviews Neuroscience* 5:747-757.
- Wassle H, Heinze L, Ivanova E, Majumdar S, Weiss J, Harvey RJ, Haverkamp S (2009) Glycinergic transmission in the Mammalian retina. *Frontiers in molecular neuroscience* 2:6.
- Werblin F (1991) Synaptic connections, receptive fields, and patterns of activity in the tiger salamander retina. A simulation of patterns of activity formed at each cellular level from photoreceptors to ganglion cells [the Friedenwald lecture]. *Investigative ophthalmology & visual science* 32:459-483.
- Werblin FS (2010) Six different roles for crossover inhibition in the retina: correcting the nonlinearities of synaptic transmission. *Visual neuroscience* 27:1-8.
- Wilhelm BT, Landry JR, Takei F, Mager DL (2003) Transcriptional control of murine CD94 gene: differential usage of dual promoters by lymphoid cell types. *Journal of immunology* 171:4219-4226.
- Wong RO (1999) Retinal waves and visual system development. *Annual review of neuroscience* 22:29-47.
- Wong RO, Meister M, Shatz CJ (1993) Transient period of correlated bursting activity during development of the mammalian retina. *Neuron* 11:923-938.
- Wong RO, Oakley DM (1996) Changing patterns of spontaneous bursting activity of on and off retinal ganglion cells during development. *Neuron* 16:1087-1095.
- Wu SM (1991) Input-output relations of the feedback synapse between horizontal cells and cones in the tiger salamander retina. *Journal of neurophysiology* 65:1197-1206.
- Wu SM, Gao F, Maple BR (2000) Functional architecture of synapses in the inner retina: segregation of visual signals by stratification of bipolar cell axon terminals. *The Journal of neuroscience: the official journal of the Society for Neuroscience* 20:4462-4470.
- Xin D, Bloomfield SA (1999) Comparison of the responses of All amacrine cells in the dark- and light-adapted rabbit retina. *Visual neuroscience* 16:653-665.
- Xu Y, Dhingra A, Fina ME, Koike C, Furukawa T, Vardi N (2012) mGluR6 deletion renders the TRPM1 channel in retina inactive. *Journal of neurophysiology* 107:948-957.
- Yang Y, Beyer BJ, Otto JF, O'Brien TP, Letts VA, White HS, Frankel WN (2003) Spontaneous deletion of epilepsy gene orthologs in a mutant mouse with a low electroconvulsive threshold. *Human molecular genetics* 12:975-984.
- Yee CW, Toychiev AH, Sagdullaev BT (2012) Network deficiency exacerbates impairment in a mouse model of retinal degeneration. *Frontiers in systems neuroscience* 6:8.
- Zaghloul KA, Boahen K, Demb JB (2003) Different circuits for ON and OFF retinal ganglion cells cause different contrast sensitivities. *The Journal of neuroscience : the official journal of the Society for Neuroscience* 23:2645-2654.

- Zeit C, Jacobson SG, Hamel CP, Bujakowska K, Neuille M, Orhan E, Zanlonghi X, Lancelot ME, Michiels C, Schwartz SB, Bocquet B, Congenital Stationary Night Blindness C, Antonio A, Audier C, Letexier M, Saraiva JP, Luu TD, Sennlaub F, Nguyen H, Poch O, Dollfus H, Lecompte O, Kohl S, Sahel JA, Bhattacharya SS, Audo I (2013) Whole-exome sequencing identifies LRIT3 mutations as a cause of autosomal-recessive complete congenital stationary night blindness. *American journal of human genetics* 92:67-75.
- Zhang C, Bettler B, Duvoisin RM (1998) Differential localization of GABA(B) receptors in the mouse retina. *Neuroreport* 9:3493-3497.
- Zhang J, Diamond JS (2009) Subunit- and pathway-specific localization of NMDA receptors and scaffolding proteins at ganglion cell synapses in rat retina. *The Journal of neuroscience: the official journal of the Society for Neuroscience* 29:4274-4286.
- Zhang J, Jeffrey BG, Morgans CW, Burke NS, Haley TL, Duvoisin RM, Brown RL (2010) RGS7 and -11 complexes accelerate the ON-bipolar cell light response. *Investigative ophthalmology & visual science* 51:1121-1129.
- Zhang J, Jung CS, Slaughter MM (1997) Serial inhibitory synapses in retina. *Visual neuroscience* 14:553-563.
- Zhang J, Li W, Trexler EB, Massey SC (2002) Confocal analysis of reciprocal feedback at rod bipolar terminals in the rabbit retina. *The Journal of neuroscience: the official journal of the Society for Neuroscience* 22:10871-10882.
- Zhang J, Slaughter MM (1995) Preferential suppression of the ON pathway by GABAC receptors in the amphibian retina. *Journal of neurophysiology* 74:1583-1592.
- Zhang J, Wu SM (2009) Immunocytochemical analysis of photoreceptors in the tiger salamander retina. *Vision research* 49:64-73.
- Zimov S, Yazulla S (2008) Novel processes invaginate the pre-synaptic terminal of retinal bipolar cells. *Cell and tissue research* 333:1-16.

CURRICULUM VITAE

Kathryn Marie Heath Fransen

BUSINESS ADDRESS

Dept of Ophthalmology & Visual Sciences
Kentucky Lions Eye Research Institute
University of Louisville
Louisville, KY 40202
(502)-852-0162: laboratory

HOME ADDRESS

2525 Glenmary Apt. 6
Louisville, KY 40204

PERSONAL INFORMATION

Citizenship: United States

EDUCATION

B.S. Indiana University
Bloomington, Indiana 47405

Psychology 2007

Ph.D. Department of Psychological and Brain Sciences
University of Louisville
Louisville, Kentucky 40202

Experimental Psychology 2014

PROFESSIONAL EXPERIENCE

Research Positions:

Fall 2007 – 2014 Graduate Student
Summer 2009- 2014 Graduate Research Assistant
Department of Psychological & Brain Sciences
University of Louisville

Teaching Positions:

Fall 2007-Spring 2009 Graduate Teaching Assistant
Department of Psychological & Brain Sciences
University of Louisville

Course titles: Introduction to Psychology (Undergraduate)
Statistics I (Undergraduate)

Professional Society Affiliations:

Member - Society for Neuroscience

Member - Association for Research in Vision and Ophthalmology

Awards:

1. Society for Neuroscience Indianapolis Chapter Poster Presentation Award Winner (2006)
2. Indiana University STARS Travel Grant (attended Society for Neuroscience, 2007)
3. ARVO Foundation for Eye Research/Tyson Research Initiative/PAOF/Retina Research Foundation Travel Grant (2011)
4. Doctoral Dissertation Completion Award (University of Louisville, 2014)
5. Graduate Teaching Assistant Academy (University of Louisville, 2014)
6. Dean's Citation Award (University of Louisville, December 2014)

PUBLICATIONS

Published Papers:

1. McDowell, AL; **Heath, KM**; Garraghty, PE The Effects of Sex and Chronic Restraint on Instrumental Learning in Rats Neuroscience Journal, vol. 2013, Article ID 893126 (2013) doi:10.1155/2013/893126
2. Ray, TA*; **Heath, KM***; Hasan, N; Noel, JM; Samuels, IS; Martemyanov, KA; Peachey, NS; McCall, MA; Gregg, RG GPR179 is required for high sensitivity of the mGluR6 signaling cascade in depolarizing bipolar cells Journal of Neuroscience, 34(18):6334-43. (2014) *Equal Contribution

Abstracts:

1. **Heath, KM**, Heflin, SJ, Nobles, RD, McCall, MA Mutational Variations in *Grm6* Result in Different Retinal Ganglion Cell Light Responses in the Mouse Retina (Research Louisville Poster in Louisville, KY, 2010).

2. **Heath, KM**, Noel, J, Gregg, R, Peachey, N, McCall, MA *Gpr179^{nob5}* Mouse Exhibits A Unique No b-wave Electrophysiological Phenotype (FASEB Retinal Neurobiology & Visual Processing, 2012).
3. **Heath, KM** and McCall, MA Different Properties Of *Nyx^{nob}* And *Grm6^{-/-}* Rod BCs May Cause Differences In Their RGC Spontaneous Rhythmic Spiking (FASEB Retinal Neurobiology & Visual Processing, 2014).
4. Noel, J, **Heath, KM**, Hasan, N, Ray, T, McCall, MA, Gregg, R Proper Localization and Function of TRPM1 Depends on LRIT3 Expression in Rod Depolarizing Bipolar Cells (FASEB Retinal Neurobiology & Visual Processing, 2014).

Invited Presentations:

1. Animal Models of Congenital Stationary Night Blindness – Exploration of Underlying Circuitry (University of Louisville, Experimental Psychology Seminar, 2010)
2. Allelic *Grm6* Variants Create Different Light-Evoked Murine Retinal Ganglion Cell Responses (ARVO Paper Presentation, 2011)